AN ABSTRACT OF THE THESIS OF

Lii-ping Leu for the degree of Doctor of Philosophy

in Chemical Engineering presented on June 11, 1981

Title: Dynamics and Control of Continuous Crystallizers

Abstract approved: Redacted for Privacy

Dr. Thomas J. Fitzgerald

The theoretical analysis of an unseeded, isothermal mixed-suspension mixed-product-removal (MSMPR) crystallizer with a fines trap is developed. The lumped parameter system equations are presented for a homogeneous nucleation and a number-dependent secondary-nucleation model. Linear stability analysis and system simulations are used to investigate the system's dynamic behavior.

Modal control algorithms for the above systems are developed using throughput rate or fines-recirculation rate or both as the manipulated variables. The system performance is significantly improved when modal control is applied whether the system is stable or unstable.

The characteristic equation for size-dependent growth rate in an MSMPR crystallizer is found by linear stability analysis. The case in which the growth rate is size-dependent for small crystals and size-independent for large crystals; and the case in which the growth rate is given by the Abegg-Stevens-Larson (ASL) equation are solved to illustrate the effect of size-dependent growth rate on stability.

A new on-line probe was developed to measure the particle size distribution. Its theory, limitations (it is useful for large particles) and applicability are discussed.

Dynamics and Control of Continuous Crystallizers

by

Lii-ping Leu

A THESIS

submitted to

Oregon State University

in partial fulfillment of
the requirements for the
degree of

Doctor of Philosophy

Completed June 11, 1981

Commencement June 1982

APPROVED:

Redacted for Privacy

Professor of Chemical Engineering in charge of major

Redacted for Privacy

Head of Department of Chemical Engineering

Redacted for Privacy

Dean of Graduate School

Date thesis is presented June 11, 1981

Typed by Young Sook Pahk for Lii-ping Leu

ACKNOWLEDGEMENT

First and foremost, I would like to express my sincere appreciation to my major professor, Dr. Thomas Fitzgerald for his expert direction and guidance. This work would not have been possible without his help. I am also grateful for his timely editing of this thesis.

I would like to thank Professor F. Kayihan for introducing me the modal control theory and for his constant source of help and inspiration.

My appreciation is also extended to Professor O. Levenspiel for his invaluable discussions and constructive suggestions.

Many thanks are due to the faculty members of the Department of Chemical Engineering, especially Dr. C.E. Wicks, Department Head, for financial support and for use of departmental facility.

Mr. Riley Chan's technical assistance in the experimental work of my thesis is kindly acknowledged.

I am also thankful to the members of graduate committee, Dr. W. Bublitz, Dr. R. Adams, and Dr. R. Davis for their logistic support and constructive comments on the thesis draft.

I am also grateful for the fellowship support from the National Science Foundation of Taiwan (1976-1977) and for the unsponsored research fund from Oregon State University Computer Center.

Special thanks go to my wife Helen for constant encouragement and never-ending support.

Finally, I acknowledge my daughter Bekki, for all that she has given to me and for being herself.

TABLE OF CONTENTS

Appendices

LIST OF FIGURES

LIST OF TABLES

DYNAMICS AND CONTROL OF CONTINUOUS CRYSTALLIZERS

CHAPTER I. INTRODUCTION

Crystallization from solution is a separation and purification process often used in the chemical, pharmaceutical, and food processing industries. Crystal size distribution (CSD) is one of the most important and difficult to predict properties of the crystallization process and better knowledge and control of crystal size is essential to the improvement of the crystallization process. Crystal size distribution affects the end uses of the crystalline product and interacts strongly with the crystallization process itself; it influences crystal purity, stability of operation, and other aspects of crystallization.

Although crystallization is a very old unit operation, the industrial operation of continuous crystallizers is still something of an art, and often depends to a considerable degree on experience. The main difference between the continuous crystallizer process and most other continuous reactors is the simultaneous occurrence of nucleation and growth, which produces cyclic instability of the crystal size distribution.

For example, an increase of the supersaturation leads to a higher nucleation rate, but as the total crystal surface area increases due to the growth of the nuclei, the supersaturation decreases again, thus reducing the nucleation rate. The total crystal surface area decreases when the product crystals are withdrawn, and this in turn causes an

increase of the supersaturation and the establishment of a new corresponding nucleation rate, and so on. The steady state condition can be expected. Due to the considerable time lag, because newly formed nuclei have no appreciable surface for a long time, a large number of nuclei might be formed which will later reduce the supersaturation below its steady state value. The resulting slow nucleation will lead to a decrease of the total crystal surface area below its steady state value, and this in turn will cause an increase of the supersaturation above its steady state, and so on. The result of this sequence of events will be the occurrence of limit cycles. Similar phenomena have been observed in some continuous polymerization and fermentation processes which also involve nucleation and growth. (39, 40, 41)

(A) CSD Dynamics and Stability

It would be wise to distinguish between CSD transients and instability. Dynamics of the former type are caused by upsets outside the crystallizer such as changing the feed rate or composition; while an unstable CSD results from the particular form of crystallizer configuration and the operating parameters imposed on the given system kinetics. Transients result from time dependent outside forcing functions, while instability results from the structure of the system equations.

Analytical work on CSD dynamics dates back to the early 1960's and was motivated by the unstable limit-cycle behavior in ammonium sulfate system (30).

Randolph and Larson (30) presented the crystal population balance as a very useful tool in the study of CSD transient. Hulburt and Katz (14)

and Randolph (25) treated the population balance as a fundamental concept in the particulate system and discussed distributed forms of the balance equations and moment transformations. Randolph and Larson (29) studied CSD dynamics in a class II (high yield) mixed suspension mixed product removal (MSMPR) crystallizer and derived the now classical constraint for homogeneous nucleation. Sherwin et al. (34) analyzed the stability of a class I (variable yield) MSMPR crystallizer in terms of the nucleation/growth sensitivity parameter, b_c/g_c which is defined in terms of the nucleation rate B and growth rate G as lnB/lnG. Hulburt and Stefango (15) investigated the dynamic behavior in a class I MSMPR crystallizer with clear liquid overflow. Sherwin et al. (35) studied an idealized classified crystallizer, and they found a dramatic influence of product classification on CSD stability. Lei et al. (19) studied similar effects of fines removal and Randolph et al. (26) examined the product classification with fines removal. These studies showed that product classification has a drastic destabilizing effect on CSD whereas seeding of the feed increases system's stability.

Recently, Liss and Shinnar (20) studied the stability of a MSMPR crystallizer in which crystallizer kinetics depend on the magma suspension. Epstein and Sowul (7) studied the stability of the class II MSMPR crystallizer with secondary nucleation kinetics including crystal number dependent, crystal length dependent, crystal surface area dependent, and crystalline mass dependent.

(B) CSD Control

A few studies on the control of CSD have been reported. Control studies are divided into two categories since there are two dynamic modes that a crystallizer may experience, namely, dynamics due to external disturbance, and self-sustained limit cycle behavior.

Han (12) analyzed the stability of class I MSMPR crystallizer which was derived by Sherwin et al. (34), and investigated a feed-forward scheme which controlled supersaturation using feed rate as the manipulated variable. Good control was predicted when the crystallizer was operated in a stable region. However, the controller did not reduce sustained limit-cycle behavior in the unstable region. Gupta and Timm (11) studied the control of the class II MSMPR crystallizer by applying predictive/corrective scheme, they utilized zeroth and second moment by using fines seeding and destruction as the manipulated variable. They found that by controlling the zeroth moment they could eliminate sustained limit cycling. On the other hand, control of the second moment might drive a normally stable crystallizer unstable. Lei et al. (18) studied the convensional proportional feedback control of class I MSMPR crystallizer with point fines trap. They investigated control of fines crystal area by manipulating either throughput rate or fines destruction rate. It was found that an unstable system could be stabilized by manipulation of throughput rate but not by manipulation of fines destruction rate. Bechman et al. (3) studied a class II complex R-z crystallizer (equipped fines destruction, clear liquor advance and product classification). In their studies, the conventional proportional feedback control was

used with two control schemes: using the nuclei density as the controlled variable and the fines destruction rate as the manipulated variable, or using the slurry density as the controlled variable and the slurry withdraw rate as the manipulated variable. The result of their work showed successful elimination of a long term oscillatory transit by the first scheme.

A comprehensive and methodical treatment of continuous crystallizer based on the population balance concept appears in a book by Randolph and Larson (28). An excellent review of the state of the art in the CSD dynamics and control is provided by Randolph (24).

(C) Scope of the Present Research

It is the intention of this work to show the dynamic behavior of an isothermal class I MSMPR crystallizer with fines trap (an MSMPR crystallizer is a special case) due to self-perpetuated limit cycles or as affected by disturbance of the feed conditions, and present the design of a control system to improve the dynamics of the uncontrolled system. The approach chosen for a control scheme was modal control which seems to have definite advantages over the conventional feedback control.

The basic technique for designing a modal controller has been discussed by Rosenbrock (32), Gould and Lasso (10), Crossley (5), Mayne and Murdoch (21), and Takahashi et al. (37). These ideas were adapted for designing a controller to control the CSD in a MSMPR with or without a trap for fines. The number of the crystals, the total length of the

crystals, the surface area of the crystals, and the mass of the crystals would be controlled using either throughput flow rate or fines destruction rate or using both as the manipulated variables and the feed concentration as the input disturbance.

Finally, the stability analysis of a class I MSMPR crystallizer with size-dependent growth rate, (where the McCabe ΔL law does not hold) will be discussed.

In the second part of this work, an on-line probe for particle size measurement is developed and discussed. It is the first, and perhaps the most basic step in developing the control technology of the continuous crystallizer.

CHAPTER II. DERIVATION OF THE MODEL

In this section, the basic differential equations for a continuous crystallizer with a fines trap will be set down. A diagram of this type of operation discussed is shown in Fig. 2-1. A crystallizer of this type is usually used to increase the crystal product size. The removal of flows of liquor associated with the fines dictates that they be dissolved and the pure liquid recycled. The net effect of fines destruction is to force the growth rate to higher levels, producing the same product in fewer crystals but of large average crystal size.

A feed material containing pure solute at concentration C_i (gm/cm^3) is fed to a crystallizer of working volume V (cm^3) at a volumetric flow rate q (cm^3/sec). A product slurry of crystallizer is withdrawn at the volumetric flow rate q, in addition a continous removal of fines or very small crystals (or crystals below a certain size) from the crystal magma at the volumetric flow rate q_o (cm^3/sec). They are drawn off to a heater in which the smaller crystals are dissolved, or to a mechanical fines-removing device and the clear solution is fed back to the crystallizer body.

(A) Homogeneous Nucleation Model

In this section the system equations of a homogeneous nucleation model will be developed, and a secondary nucleation model will be developed in the following section.

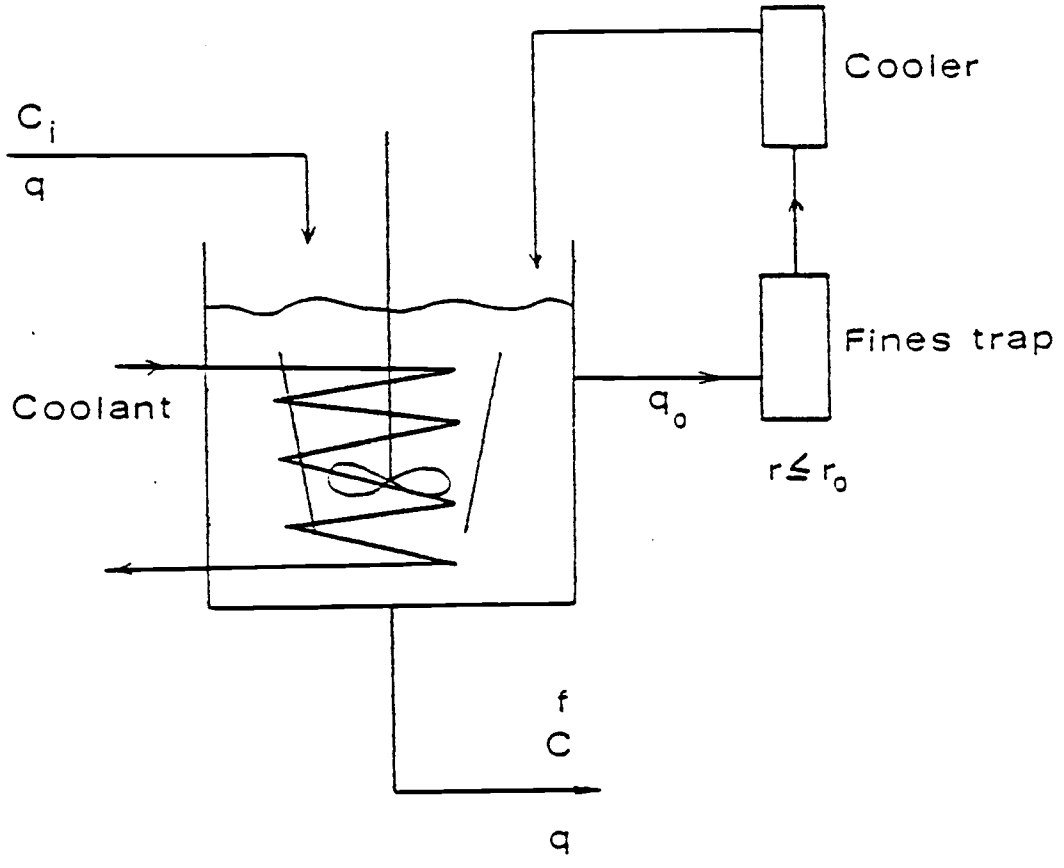

Fig. 2-1. Schematic diagram of a continuous crystallizer with a fines trap.

In addition to simplify the development, the following basic assumptions are made:

1. The crystallizer is ideally mixed.

2. The crystals in the system are geometrically similar and the solid density is constant.

3. The growth rate G (cm/sec) = dr/dt is independent of particle size, i.e. the McCabe ΔL law holds, and is proportional to the supersaturation

$$G = k_g(C-C_s)$$

where C_s is the saturation concentration at the given temperature and k_g is the growth rate constant.

4. The nucleation rate $B(no/cm^3\ sec)$ is defined by the Mier form:

$$B = k_b\ (C-C_m)^{n'}\ ,\quad n' \geq 1$$

where C_m is some critical concentration level higher than the saturation concentration C_s.

5. The crystallizer is isothermal, with the instant cooling of the feed resulting in a supersaturation driving force for the subsequent nucleation and growth.

6. The volume of the crystallizer and the volumetric flow rate are based on the total slurry, and the total volume of the crystallizer is kept constant.

7. No solids or seeds exist in the input feed stream.

8. The fines destruction size r_o and the fines retention time θ_0 $(= V/q_0)$ are very small, however, their ratio is finite. This corresponds to a crystallizer with a point fines trap.

The basic governing equations may be described by the following set of equations.

(i) Population balance:

By Hulburt and Katz (14), the population balance equation is taken to be:

$$V \frac{\partial f}{\partial t} + VG \frac{\partial f}{\partial r} = -qf, \quad r > 0 \qquad (2\text{-}1a)$$

where:

f = population density of crystal particles at size r and at time t ($no/cm^3 cm$)

G = growth rate (cm/sec)

q = volumetric flow rate (cm^3/sec)

r = characteristic size of the crystals (cm)

t = time (sec)

V = volume of the crystallizer (cm^3)

The terms in Eq.(2-1a) represent, in order, the accumulation of the crystals at size r, the net flux of crystals away from size r due to growth, and the withdrawal of particles of size r due to the product removal.

The boundary condition will be (19)

$$Gf = \varepsilon B\, e^{-r_o q_0/GV}, \quad r = 0 \qquad (2\text{-}1b)$$

where ε is the liquid volume fraction in the crystallizer, and it will be represented as

$$\varepsilon = 1 - k \int_0^\infty f\, r^3 dr \qquad (2\text{-}1c)$$

and $k(1/no)$ is the geometrical shape factor. Here also, r_o is the fines destruction size, and q_o the fines removal rate.

The boundary condition (2-1b) means the formation of new crystals because of nucleation at size $r = 0$, but the fraction $1 - \exp(-r_o q_0/GV)$ of nuclei formed is destroyed due to the fines trap.

(ii) Solute and Crystal balance:

The overall mass balance on solute and crystal material in the system is:

$$V \frac{d}{dt} \{C\varepsilon + (1-\varepsilon)\rho_s\} = qC_i - q \{C\varepsilon + (1-\varepsilon)\, \rho_s\} \qquad (2\text{-}1d)$$

where C and C_i represent the concentration of solute within the crystallizer (and the output) and the input feed, respectively, and ρ_s represents the solid crystal density.

The terms in Eq. (2-1d) represent, in order, the accumulation of solute and crystals within the crystallizer, the input of solute by

feed stream, and the removal of solute and crystals from the crystallizer due to the product withdrawal.

(iii) Moment Equations

If it is not necessary to determine how the population distribution f varies with time; a knowledge of the variation of its moments with time is satisfactory. This set can be transformed to a group of ordinary differential equations.

The nth moment of f will be called μ_n,

$$\mu_n(t) = \int_0^\infty f r^n dr$$

the physical significance of the moments of f is shown below:

$\mu_0 = \int_0^\infty f dr$	= total number of crystals per unit volume of crystallizer
$\mu_1 = \int_0^\infty f r dr$	= total radius of crystals per unit volume of crystallizer
$3\,k\mu_2 = 3k\int_0^\infty f r^2 dr$	= total surface area of crystals per unit volume of crystallizer
$k\mu_3 = k\int_0^\infty f r^3 dr = 1 - \varepsilon$	= volume fraction of solids in crystallizer

The moments of higher order can be defined similarly, but their physical significances are not so obvious as the first four leading moments.

Multiplying Eq. (2-1a) through by r^n, and integrating with respect to r from 0 to ∞, one generates the moment equations.

$$\frac{d\mu_0}{dt} = -\frac{q}{V}\mu_0 + \varepsilon\, B e^{-r_o/G\theta_0}$$

$$\frac{d\mu_n}{dt} = -\frac{q}{V}\mu_n + nG\mu_n - 1$$

$$(n = 1,2,3,.....)$$

It is convenient to introduce a crystal-solute function

$$\psi = (1-k\mu_3)C + k\mu_3\rho_s \qquad (2\text{-}2)$$

Then using Eq. (2-1d), the system equations will be:

$$\frac{d\mu_0}{dt} = -\frac{q}{V}\mu_0 + \varepsilon\, Be^{-r_o/\theta_0 G} \qquad (2\text{-}3a)$$

$$\frac{d\mu_1}{dt} = -\frac{q}{V}\mu_1 + G\,\mu_0 \qquad (2\text{-}3b)$$

$$\frac{d\mu_2}{dt} = -\frac{q}{V}\mu_2 + 2G\mu_1 \qquad (2\text{-}3c)$$

$$\frac{d\mu_3}{dt} = -\frac{q}{V}\mu_3 + 3G\mu_2 \qquad (2\text{-}3d)$$

$$\frac{d\psi}{dt} = \frac{q}{V}C_i - \frac{q}{V}\psi \qquad (2\text{-}3e)$$

Although $n = 3$ is enough to form the closed complete set of equations all moments should exist mathmatically (1).

(iv) Steady State Solutions

The steady state moments can now be obtained by letting $\frac{d}{dt} = 0$ in Eq. (2-3).

$$\mu_0^* = \theta^* \varepsilon^* B^* e^{-\lambda} \tag{2-4a}$$

$$\mu_n^* = n\theta^* G^* \mu_{n-1}^* \quad (n = 1,2,3,.....) \tag{2-4b}$$

$$C_i^* = \psi^* \tag{2-4c}$$

where $\lambda = \frac{r_o q_0^*}{VG^*}$, $\theta^* = \frac{V}{q^*}$

the superscript"*" means steady state value. The parameter "λ" characterizes the operation of fines trap: when r_o is small, the value r_o/G^*, the time a nucleus needs to grow to size r_o, is small with respect to the mean residence time θ, but it is finite with respect to the much smaller mean recirculation time θ_0, and if r_o is small, the destruction of nuclei in the fines trap is instantaneous.

(v) Linearization

In order to determine the stability condition and apply linear control theory, the set of equations describing the system, Eq. (2-3) must be linearized about the steady state value. The quantities "δ" denote the departure from the steady state value.

The feed rate and concentration can vary in time in the form:

$$C_i(t) = C_i^* + \delta C_i \tag{2-5a}$$

$$q(t) = q^* + \delta q \tag{2-5b}$$

$$\psi(t) = \psi^* + \delta\psi \tag{2-5c}$$

$$C(t) = C^* + \delta C \tag{2-5d}$$

The performance variables are represented by:

$$\mu_n(t) = \mu_n^* + \delta\mu_n \quad (n = 0,1,2,3,.....) \tag{2-6}$$

The kinetic terms for small displacement can be written as:

$$B(t) = B^* + \frac{\partial B}{\partial C}\ \delta C \tag{2-7a}$$

$$G(t) = G^* + \frac{\partial G}{\partial C}\ \delta C \tag{2-7b}$$

Now substitution of Equations (2-5), (2-6) and (2-7) into Eq. (2-3) and utilization of the steady state relations Eq. (2-4), retaining only the first order term of "δ" in each term results in the following linearized set:

$$\begin{aligned}\frac{d\delta\mu_0}{dt} = &-\frac{\mu_0}{V}\delta q - \frac{\mu_0^*}{V}\delta\mu_0 \\ &- B^*(1 - k\mu_3^*)\exp\left(\frac{-r_o q_0^*}{VG^*}\right)\frac{r_o}{VG^*}\delta q_0 \\ &+ B^*\exp\left(\frac{-r_o q_0^*}{VG^{*2}}\right)\left(\frac{dB}{dc}\frac{1}{B^*} + \frac{r_o}{VG^{*2}}q_0^*\frac{dG}{dc}\right)\delta\psi \\ &- kB^*\exp\left(\frac{-r_o}{V}\frac{q_0^*}{G^*}\right)\left\{\left(\frac{dB}{dcB^*} + \frac{r_o q_0^*}{VG^{*2}}\frac{dG}{dc}\right)\right. \\ &\left.(\rho_s - C^*) + 1\right\}\delta\mu_3\end{aligned} \tag{2-8a}$$

$$\delta\mu_0(0) = 0 \tag{2-8b}$$

$$\frac{d\delta\mu_n}{dt} = -\frac{\mu_n^*}{V}\delta q - \frac{q^*}{V}\delta\mu_n + nG^*\delta\mu_{n-1}$$

$$+ n\frac{dG}{dc}\mu_{n-1}^*\frac{\delta\psi}{(1-k\mu_3^*)}$$

$$- nk\frac{(\rho_s - c^*)}{1-k\mu_3^*}\frac{dG}{dc}\mu_{n-1}^*\delta\mu_3 \tag{2-8c}$$

$$(n = 1,2,3,....)$$

$$\delta\mu_n(0) = 0 \tag{2-8d}$$

$$\frac{d\delta\psi}{dt} = \frac{q^*}{V}\delta C_i - \frac{q^*}{V}\delta\psi \tag{2-8e}$$

$$\delta\psi(0) = 0 \tag{2-8f}$$

Now defining the following dimensionless parameters and variables, one obtains

$$\frac{\delta \mu_n}{\mu_n^*} = Z_n'$$

$$t' = \frac{t}{\theta^*} \quad (\theta^* = \frac{V}{q^*})$$

$$g_c = 6\, k\, (\rho_s - C^*)\, \theta^{*4}\, G^{*3}\, B^*\, \frac{dG}{dc}\, \frac{1}{G^*}$$

$$= \alpha\, (\rho_s - C^*)\, \frac{1}{G^*}\, \frac{dG}{dc}$$

$$b_c = 6\, k\, B^* G^{*3} \theta^{*4}\, \{1 + (\rho_s - C^*)\, \frac{dB}{dc}\, \frac{1}{B^*}\}$$

$$= \alpha\, \{1 + (\rho_s - C^*)\, \frac{1}{B^*}\, \frac{dB}{dc}\}$$

$$\alpha = 6k\, B^* G^{*3} \theta^{*4}$$

$$q' = \delta q / q^*$$

$$q_0' = \delta q_0 / q_0^*$$

$$L = \frac{\rho_s - C_s}{C_i^* - C_s}$$

$$M = \frac{C^* - C_s}{C_i^* - C_s}$$

$$F' = \frac{\delta\psi}{\psi^*}$$

$$h' = \frac{\delta C_i}{C_i^*}$$

$$P = \frac{1}{\alpha(L-M)(1-k\mu_3^*)(1-\frac{C_s}{C_i^*})}$$

We obtain following set of dimensionless equations.

$$\frac{dZ_0'}{dt'} = -q'-\lambda q_0'-Z_0' -(b_c+\lambda g_c)e^{-\lambda}Z_3' + (\lambda g_c+b_c-\alpha)PF' \quad (2\text{-}9a)$$

$$\frac{dZ_1'}{dt'} = -q'+Z_0'-Z_1'-g_c e^{-\lambda}Z_3' + g_c PF' \quad (2\text{-}9b)$$

$$\frac{dZ_2'}{dt'} = -q'+Z_1'-Z_2'-g_c e^{-\lambda}Z_3+ g_c PF' \quad (2\text{-}9c)$$

$$\frac{dZ_3'}{dt'} = -q'+Z_2'-(1+g_c e^{-\lambda})Z_3' + g_c PF' \quad (2\text{-}9d)$$

$$\frac{dF'}{dt'} = -F' + h' \quad (2\text{-}9e)$$

Eq. (2-9) is the system equation linearized about the steady state value for a continuous crystallizer with a point fines trap. Its dynamic behavior depends on the several dimensionless parameters; these are

growth rate sensitivity g_c, nucleation sensitivity b_c and the parameter for the fines trap λ.

Eq. (2-9) can be written in a more compact matrix form by letting

$$X = (Z_0', \ Z_1', \ Z_2', \ Z_3', \ F')^T \quad = \text{state variable vector}$$

$$U = (q_0', \ q')^T \quad = \text{control variable vector}$$

$$V = h' \quad = \text{input}$$

Then, Eq. (2-9) becomes

$$\dot{X} = AX + BU + DV \tag{2-10}$$

where

$$A = \begin{bmatrix} -1 & 0 & 0 & -(b_c + \lambda g_c)\, e^{-\lambda} & (\lambda g_c + b_c - \alpha)P \\ 1 & -1 & 0 & -g_c\, e^{-\lambda} & g_c P \\ 0 & 1 & -1 & -g_c\, e^{-\lambda} & g_c P \\ 0 & 0 & 1 & -(1+g_c e^{-\lambda}) & g_c P \\ 0 & 0 & 0 & 0 & -1 \end{bmatrix} \tag{2-11a}$$

$$B = \begin{bmatrix} -\lambda & -1 \\ 0 & -1 \\ 0 & -1 \\ 0 & -1 \\ 0 & 0 \end{bmatrix} \tag{2-11b}$$

$$D = \begin{bmatrix} 0 \\ 0 \\ 0 \\ 0 \\ 1 \end{bmatrix} \qquad (2\text{-}11c)$$

From state space analysis, V represents the forcing function, U represents the manipulated variable. The matrix A represents the state space matrix, and X represents the state variable vector.

(B) Secondary Nucleation Model

In the previous section, a system model of an MSMPR crystallizer with a point fines trap for the homogeneous nucleation was developed. Usually, crystal nucleation in homogeneous solutions requires a much higher degree of supersaturation than that required for solutions containing a suspended crystalline phase. The heterogeneous, crystalline phase apparently has an autocatalytic effect upon the formation of incipient crystals.

Recent studies of continuous mixed-suspension crystallizers provide growing evidence that the secondary rather than homogeneous nucleation is the dominant source of nuclei. In continuous mixed suspension crystallizers, the secondary nucleation rate normally depends on the leading moments of the crystal distribution. The homogeneous nucleation model of Miers can be extended to secondary nucleation by taking this into account. All possible rate models must include

supersaturation as a variable because of its role as the fundamental mass transfer driving force. Thus, the secondary nucleation model can be mass dependent, area dependent, length dependent, and number dependent mechanism.

Although we can propose mass dependent, length dependent, area dependent, and number dependent secondary nucleation model as we can find in the literature, the research to date is not capable of distinguish between these mechanisms. All are equally adequate (6) to fit the experimental data obtained from the continuous MSMPR crystallizer, so without other evidence we can not deduce the secondary nucleation mechanism. For this reason, here we choose a number dependent nucleation model for the calculation of secondary nucleation. All other models can be treated in a similar way.

The system of equations governing the dynamic behavior of an MSMPR crystallizer with a point fines trap with number dependent nucleation kinetics can be written in the following form.

(The notations and the assumptions are same as the homogeneous nucleation except the nucleation rate.)

$$V \frac{\partial f}{\partial t} + VG \frac{\partial f}{\partial r} = -qf, \quad r > 0 \tag{2-12a}$$

$$Gf = B(c,n)e^{-r_o/\theta_0 G}, \quad r = 0 \tag{2-12b}$$

$$V \frac{d\psi}{dt} = qC_i - q\psi \tag{2-12c}$$

where

$$n = \mu_0 = \int_0^\infty f dr \quad = \text{number of crystals per unit volume}$$

For secondary nucleation, the experimental data are obtained in the presence of solid crystals and the expression for nucleations are based on total slurry volume. For this reason, the boundary condition given in Eq. (2-12b), does not include ε.

Using the same techniques as in the homogeneous case, i.e. taking moment transformation of Eqs. (2-12a) and (2-12b); and linearizing the moment equations and Eq. (2-12c) the following dimensionless equations can be derived.

$$\frac{dZ_0'}{dt'} = -(1-b_n)Z_0' - (\lambda g_1+b_1)e^{-\lambda}Z_3' - q' - \lambda q_0' + (\lambda g_c + b_c-\alpha)\, PF' \qquad (2\text{-}13a)$$

$$\frac{dZ_1'}{dt'} = Z_0' + Z_1' - g_1 e^{-\lambda}Z_3' + q' + g_c PF' \qquad (2\text{-}13b)$$

$$\frac{dZ_2'}{dt'} = Z_1' - Z_2' - g_1 e^{-\lambda}Z_3' - q' + g_c PF' \qquad (2\text{-}13c)$$

$$\frac{dZ_3'}{dt'} = Z_2' - (1+g_1 e^{-\lambda})\, Z_3' + g_c PF' - q' \qquad (2\text{-}13d)$$

$$\frac{dF'}{dt'} = h' - F' \qquad (2\text{-}13e)$$

where:

$$b_n = \frac{\mu_0^*}{B^*}\frac{\partial B}{\partial \mu_0}$$

$$g_1 = g_c/\varepsilon^*$$

$$b_1 = \frac{b_c - \alpha}{\varepsilon^*}$$

All other parameters are defined in the same way as in the homogeneous nucleation case.

And also Eq. (2-13) can be put into the matrix form as $\dot{X} = AX + BU + DV$ and each matrix can be defined as follows:

$$A = \begin{bmatrix} -(1-b_n) & 0 & 0 & -(\lambda g_1+b_1)e^{-\lambda} & (\lambda g_1+b_1)P\varepsilon^* \\ 1 & -1 & 0 & -g_1 e^{-\lambda} & g_1 P\varepsilon^* \\ 0 & 1 & -1 & -g_1 e^{-\lambda} & g_1 P\varepsilon^* \\ 0 & 0 & 1 & -(1+g_1 e^{-\lambda}) & g_1 P\varepsilon^* \\ 0 & 0 & 0 & 0 & -1 \end{bmatrix} \qquad (2\text{-}14a)$$

$$B = \begin{bmatrix} -\lambda & -1 \\ 0 & -1 \\ 0 & -1 \\ 0 & -1 \\ 0 & 0 \end{bmatrix} \qquad (2\text{-}14b)$$

$$D = \begin{bmatrix} 0 \\ 0 \\ 0 \\ 0 \\ 1 \end{bmatrix} \qquad (2\text{-}14c)$$

$$X = [\, Z_0', \; Z_1', \; Z_2', \; Z_3', \; F' \,]^T$$

$$U = [\, q_0', \; q' \,]^T$$

$$V = h'$$

CHAPTER III. STABILITY ANALYSIS

The linearized model can be used to study the dynamics and stability of the system only in localized regions around the operating point where linearization had been performed. None the less, it is often sufficient to look at such small areas while analyzing the system's stability because in many cases the linearized model provides a reasonably good approximation of the non-linear behavior. Further, in the neighborhood of a steady state for a non-linear system, the stability characteristics of the solution are the same as those for the linearized model. All inherent stability criteria are based on the concept of exponential asymptotic stability; in the time domain this translates into the requirement that all the real part of the eigenvalues of the state matrix be negative, if more than one eigenvalue has a real part which is positive, the system will be inherently unstable and the linear solution will become infinite as the time goes on.

(A) Homogeneous Nucleation Model

The characteristic equation of system equation (2-10) is

$$|A - S\,I| = 0$$

then

$$S = -1 \qquad (3\text{-}1)$$

or

$$\begin{vmatrix} -1-S & 0 & 0 & -(b_c+g_c)e^{-\lambda} \\ 1 & -1-S & 0 & -g_c e^{-\lambda} \\ 0 & 1 & -1-S & -g_c e^{-\lambda} \\ 0 & 0 & -1 & -(1+g_c e^{-\lambda})-S \end{vmatrix} = 0 \qquad (3\text{-}2)$$

Since only the stability of the system is of interest then $S \neq -1$, and from Eq. (3-2) the following characteristic equation can be found.

$$S^4 + (4+g_c e^{-\lambda})S^3 + (6+4g_c e^{-\lambda})S^2$$

$$+ (4+6g_c e^{-\lambda})S + [1+3g_c e^{-\lambda}+(b_c+\lambda g_c)e^{-\lambda}] = 0 \qquad (3\text{-}3)$$

This is the same characteristic equation obtained by Lei et al. (19) by using spectral analysis.

By the Routh test, the following relationship is found for the linear stable region:

$$\text{(i)} \quad \frac{b_c}{g_c} < -\lambda + \frac{21+87\frac{e^{\lambda}}{g_c} + 128\frac{e^{2\lambda}}{g_c^2} + 64\frac{e^{3\lambda}}{g_c^3}}{\left(1 + \frac{4e^{\lambda}}{g_c}\right)^2} \qquad (3\text{-}4a)$$

$$\text{(ii)} \quad \text{If } g_c \to \infty \ , \ b_c/g_c \to 21 - \lambda \qquad (3\text{-}4b)$$

If $\lambda = 0$ the crystallizer has no fines trap, and then $b_c/g_c \to 21$. This is the well-known MSMPR stability limit obtained by Sherwin et al. (35), and Randolph and Larson (29).

(iii) If the system is in the unstable region, two roots (eigenvalues) will have pssitive real parts.

The stability condition described by Eq. (3-3) is shown graphically in Fig. 3-1.

The result of Eq. (3-4), where b_c is termed the nucleation sensitivity parameter and g_c termed the sensitivity growth rate parameter, means that the asymptotic behavior of MSMPR crystallizer with a fines trap when the homogeneous kinetic order is less than $(21 - \lambda)$, will be linearly stable. Therefore, if $b_c/g_c > 21 - \lambda$ the system will become unstable, so the larger we take λ (the more fines we destroy), the smaller we must take b_c/g_c to ensure stable operation. If we destroy more fines we destabilize the system. It is helpful to keep in mind that the stable regions represent the parametric combinations which give a set of eigenvalues with exclusively negative real parts, while the unstable regions are representation of some eigenvalues with positive real parts.

(B) Secondary Nucleation Model

From Eq. (2-14a), the characteristic equation of the secondary nucleation system will be

$$S^4 + (4+g_1e^{-\lambda}-b_n)S^3 + (6+4g_1e^{-\lambda}-3b_n-g_1b_ne^{-\lambda})S^2$$

$$+ (4+6g_1e^{-\lambda}-3b_n-3g_1e^{-\lambda}b_n)S$$

$$+ (3g_1e^{-\lambda}+1+\lambda g_1e^{-\lambda}-b_n-3b_ng_1e^{-\lambda}+b_1e^{-\lambda}) = 0 \qquad (3\text{-}5)$$

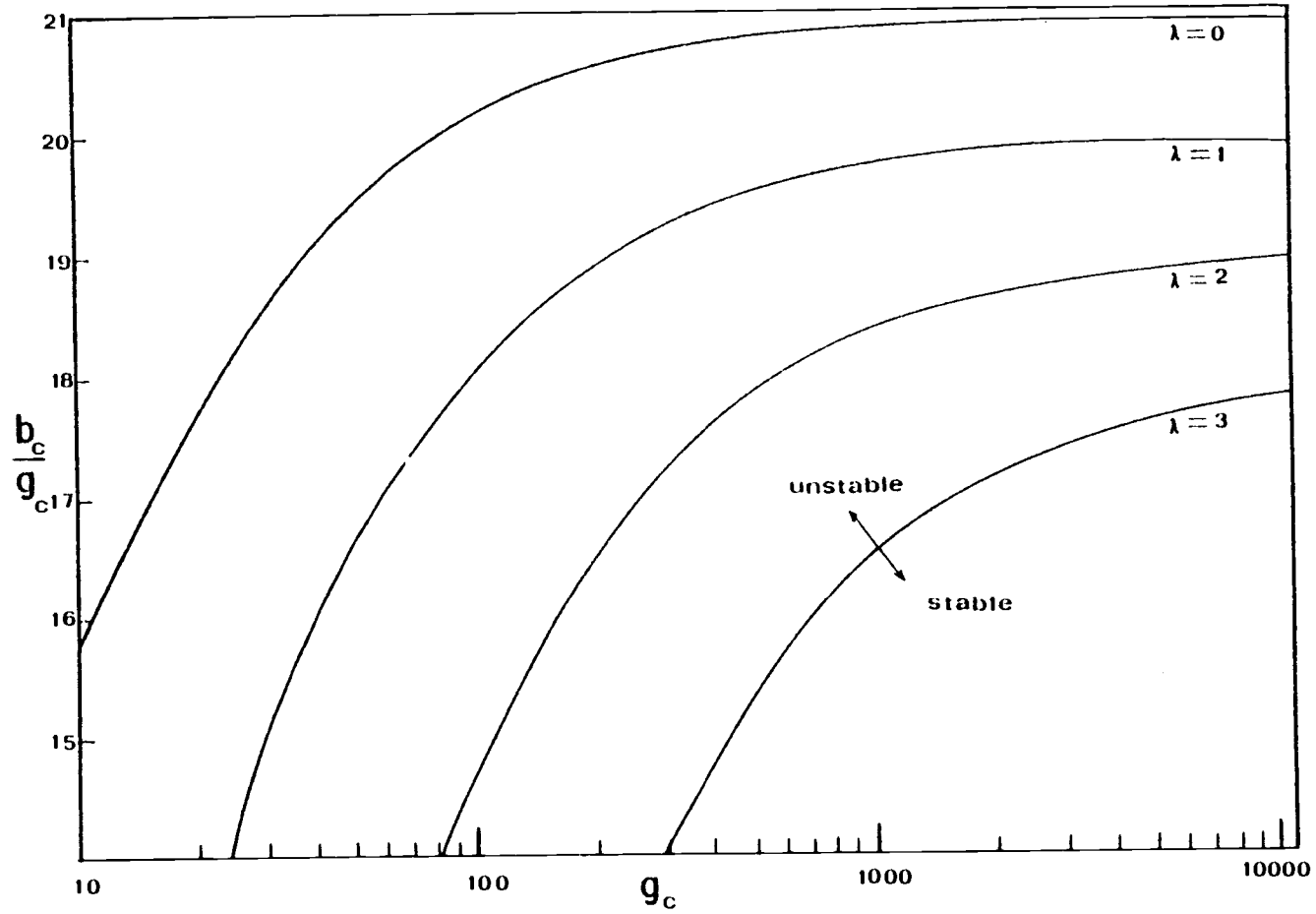

Fig.3-1. Stability curves for a crystallizer with a point fines trap.

By the Routh test, the following conditions should be satisfied for linear stability:

$$4 + g_1 e^{-\lambda} - b_n > 0 \tag{3-6a}$$

$$3g_1 e^{-\lambda} + 1 + \lambda g_1 e^{-\lambda} + b_1 e^{-\lambda} - b_n - 3\, b_n g_1 e^{-\lambda} > 0 \tag{3-6b}$$

$$(4+g_1 e^{-\lambda}-b_n)(6+4g_1 e^{-\lambda}- 3b_n - g_1 b_n e^{-\lambda})$$
$$- (4 + 6g_1 e^{-\lambda} - 3b_n - 3g_1 e^{-\lambda} b_n) > 0 \tag{3-6c}$$

$$(4 + 6g_1 e^{-\lambda}- 3b_n - 3g_1 e^{-\lambda} b_n) \{(4 + g_1 e^{-\lambda}- b_n)$$
$$\times (6 + 4g_1 e^{-\lambda}- 3b_n - g_1 b_n e^{-\lambda}) - (4 + 6g_1 e^{-\lambda}$$
$$- 3b_n - 3g_1 e^{-\lambda} b_n)\} - (4 + g_1 e^{-\lambda}-b_n)^2 (3g_1 e^{-\lambda}+ 1$$
$$+ \lambda g_1 e^{-\lambda}+ b_1 e^{-\lambda}- b_n - 3b_n g_1 e^{-\lambda}) > 0 \tag{3-6d}$$

In Appendix A the above set of equations are simplified and the stability region will be as follows:

$$b_n + 3b_n g_1 e^{-\lambda}- 3\, g_1 e^{-\lambda}- 1 - \lambda g_1 e^{-\lambda} < b_1 e^{-\lambda}$$
$$< \{(g_1 e^{-\lambda})^3 (21-15b_n + 3b_n{}^2 - \lambda) + (g_1 e^{-\lambda})^2$$
$$(87-81b_n -8\lambda b_n +27b_n{}^2 - 3b_n{}^3) + (g_1 e^{-\lambda})$$

$$(128 - 148b_n + 8\lambda b_n - 16\lambda + 62b_n^2 - \lambda b_n^2 - 9b_n^3)$$

$$+ (64 - 96b_n + 48b_n^2 - 8b_n^3)\} \,/(4 + g_1 e^{-\lambda} - b_n)^2 \qquad (3\text{-}7a)$$

$$g_1 e^{-\lambda} > -\frac{3b_n - 4}{3b_n - 6}, \quad b_n < 2 \qquad (3\text{-}7b)$$

If $\lambda = 0$, i.e. the MSMPR crystallizer has no fines trap, the above relations reduce to the results obtained by Liss and Shinnar (20). These results are plotted on $b_1 e^{-\lambda}$ vs $g_1 e^{-\lambda}$ in Fig. 3-2 for using parameter b_n. Unlike to the homogeneous nucleation model, the direct relationship between the fines destruction rate and stable region can not be found. In Fig. 3-3, the minimum stable value of $g_1 e^{-\lambda}$ is plotted as a function of b_n. If $b_n = 2$ the disturbance tends to autoaccelerate itself explosively. It is also interesting to consider the asymptotic behavior of the stability criteria of Eq. (3-7). In Fig. 3-4 the values of b_1/g_1 (or $b_1 e^{-\lambda}/g_1 e^{-\lambda}$) at the critical stability limits are plotted as a function of b_n. From these plots, we find that the stable region is rather narrow, which means that the secondary nucleation is less stable comparing to the homogeneous nucleation.

The number of eigenvalues which have a positive real part when the system is an unstable region is rather complicated to compute but in normal operating region ($b_n < 2$, and $g_1 > 0$), only two eigenvalues have a positive real part. This fact is good for control (as will be shown later).

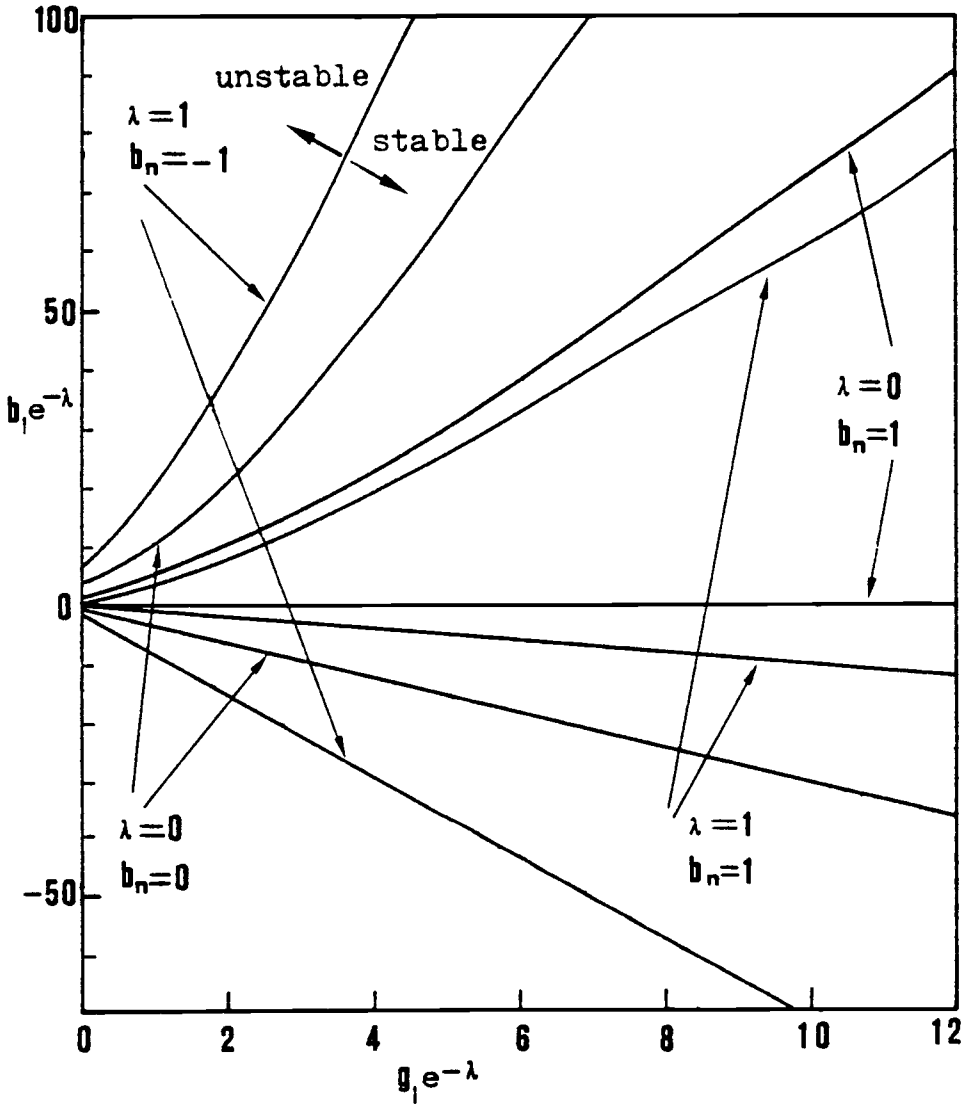

Fig.3-2. Stability curves of a secondary nucleation model for a crystallizer with a point fines trap.

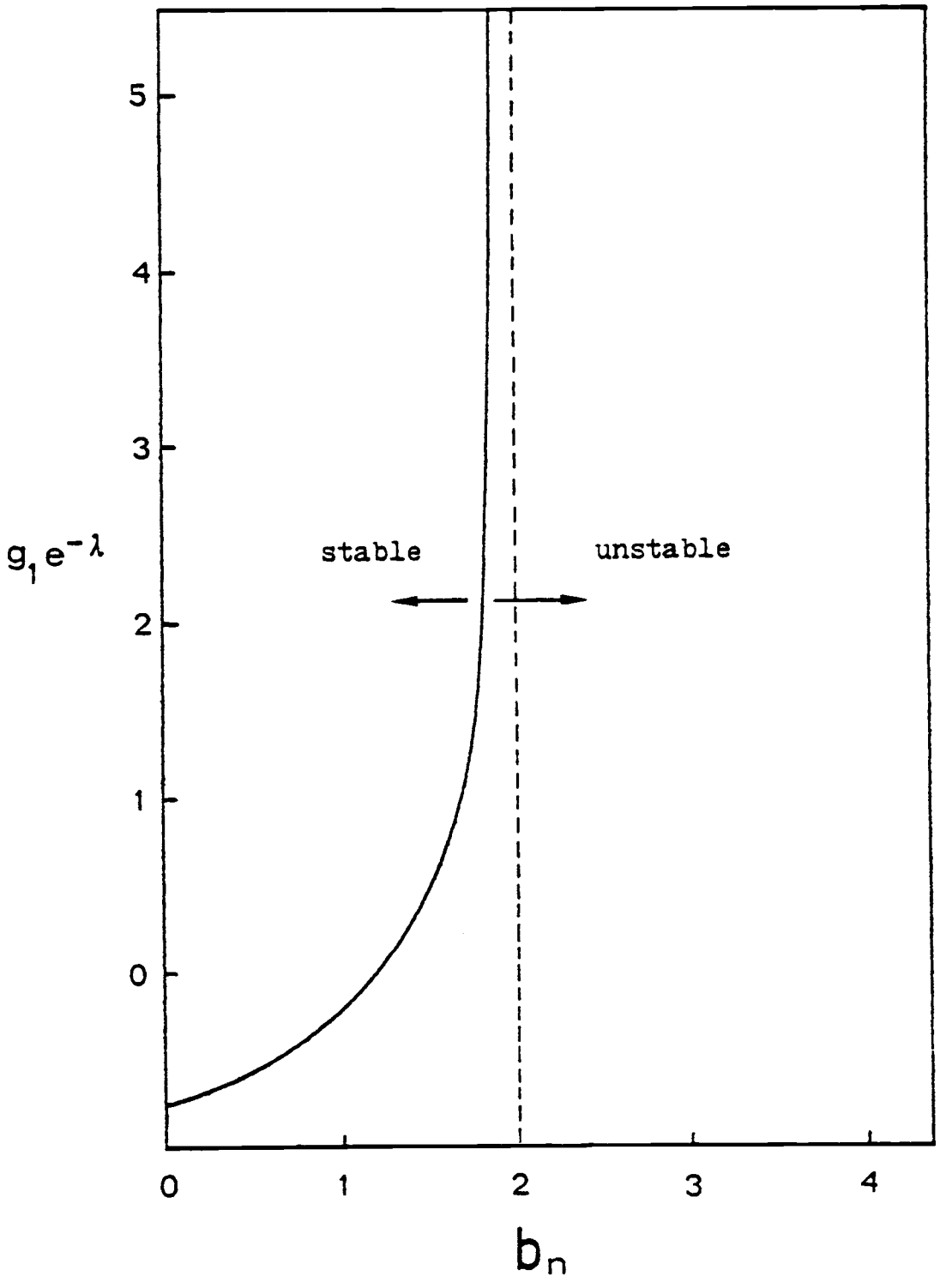

Fig.3-3. Stability limit of b_n for number dependent model for a crystallizer with a point fines trap.

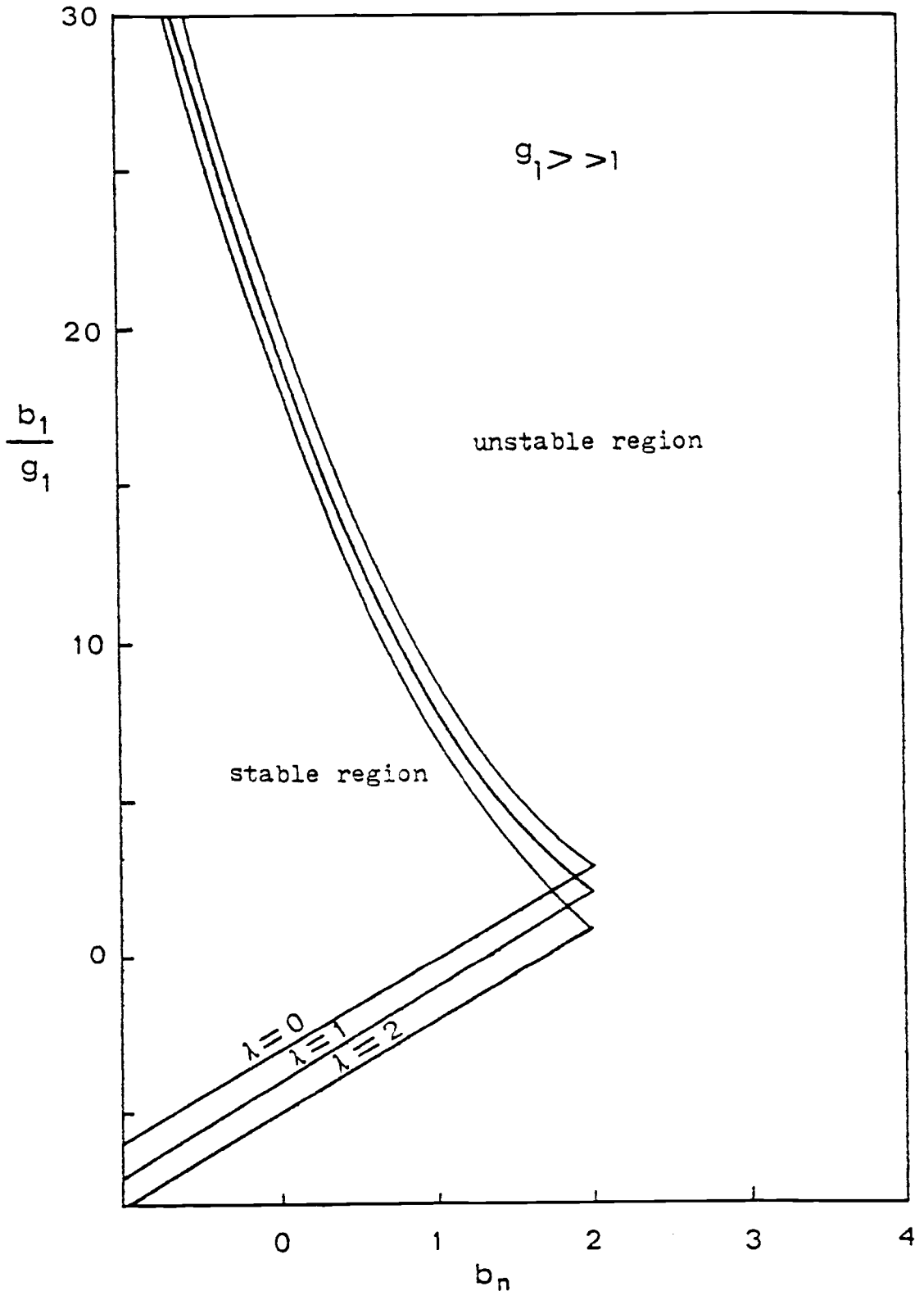

Fig.3-4. Asymptotic stability limit of number dependent nucleation model for a crystallizer with a point fines trap.

CHAPTER IV. MODAL CONTROL OF CONTINUOUS MSMPR CRYSTALLIZERS

In the conventional feedback control system, the manipulated variables are based upon the change of a deviation occurs in our measuring state variable. The traditional approach is inappropriate for many problems of process control for the following reasons:

1. It conceals the behavior of many variables which may in fact have to be considered.

2. It offers no direct assistance in choosing the particular variables as manipulated or controlled variables.

3. It does not show how these variables are to be chosen so as to avoid interaction.

Modal design of multivariable system control was first proposed by Rosenbrock (32), who consider the case when both matrix B and C in the system equations

$$\dot{X} = AX + BU + DV$$

$$U = - CX$$

could be chosen.

Takahashi et al. (37) extended this idea to the more general non-ideal system when B and C could not be freely chosen. Based on their idea our approach is to change the first r-largest eigenvalues of the system (if there are r manipulated variables).

Ellis and White (42), Mayne and Murdoch (21), Crossley (5) extended modal control to a single-input control system. Based on these ideas we change more than one eigenvalue even if there was only one manipulated variable.

The details and techniques of modal control can be found in the above sources and we will not repeat them here. Here we use the modal control algorithm by Takahashi et al. for multiple input control, and use Mayne and Murdoch's algorithm for the single input control.

For a continuous MSMPR crystallizer with a fines trap whose dynamic equations are described above, the input variables are input concentration C_i, feed flow rate q and fines recirculation rate q_0; the output variables are number of particles $\mu_0(t)$, particle size $\mu_1(t)$, surface area $\mu_2(t)$, volume of magma $\mu_3(t)$, and the total mass of solute and crystals, $\psi(t)$. Alternately, the feed concentration can be assumed as an input disturbance or noise, with the feed rate and (or) fines recirculation rate as the manipulated variables. On the measurement of the state variables μ_0, μ_1, μ_2, μ_3, ψ the controller manipulates the feed flow rate and (or) fines recirculation rate to hold the deviation of output to zero. The schematic diagram of the control system is shown graphically in Fig. 4-1, and the block diagram is shown in Fig. 4-1a.

(A) Simulation Results and Discussions

Numerical simulations of the system's response to various input were performed on a Cyber 73 digital computer. The existing computer

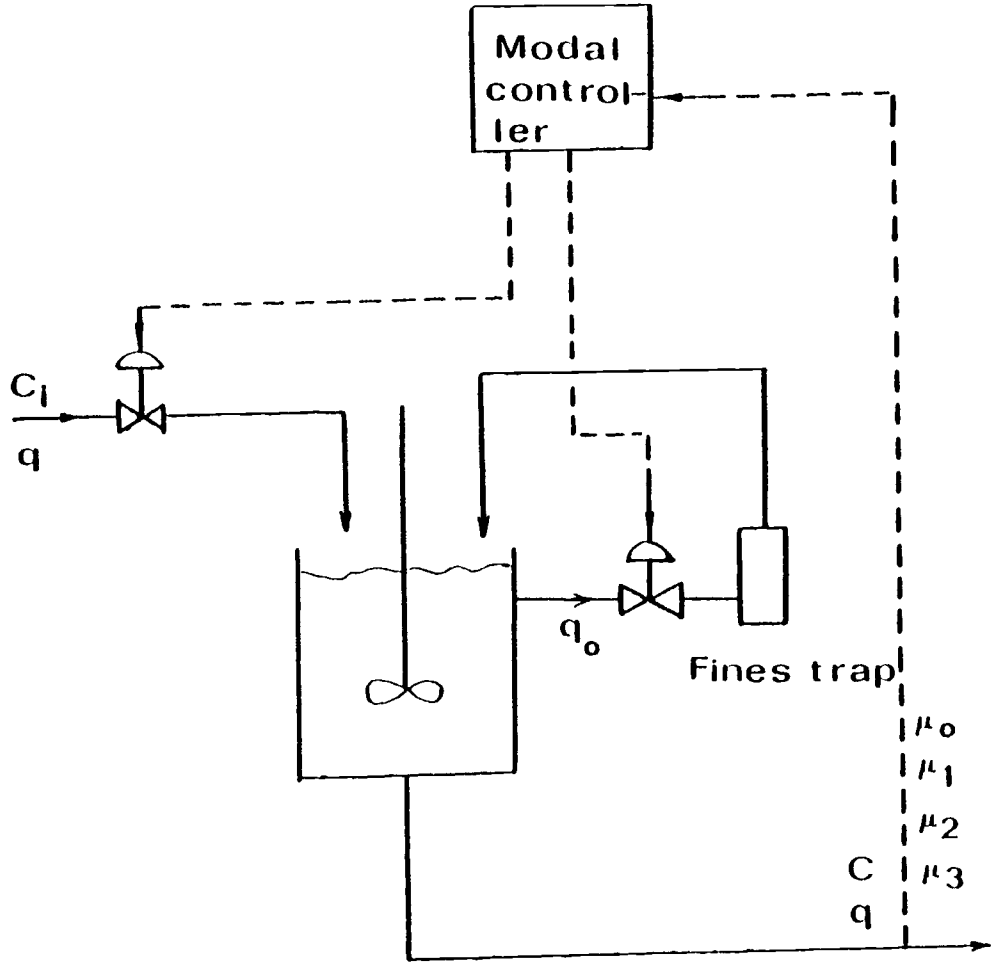

Fig.4-1. Schematic diagram of a modal controlled crystallizer with a point fines trap.

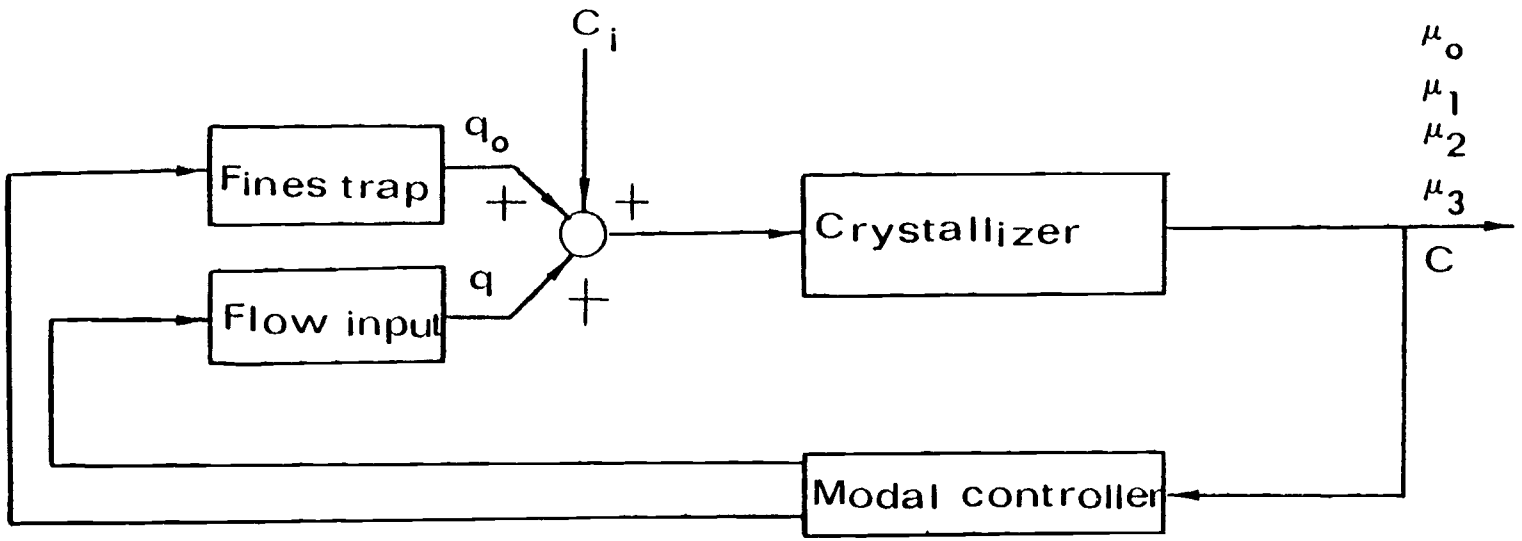

Fig. 4-1a. Block diagram of a modal controlled crystallizer with a point fines trap.

subroutines in IMSL package (International Mathematical and Statistical Library Package) were taken to compute the eigenvalues and eigenvectors of the real matrix, the inverse of the complex matrix, and to solve simultaneous non-linear differentail equations.

Non-linear Equations (2-8) and (2-12) were made dimensionless (in Appendix B) along with appropriate initial pertubations, and were solved numerically by computer. The parameters were calculated from steady state values and were shown in Table 4-1.

Figure 4-2 to 4-5 show the dynamic response of the homogeneous nucleation system. The values are normalized (with respect to the steady state value) and represent number, total length, total surface area, total mass, and total solute concentration, with reduced time corresponding to the step change of input feed concentration. It is found that both the linearized model and non-linear model predict the transient behavior of MSMPR crystallizer with a fines trap very closely. Figures 4-2 to 4-5 also demonstrate the dynamic behavior of the system which is inherently stable, as was predicted by linear stability analysis. From these figures we find an oscillatory behavior with high frequencies and very slow decay. It is also seen that after the initial disturbance, although the total solute resource function F settles to a new steady state value, four leading moments are still in oscillatory behavior and do not settle to the new steady state value. This kind of oscillatory behavior may last up to twenty four hours or more in an industrial system (24).

The oscillatory behavior of the process is due to competition between the nucleation and the growth rates. A small increase in

Table 4-1. Parameters for Simulation

Item \ Case	I	II	III	IV
Model	Homogeneous		Secondary	
Parameters g_c	50	30		
Parameters g_1			50	50
Parameters b_c	750	480		
Parameters b_1			350	750
Parameters b_n			1	1
Parameters λ	1	1	1	1
Parameters L	6	10	6	6
Stability	stable	unstable	stable	unstable

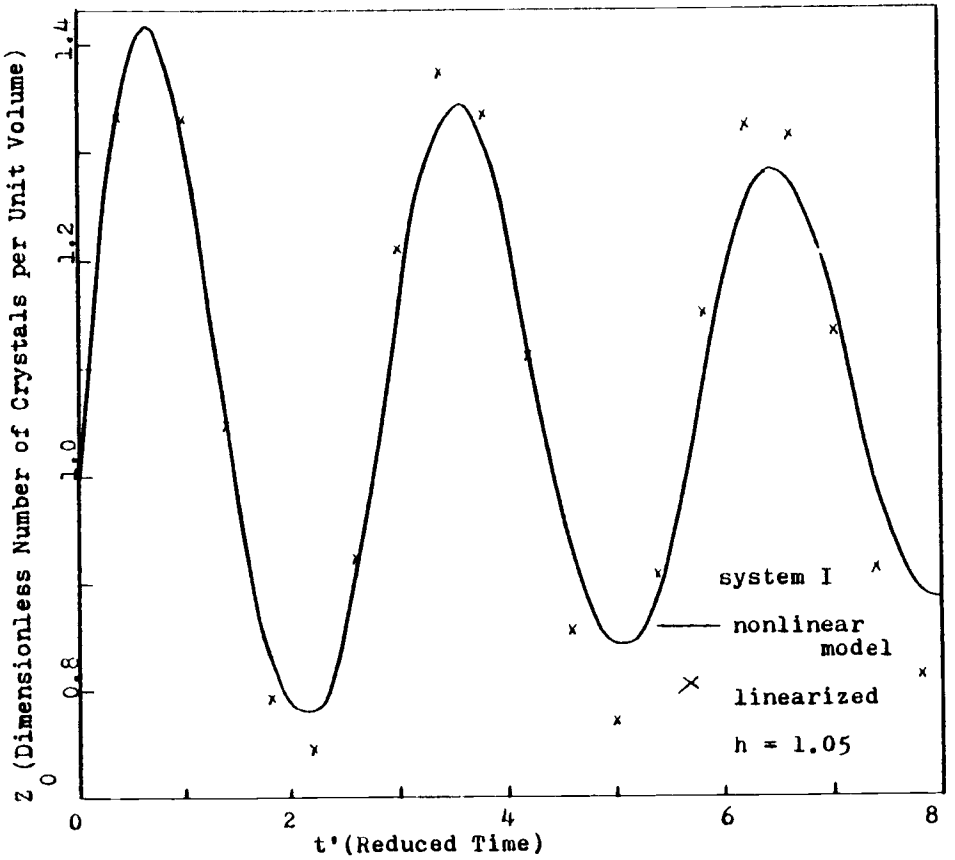

Fig.4-2. Open loop response of Z_0 of system I to input step change.

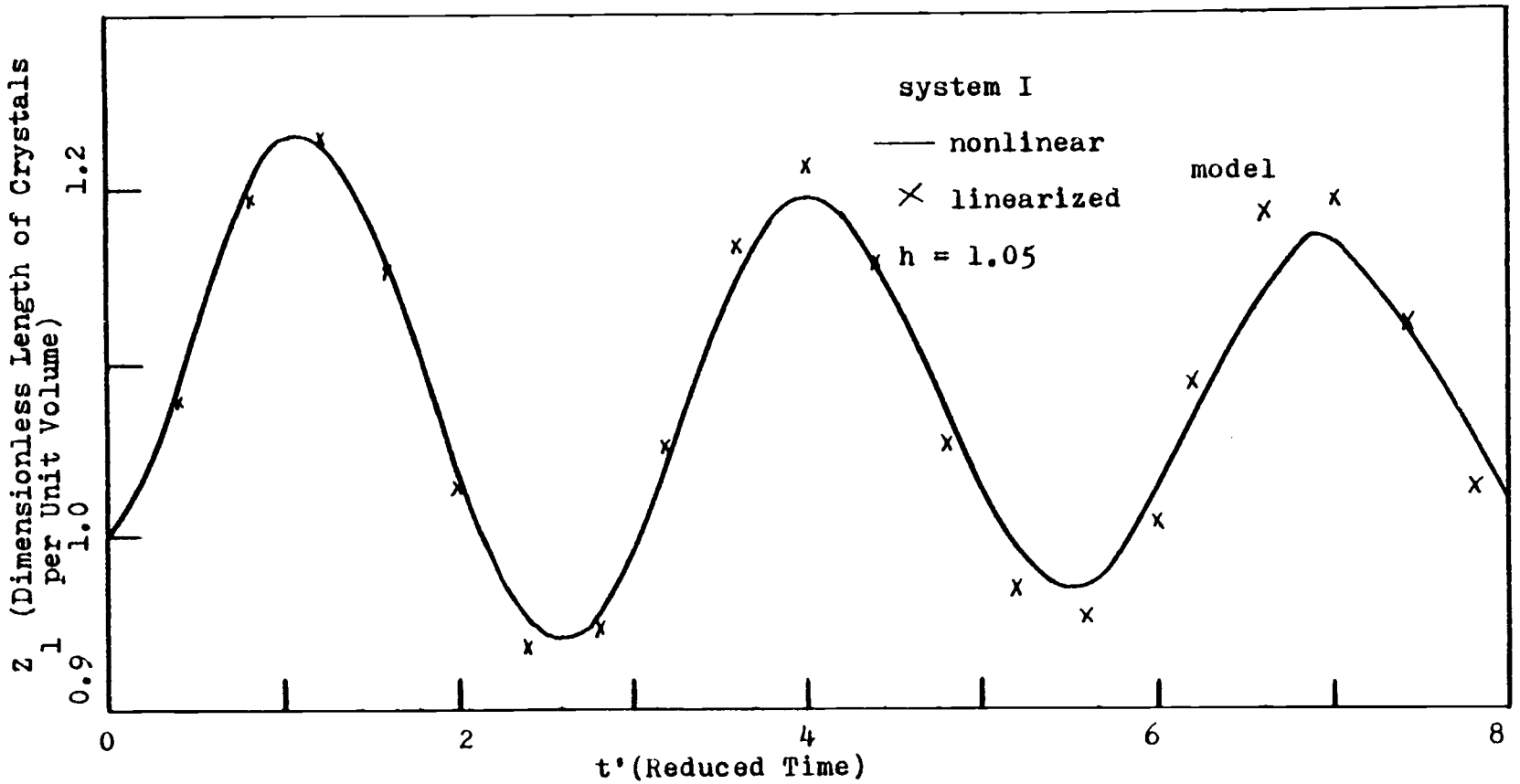

Fig.4-2a. Open loop response of Z_1 of system I to input step change.

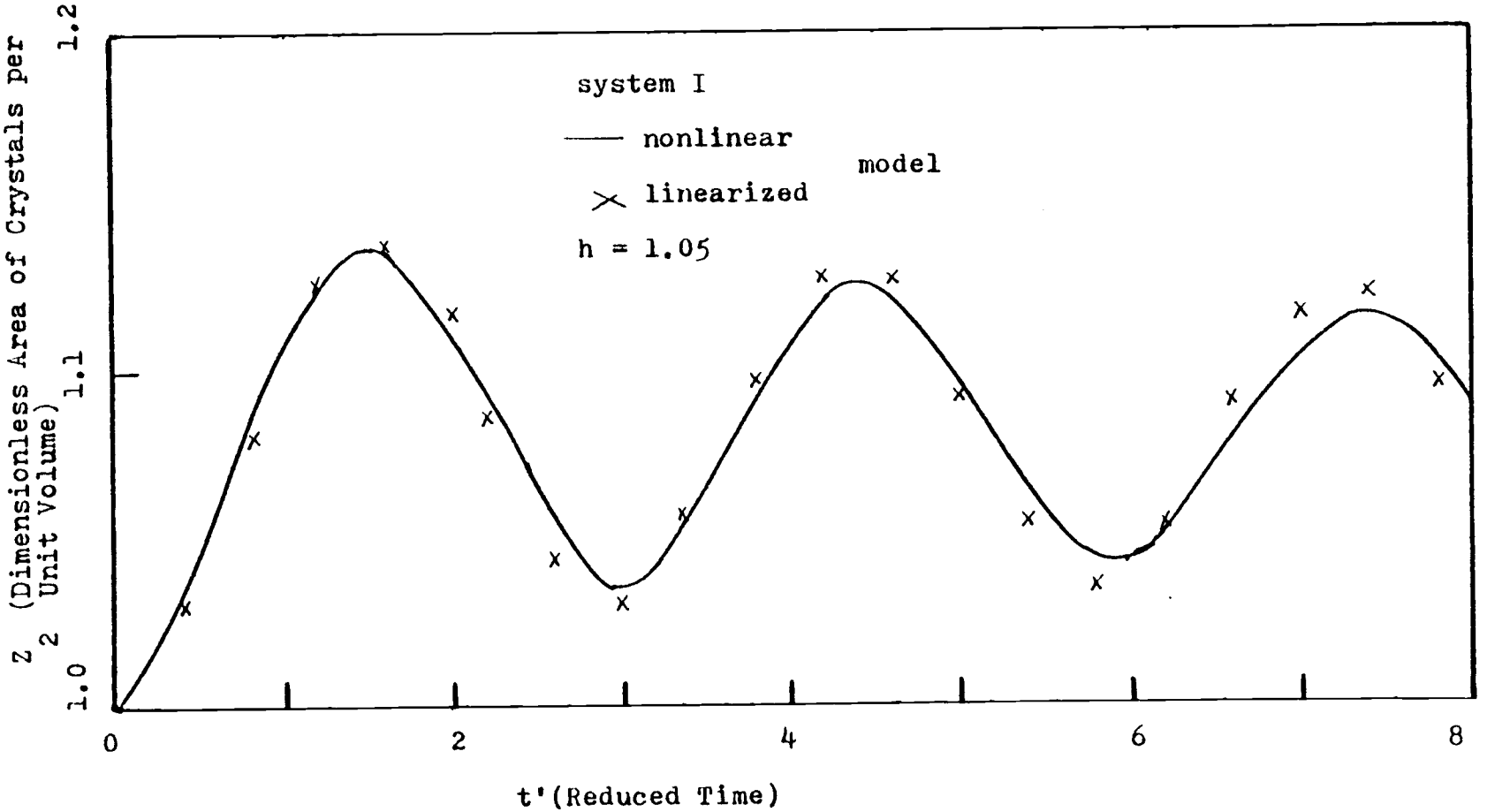

Fig.4-3. Open loop response of Z_2 of system I to input step change.

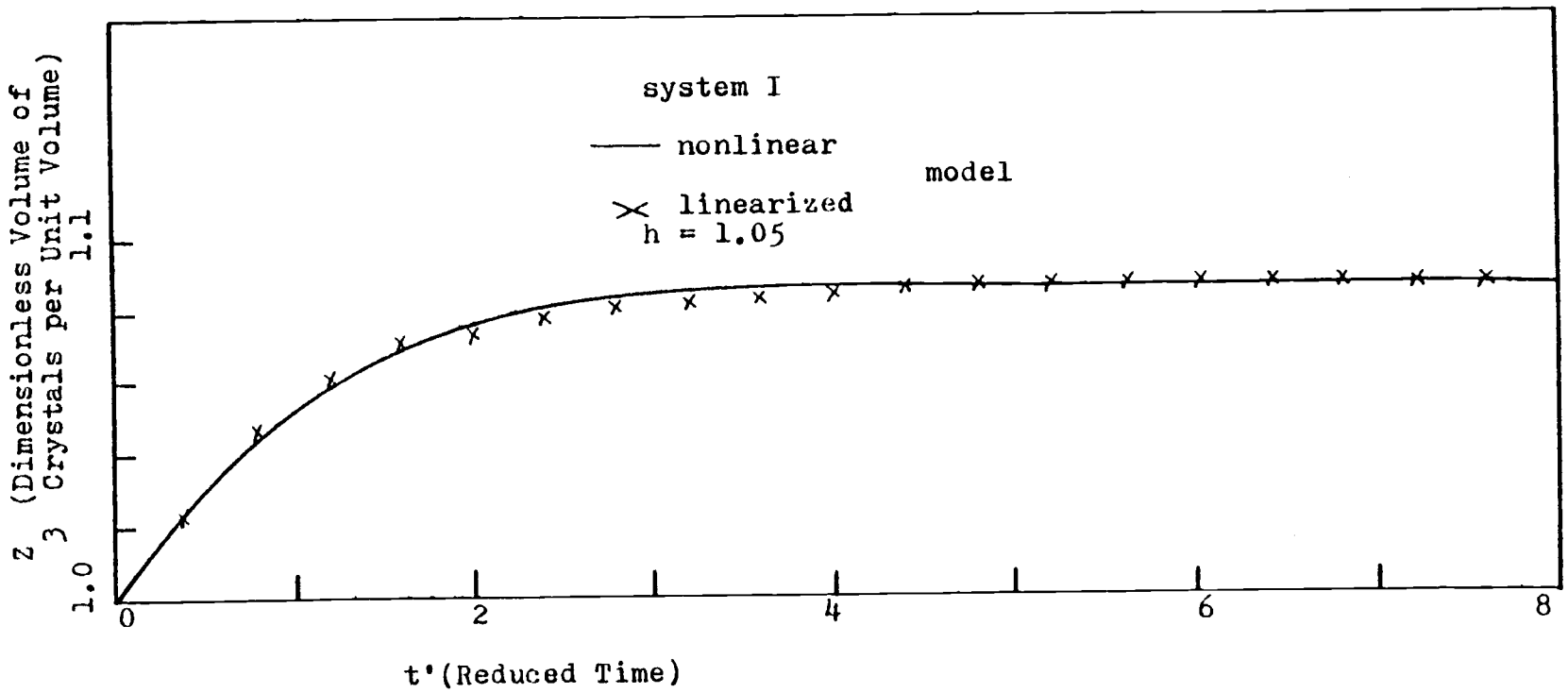

Fig.4-4. Open loop response of Z_3 of system I to input step change.

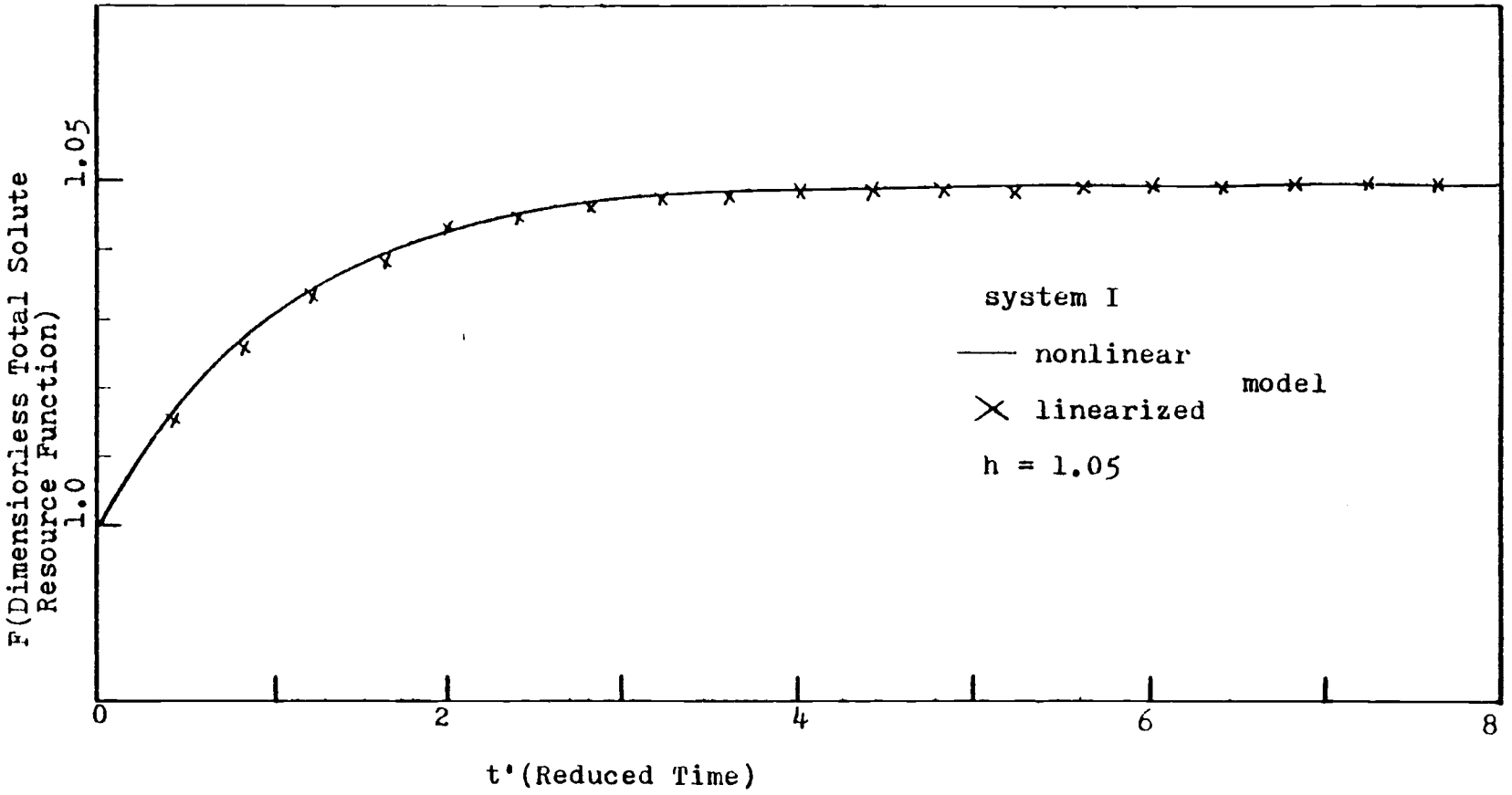

Fig.4-5. Open loop response of F of system I to input step change.

concentration causes a shower of nuclei to form, and when these nuclei grow, they supply such a large area for growth that the concentration decreases significantly. The decreasing concentration causes the nucleation rate to decrease until the removal of the crystals (and therefore area for growth) and the addition of more solute causes another shower of nuclei to occur. Thus the system generates the self-sustained oscillations.

Figures 4-6 to 4-10 show the transient response of secondary nucleation system, which is inherently unstable. Linear stability analysis predicts very successfully, that the leading moments Z_0, Z_1, Z_2, Z_3 exhibit a sustained oscillation, and the amplitude of oscillations increases and become bigger and bigger as the time elapses. The number of crystals most sensitively shows this effect.

Figures 4-11 and 4-14 show the effect on particle size of a step change in feed concentration: the number of crystals Z_0 increases as the inlet concentration increases; the effect is in the opposite direction if the input concentration step change is in the decreasing direction. Figures 4-12 and 4-15 show that the transient response to a step change of throughput flow rate is quite similar to the effect caused by inlet concentration. Increasing the input flow rate is similar to increasing the feed concentration. Figures 4-13 and 4-16 show that the transient response to a step change in fines destruction rate, is contrary to the above result. The reason is that increasing the fines destruction rate is quite similar to decreasing the feed concentration or feed flow rate. This is quite reasonable because increasing the

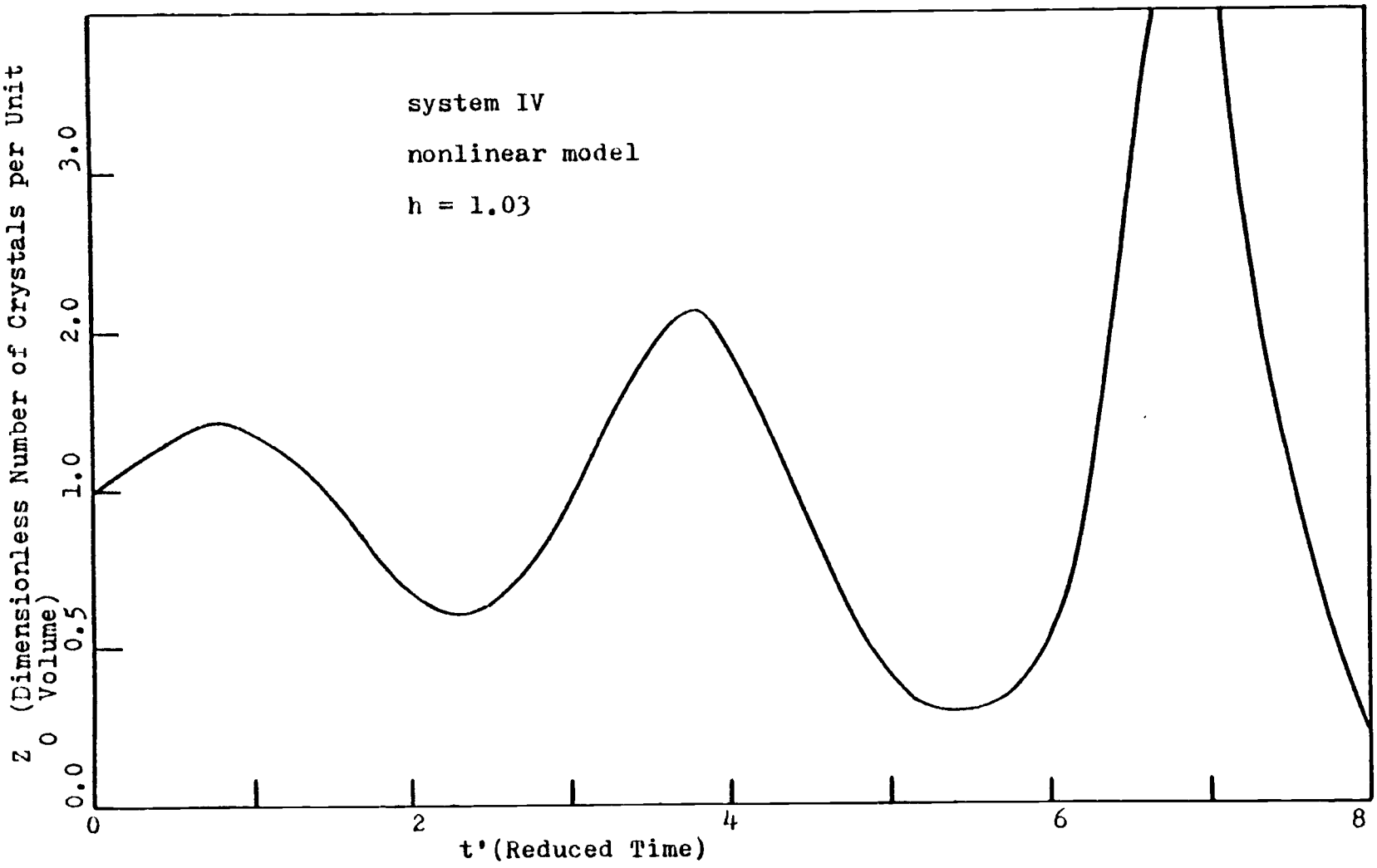

Fig.4-6. Open loop response of Z_0 of system IV to input step change.

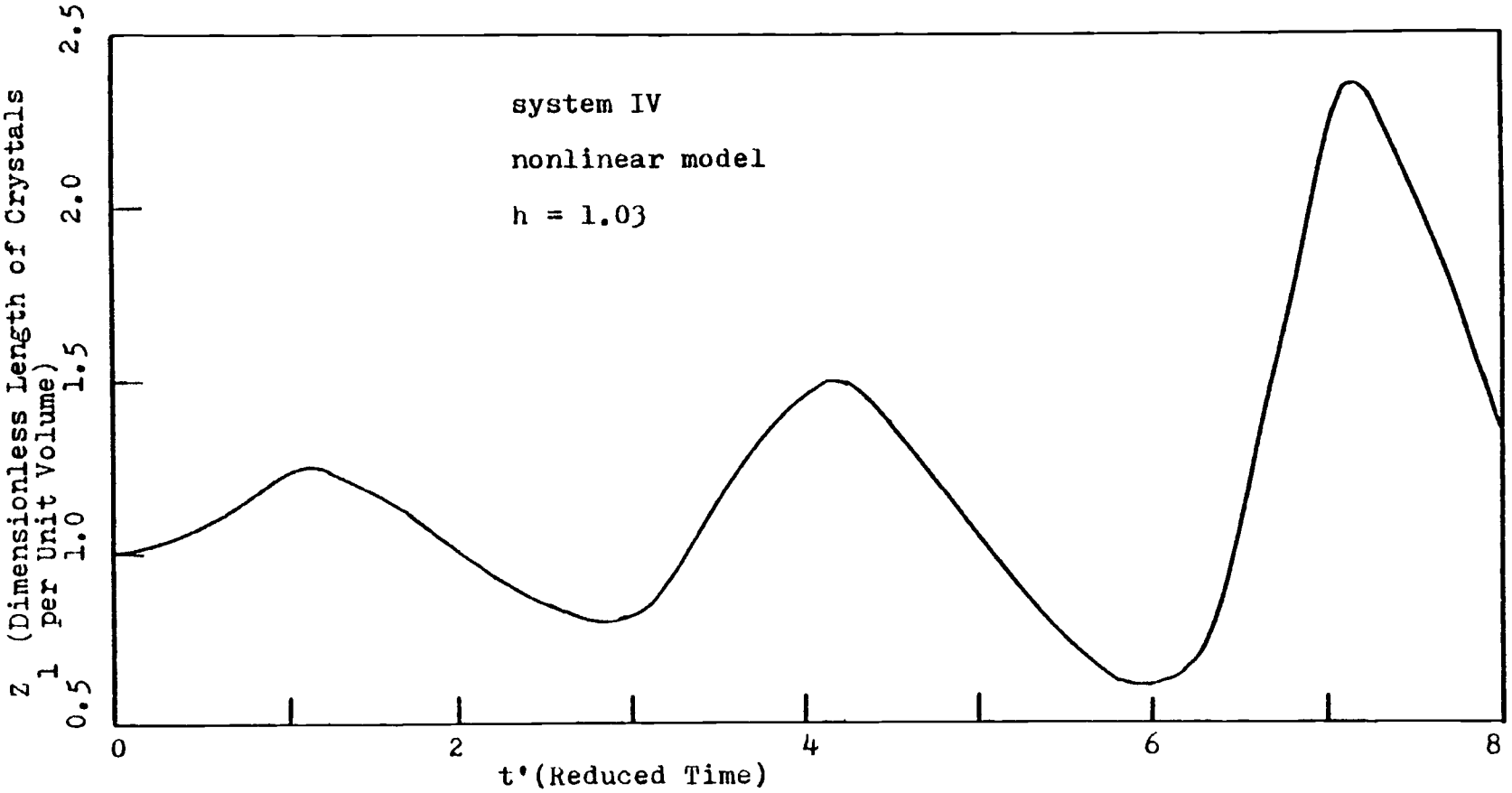

Fig.4-7. Open loop response of Z_1 of system IV to input step change.

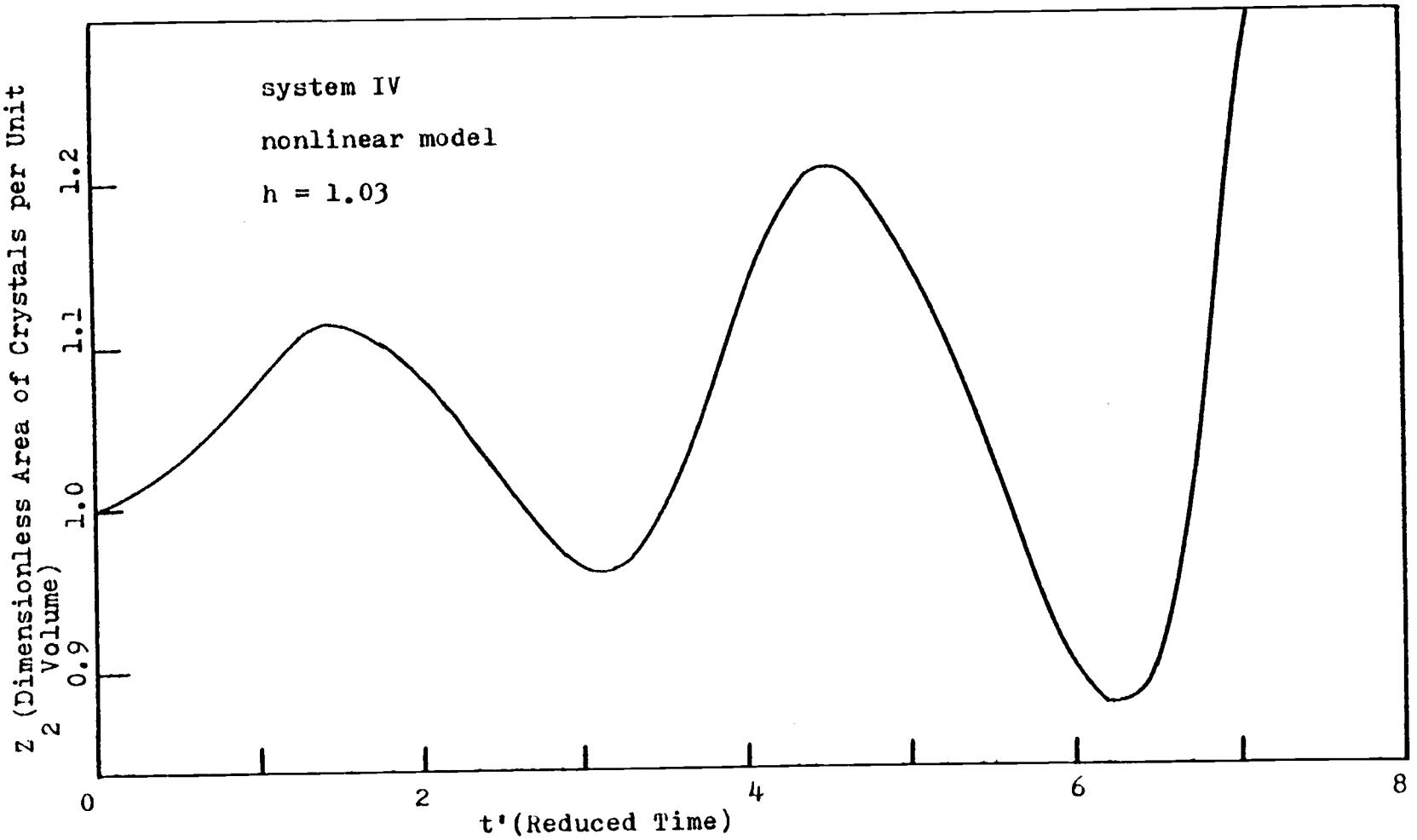

Fig.4-8. Open loop response of Z_2 of system IV to input step change.

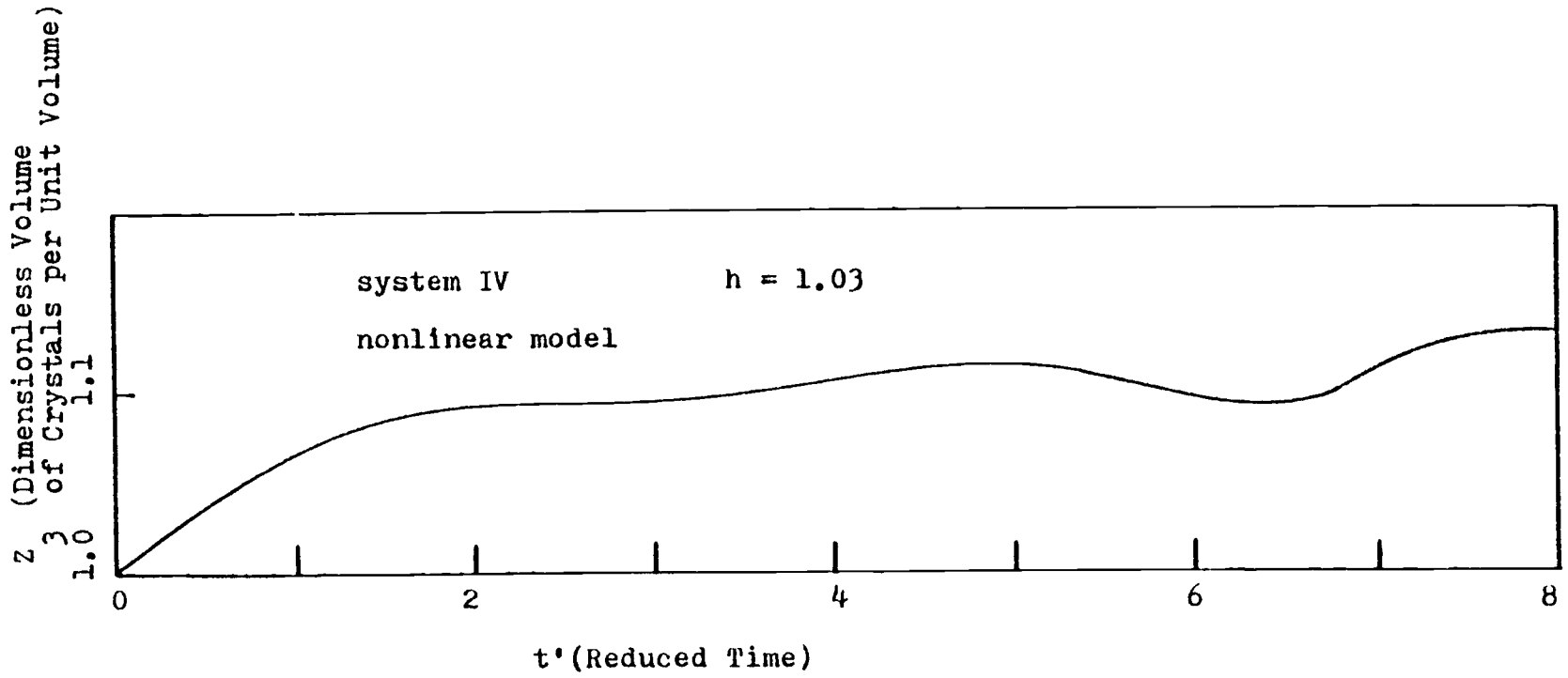

Fig.4-9. Open loop response of Z_3 of system IV to input step change.

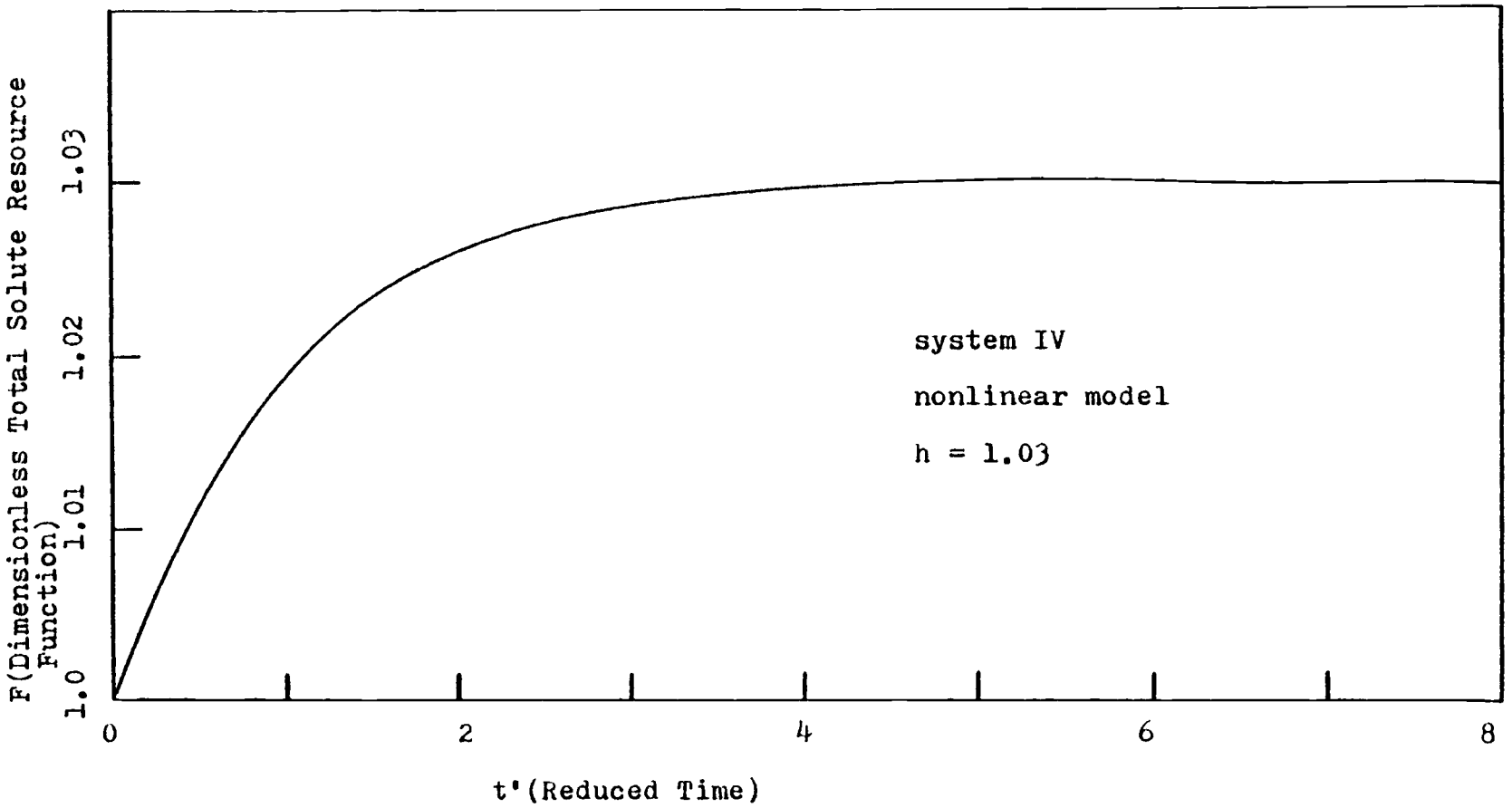

Fig.4-10. Open loop response of F of system IV to input step change.

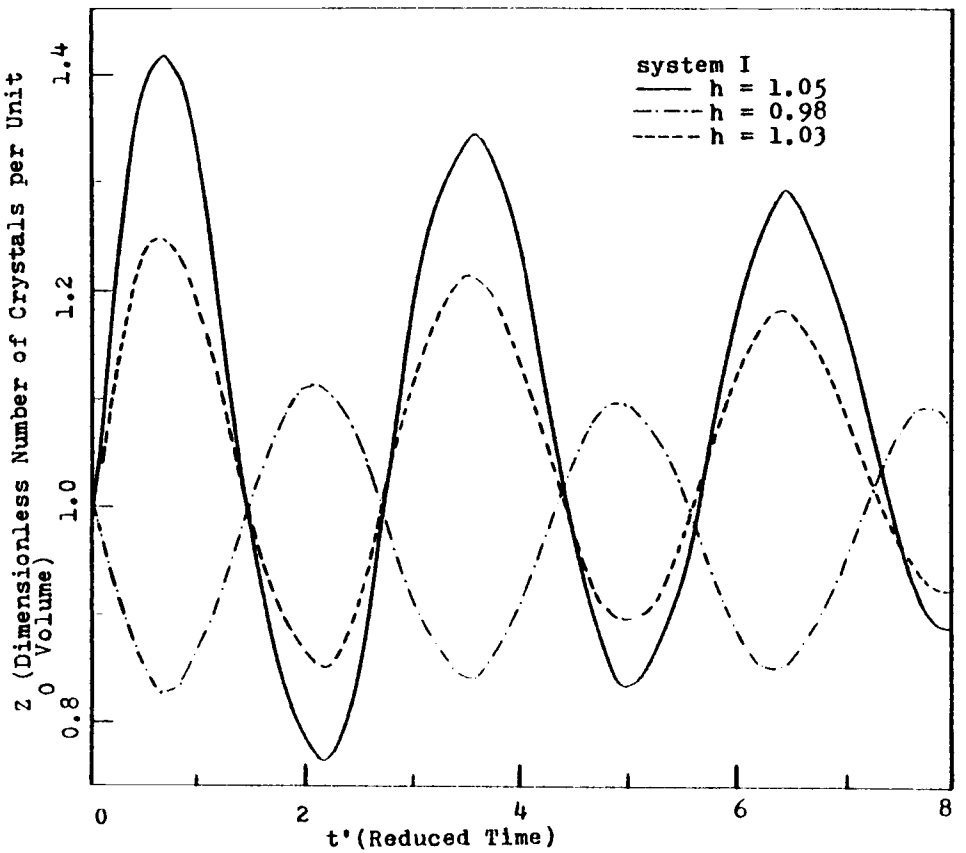

Fig.4-11. Effect of size of input step change on response of Z_0 of system I.

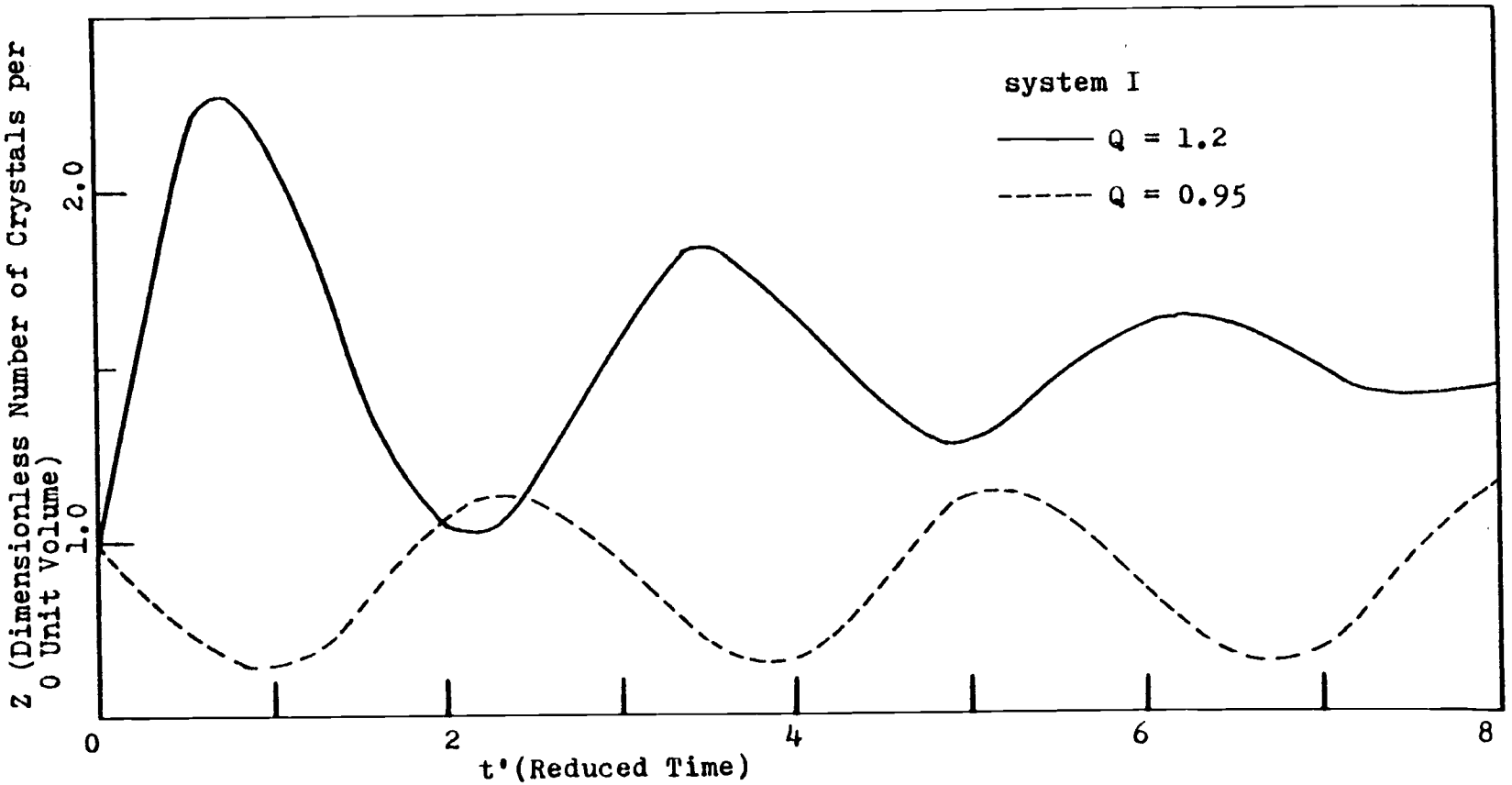

Fig.4-12. Effect of size of flow rate step change on response of Z_0 of system I.

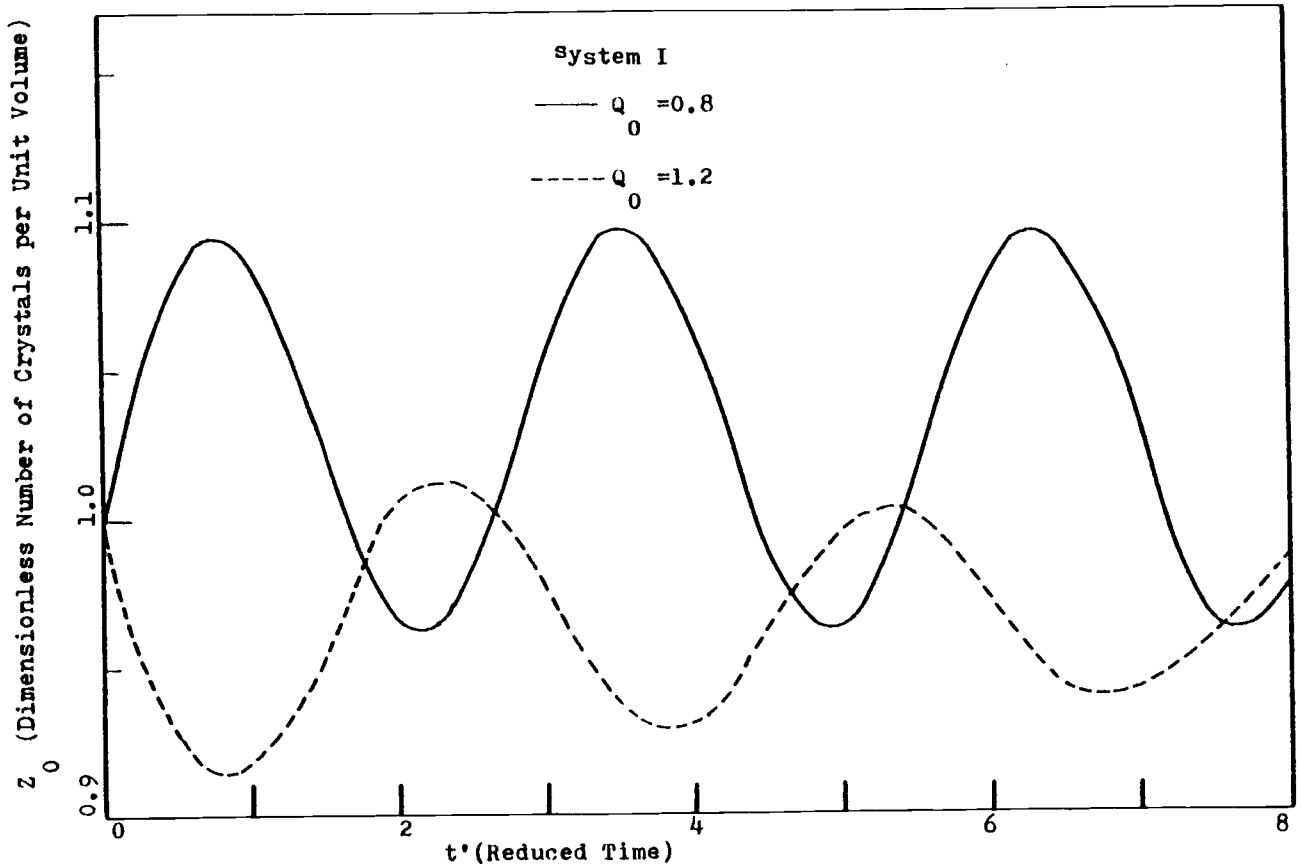

Fig.4-13. Effect of size of fines recirculation rate step change on response of Z_0 of system I.

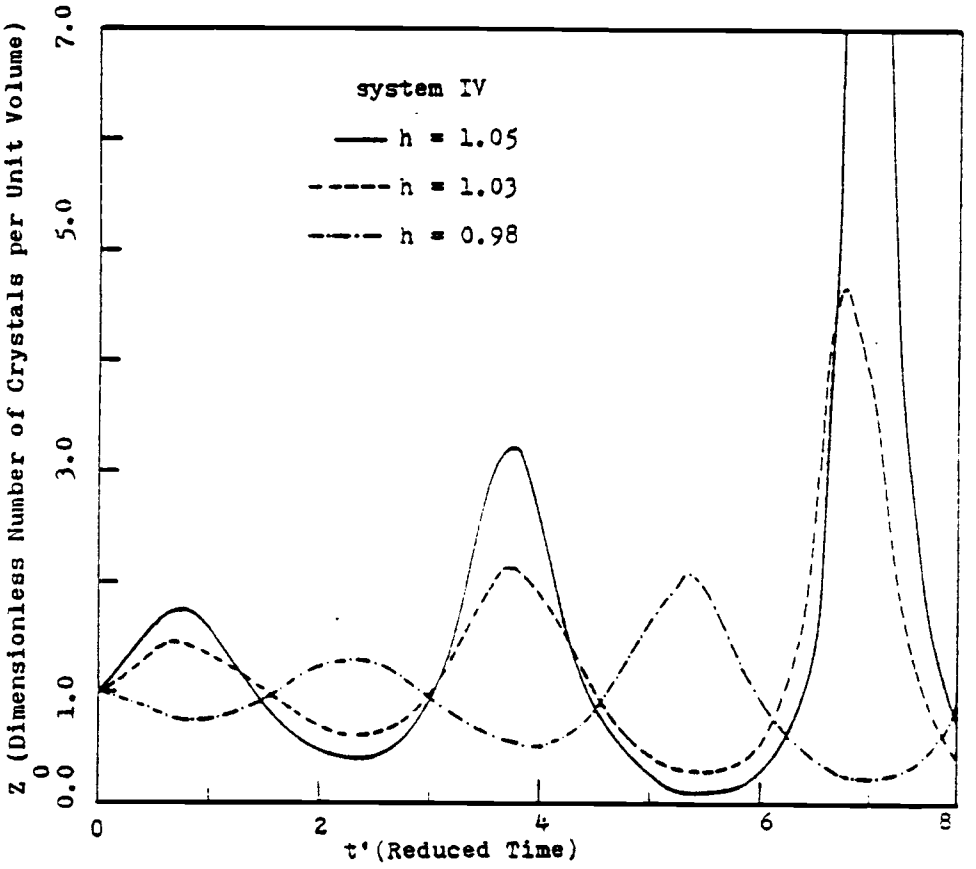

Fig.4-14. Effect of size of input step change on response of Z_0 of system IV.

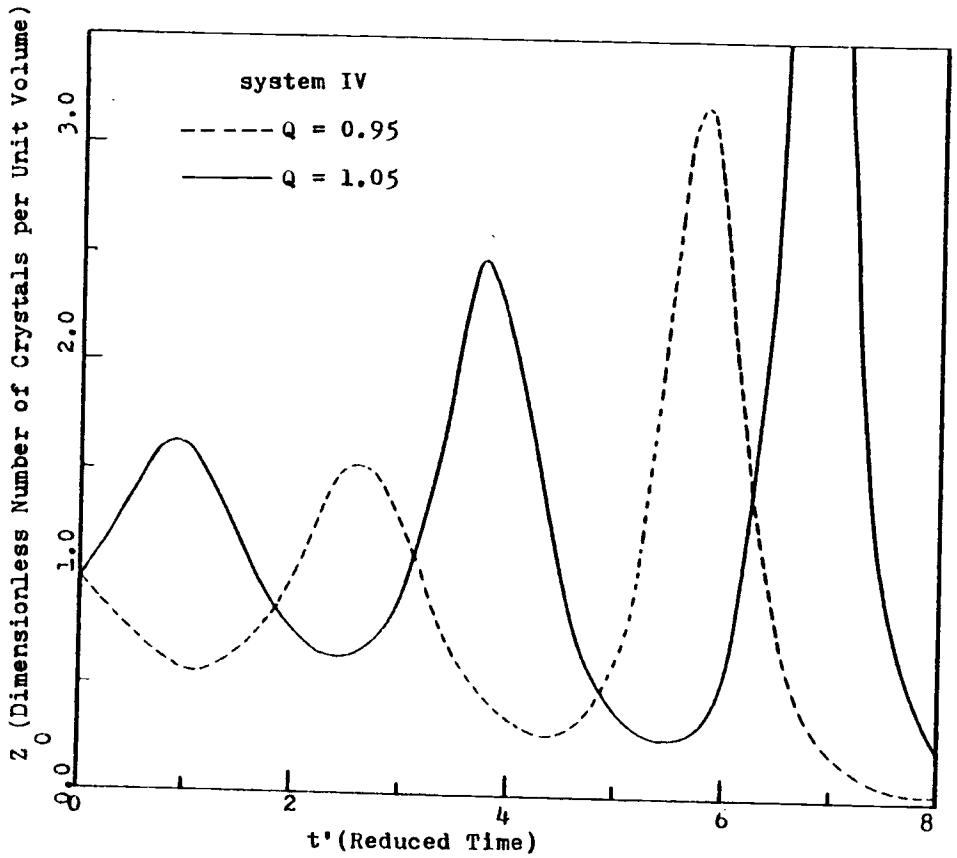

Fig.4-15. Effect of size of flow rate step change on response of Z_0 of system IV.

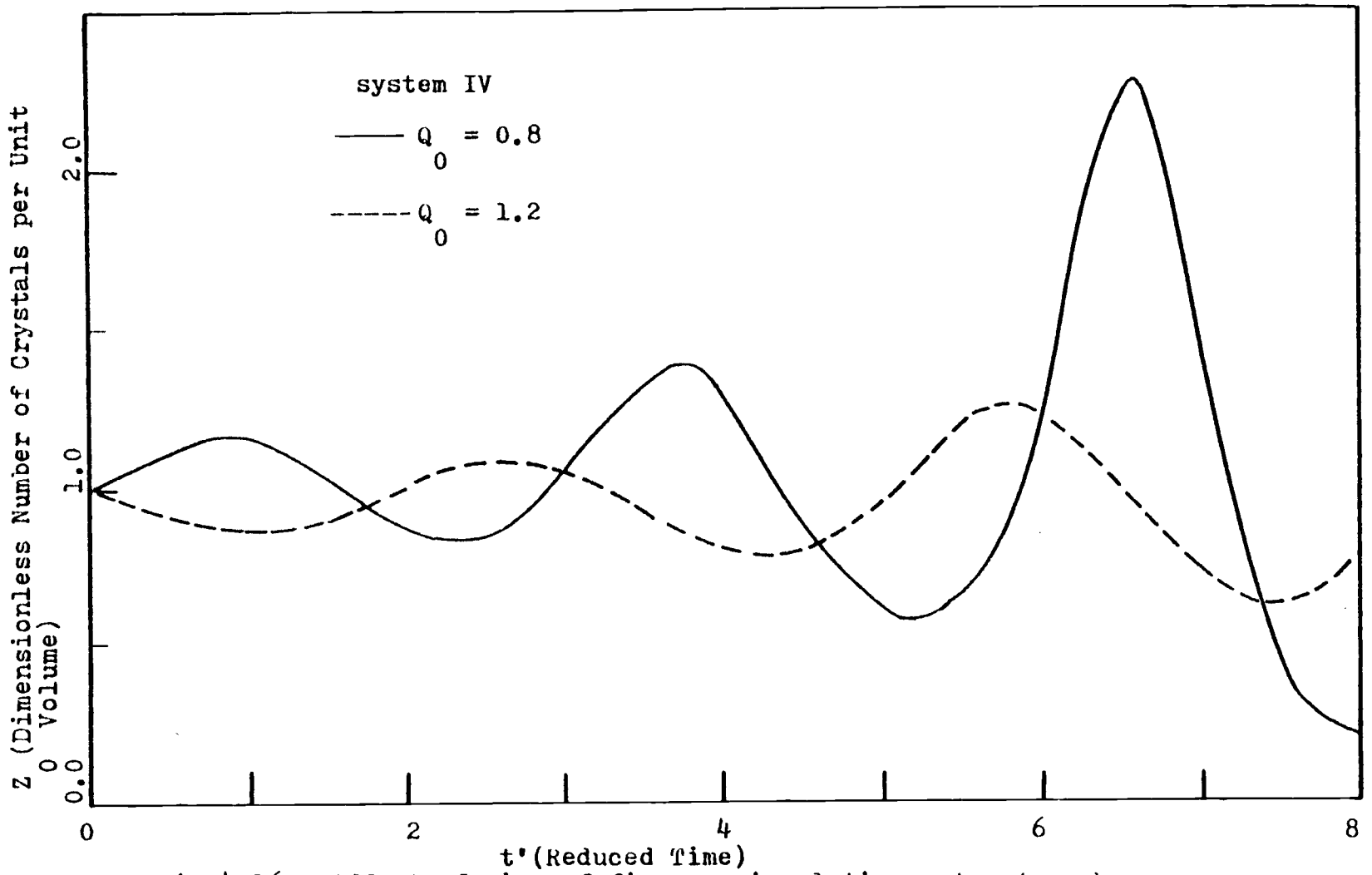

Fig.4-16. Effect of size of fines recirculation rate step change on response of Z_0 of system IV.

fines destruction rate will cause nuclei density to decrease and this effect is similar to the decreasing the feed concentration.

From the above results, we find that linear stability models the system's dynamic behavior very successfully. When linear stability analysis predicts the system is stable, we get a stable but oscillatory system; if linear stability analysis predicts the system is unstable then the system oscillate and the amplitude becomes bigger and bigger.

(B) Modal Control: Results and Discussions

Now it is quite obvious we need some control scheme to get better performance. For an unstable system the reason is very obvious: we can not operate the system; and even if the system is stable we still need to eliminate the long term oscillations in order to get a smooth system output. The modal control discussed in the previous section can be used to improve the performance of our system. The output variables Z_0, Z_1, Z_2, Z_3 and F are measured and the modal controller manipulates the feed throughput rate or fines destruction rate or both. Usually the two biggest eigenvalues of the system are shifted to improve the dynamic performance of the original (open loop) system. The eigenvalues of the system are shown in Table 4-2. The gain calculated by the modal control scheme is shown in Table 4-3.

Due to the basic structure of the Eq. (2-11a) and (2-14a), there is always an eigenvalue whose value is negative one; this value is fixed and this eigenvalue can not be changed by any method. Thus, the two biggest eigenvalues can only be shifted to negative one. Figures 4-17, 18, 19, and 20 show the modal control of a homogeneous nucleation

Table 4-2. The Eigenvalues of the System

System	Eigenvalues	Stability
I	- 0.046843 + 2.1957 i	
	- 0.046843 - 2.1957 i	
	- 1.0	stable
	- 3.9625	
	- 18.339	
II	0.025403 + 2.1929 i	
	0.025403 - 2.1929 i	
	- 1.0	unstable
	- 4.2567	
	- 10.831	
III	- 0.0036061 + 1.631 i	
	- 0.0036061 - 1.631 i	
	- 1.0	stable
	- 3.0097	
	- 21.865	
IV	0.29134 + 2.0836 i	
	0.29134 - 2.0836 i	
	- 1.0	unstable
	- 3.6189	
	- 21.846	

Table 4-3. Controller Gain

(a) Multiple-input Case

System	Gain matrix (2 x 5 Matrix)				
I	0.95315	18.39565	29.6116	-48.96009	87.75355
	0	1.17542	2.24113	-2.46338	4.43338
II	1.025375	12.49493	19.41281	-32.83147	60.41577
	0	0.7343815	1.506456	- 1.215416	2.245738
III	0.997259	21.8092	18.95959	-41.8033	73.4875
	0	3.13278	3.10969	- 5.24534	9.22115
IV	1.29131	29.00786	40.19301	-70.49161	129.18554
	0	1.95236	3.0899	- 3.75093	6.61397

(b) Single-input Case

(i) Manipulated variable Q_0

System	Gain Vector				
I	-1.906	-2.726	5.726	26.53	-47.03
II	-2.051	-3.154	5.549	29.87	-54.71
III	-1.993	-0.9856	4.323	12.21	-21.47
IV	-2.583	-2.42	7.601	34.7	-60.05

Table 4-3. Controller Gain (Cont'd)

(ii) Manipulated variable Q

System	Gain Vector				
I	0.1296	0.1505	-0.4555	-1.731	3.066
II	-2.051	-3.154	5.549	29.87	-54.71
III	0.2911	0.1001	-0.6690	-1.721	3.025
IV	-2.583	-2.42	7.601	34.17	-60.05

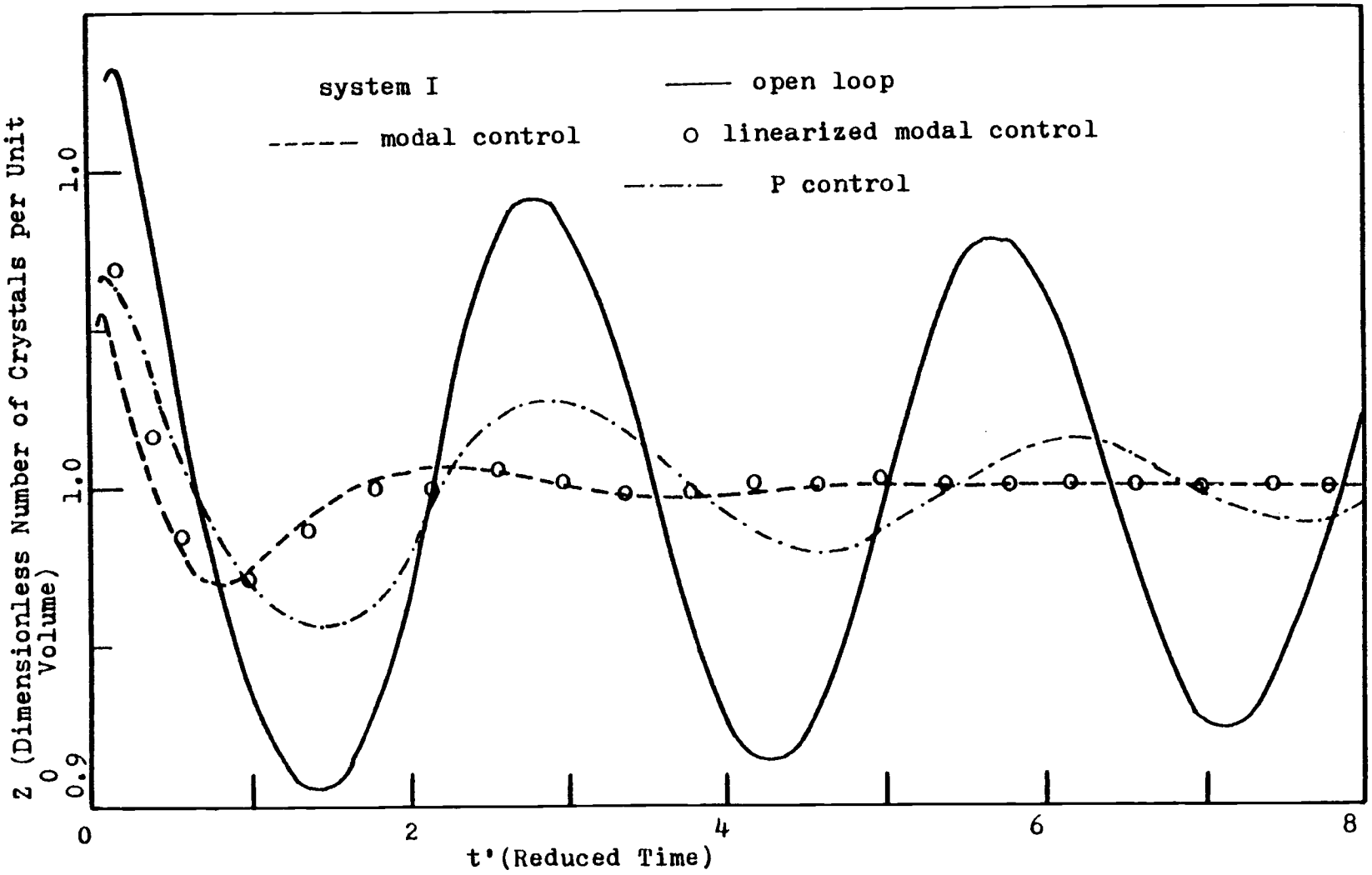

Fig.4-17. Effect of modal controller on Z_0 of system I to initial pertubation on F.

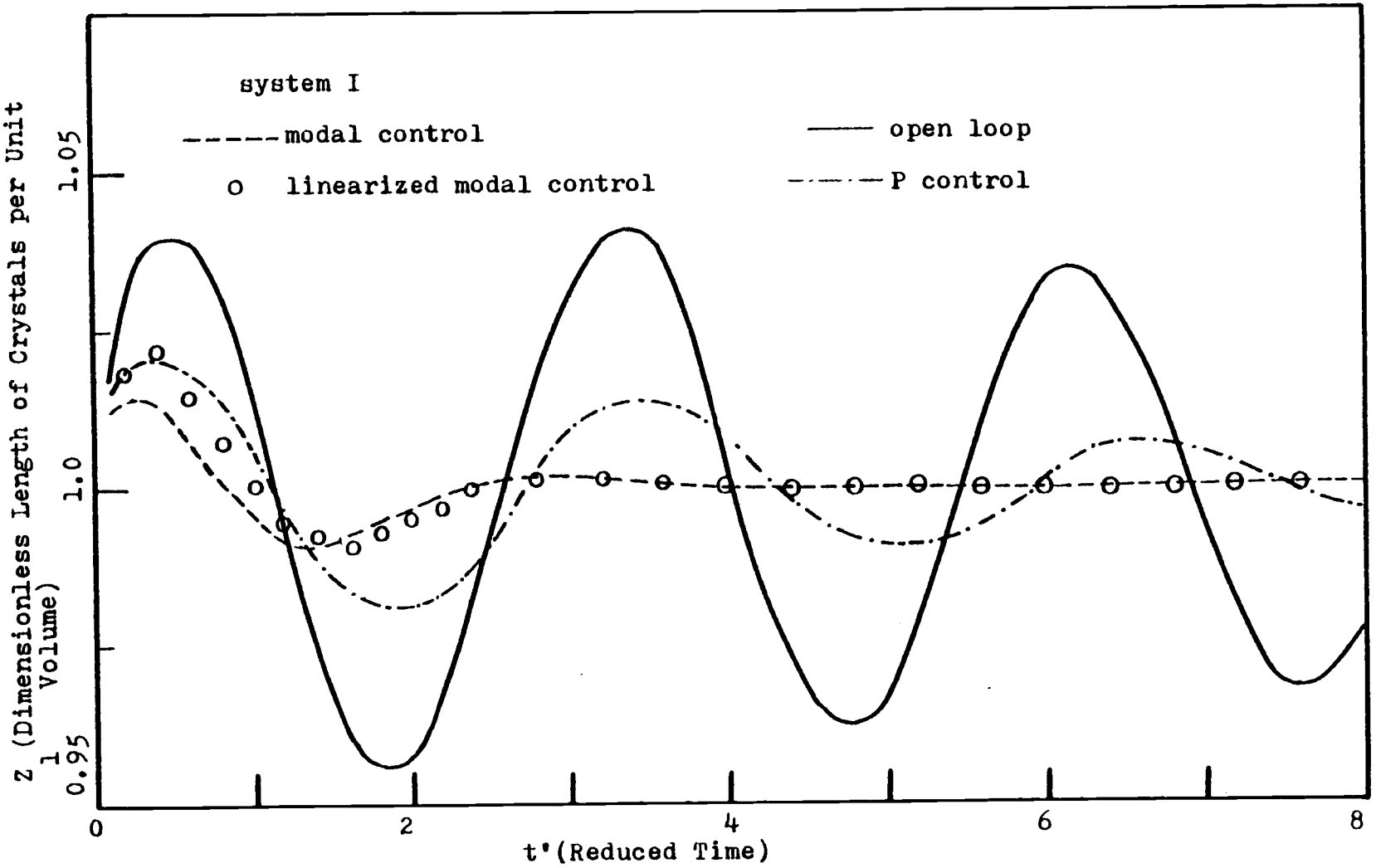

Fig.4-18. Effect of modal controller on Z_1 of system I to initial pertubation on F.

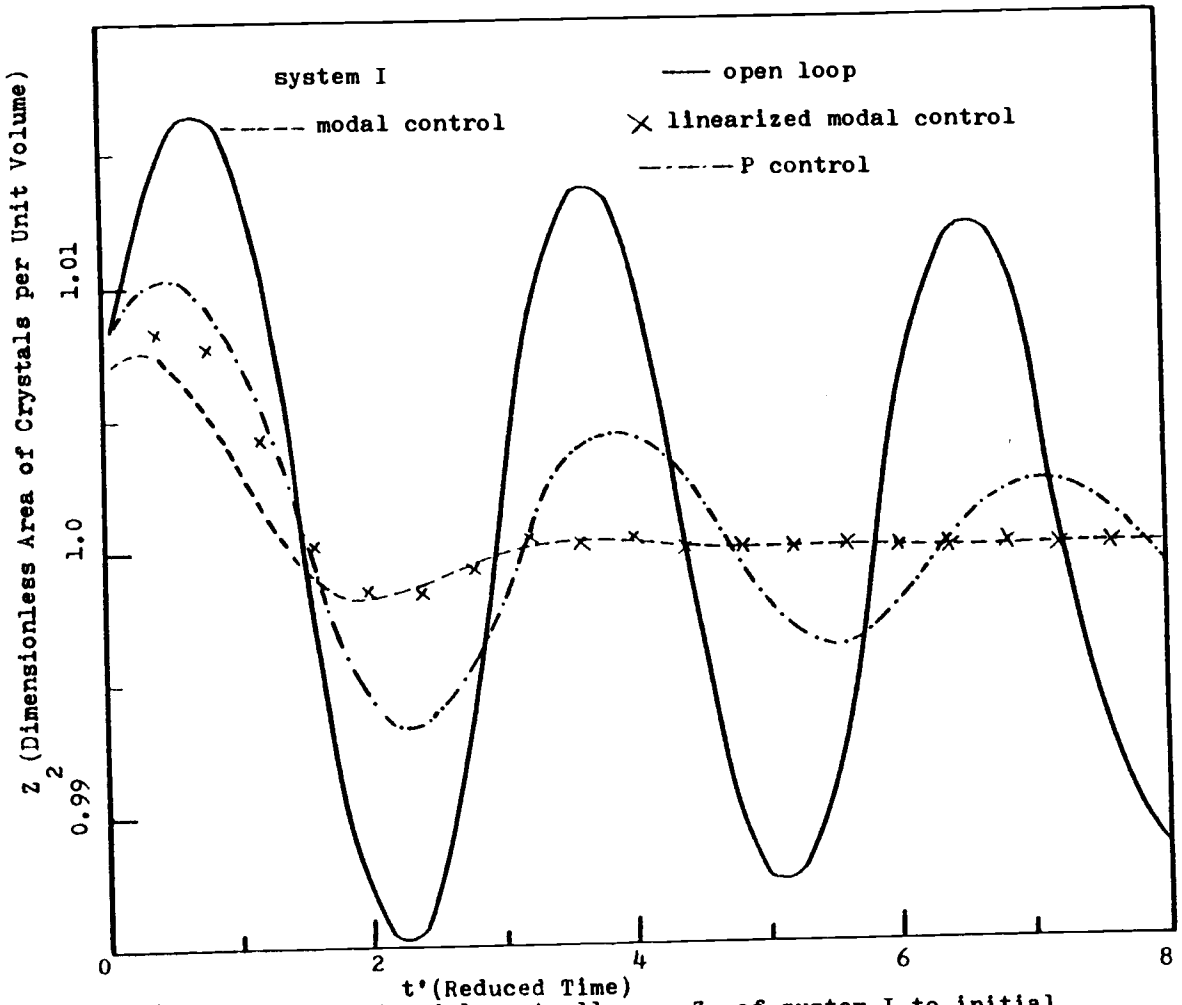

Fig.4-19. Effect of modal controller on Z_2 of system I to initial pertubation on F.

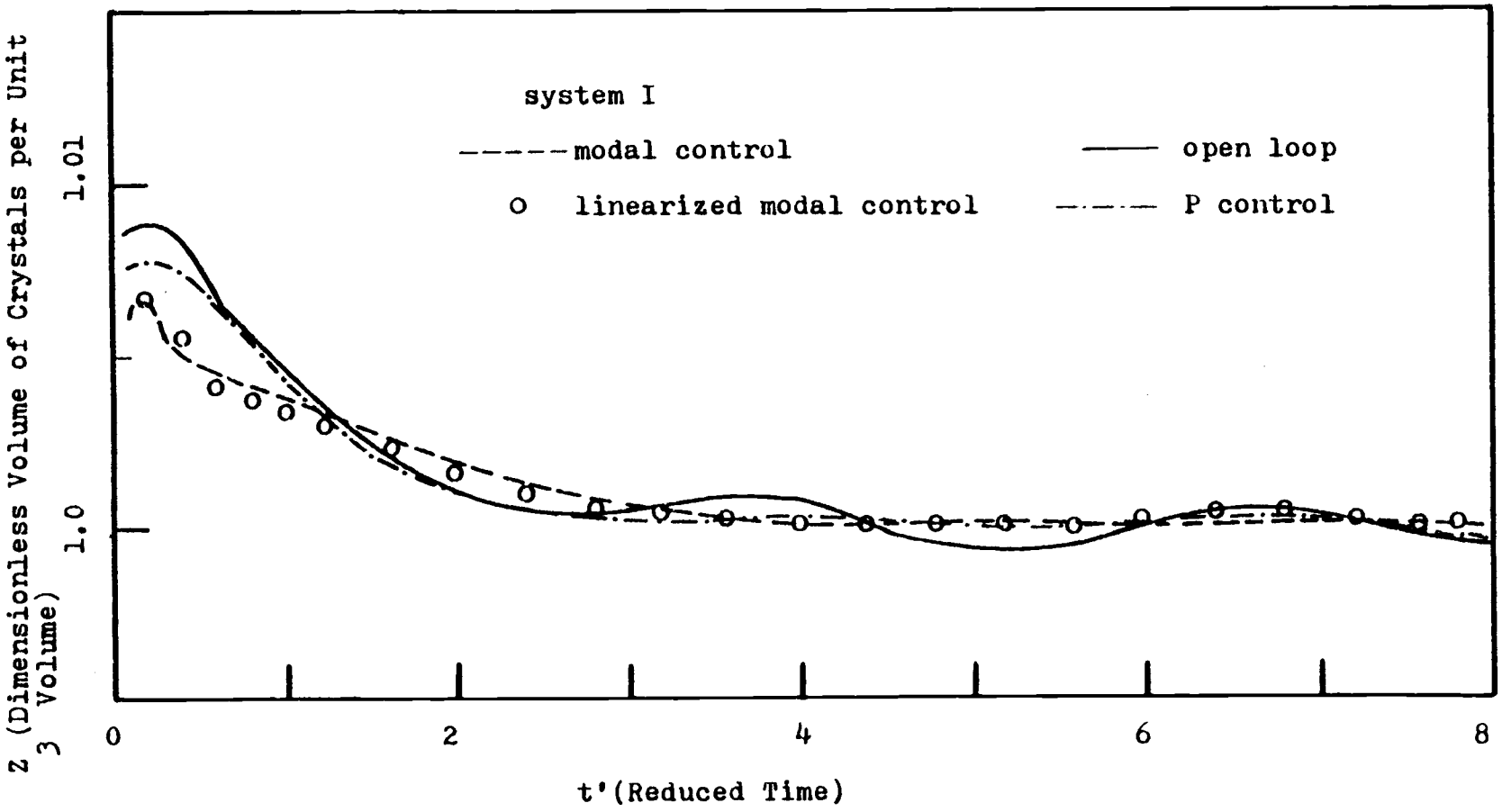

Fig.4-20. Effect of modal controller on Z_3 of system I to initial pertubation on F.

system using the throughput rate and fines destruction rate as manipulated variable if the initial pertubation on F = 1.006 (this value is equivalent to 19.58% increase in supersaturation). Comparing this response to the open loop response, we find that modal control has a tremendous effect on the system, it reduces the overshoot peak; and restores the system to its steady state very quickly; and more important, it eliminates the self-sustained oscillation. Contrary to the conventional controller, the modal controller monitors each system output variable, using the manipulated variables to control the output variable very efficiently. This means that a modal controller can produce a stable and ideal system response. A conventional feedback control can then be used as a cascade controller to control the whole system to the desired level.

In Figures 4-17, 18, 19, and 20 also show the proportional control of the same system using nuclei density as the controlled variable and using fines destruction rate as the manipulated variable. The value of the gain used in the simulation was calculated as suggested by Beckman et al. (3). Comparing this response to modal control response, we found that using proportional control was not an effective way to control the continuous crystallizer with a fines trap.

Usually we only change the real part of the biggest eigenvalues, but we can also change the imaginary parts of the changeable eigenvalues. However, this always gives rise to a higher gain value. Very high gains are normally impractical even if stable, as they lead to excessive control effect, and also to amplification of high frequency disturbances.

Fig. 4-21 shows the response of Z_0 with modal control using throughput rate or fines destruction rate as the control variables for a pertubation in F. This method is effective even though controlling both may be a more effective way to control the system than single input control. From the above graph we also find that using fines destruction rate is better than using the throughput rate in modal control. Although controlling the throughput rate is not so effective as other two methods, it gives us a very powerful method to control the continuous MSMPR crystallizer (without a fines trap).

Figures 4-24 and 4-25 show the control effect for a secondary nucleation system in which the system is inherently stable in the open loop. Improvement similar to that found for homogeneous nucleation is found in this system.

Systems which are inherently unstable show satisfactory control performance using either throughput rate or fines destruction rate or both as the manipulated variables. The unstable system shifts to a stable one within a reasonably short time period. Figures 4-22, 4-23, 4-26, and 4-27 show (by simulation) that the unstable system can be stabilized by using a modal controller. This is the special advantage of a modal controller over conventional control schemes. Han (12) used the feedforward control scheme to control the MSMPR crystallizer. The controller was designed to control the supersaturation with the feed rate as a manipulated input variable. Supersaturation is significantly improved when the controllers are applied to the system which is basically stable but they can not make a system stable if the system is basically in an unstable region.

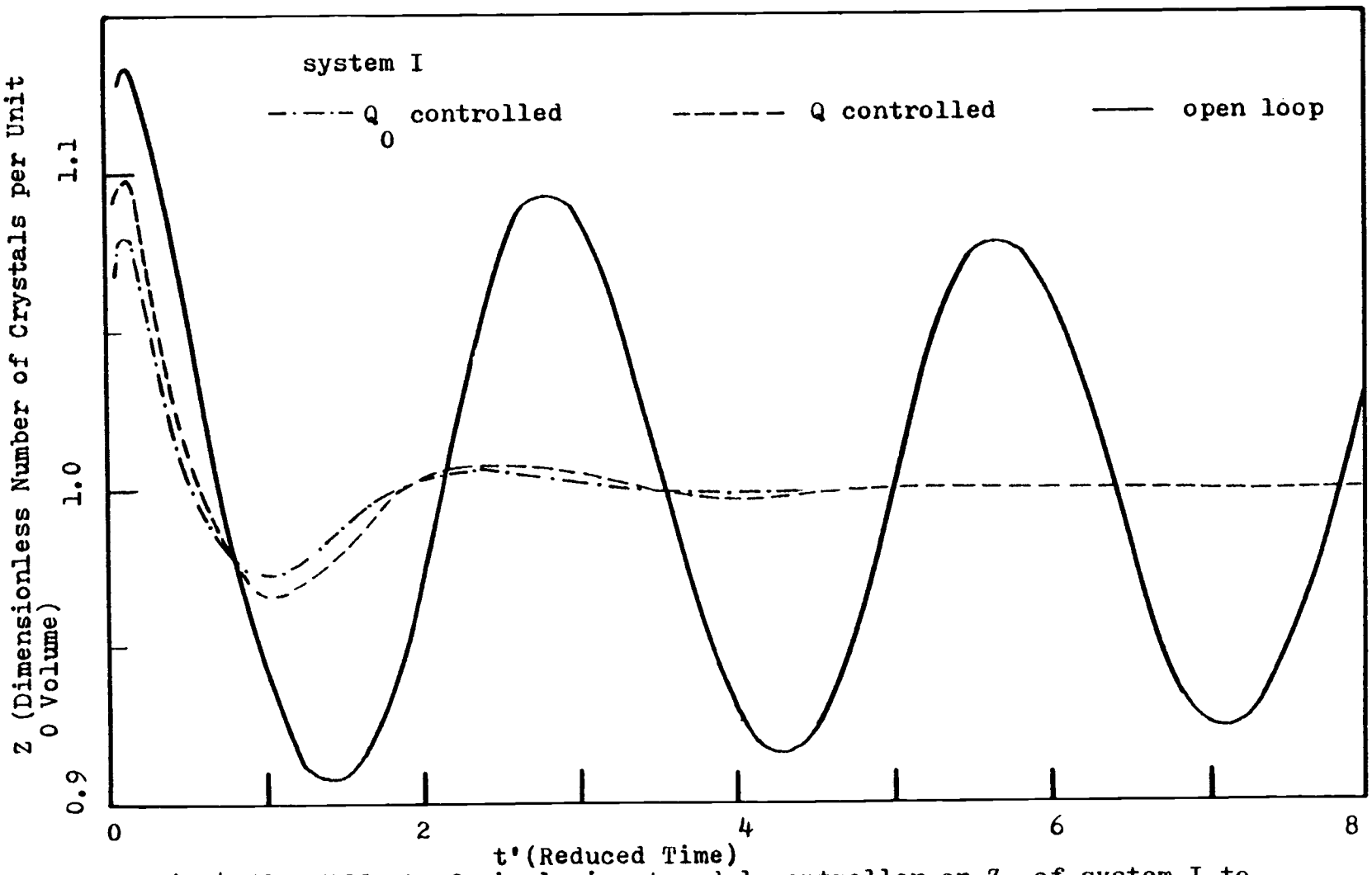

Fig.4-21. Effect of single input modal controller on Z_0 of system I to initial pertubation on F.

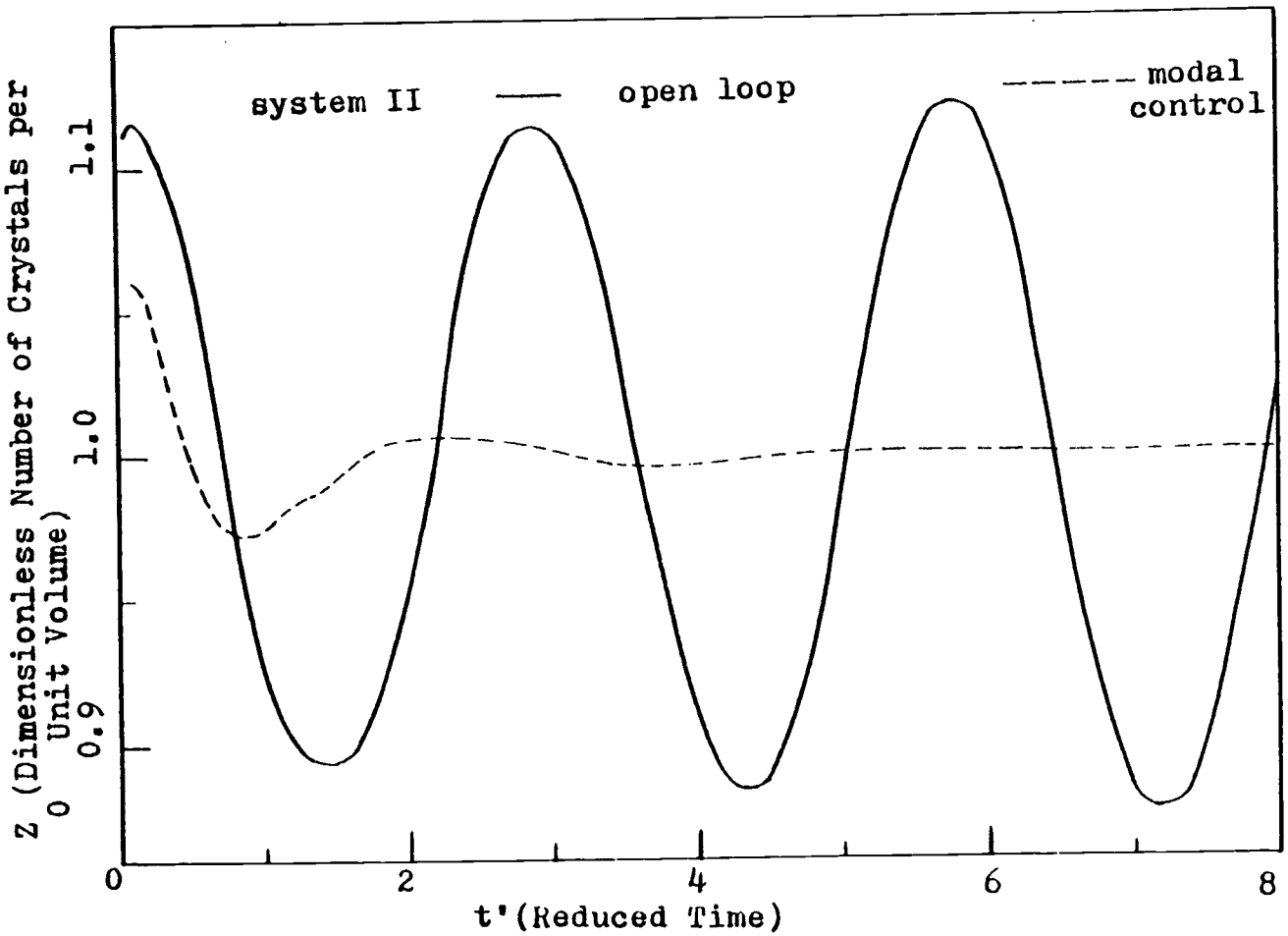

Fig.4-22. Effect of modal controller on Z_0 of system II to initial pertubation in F.

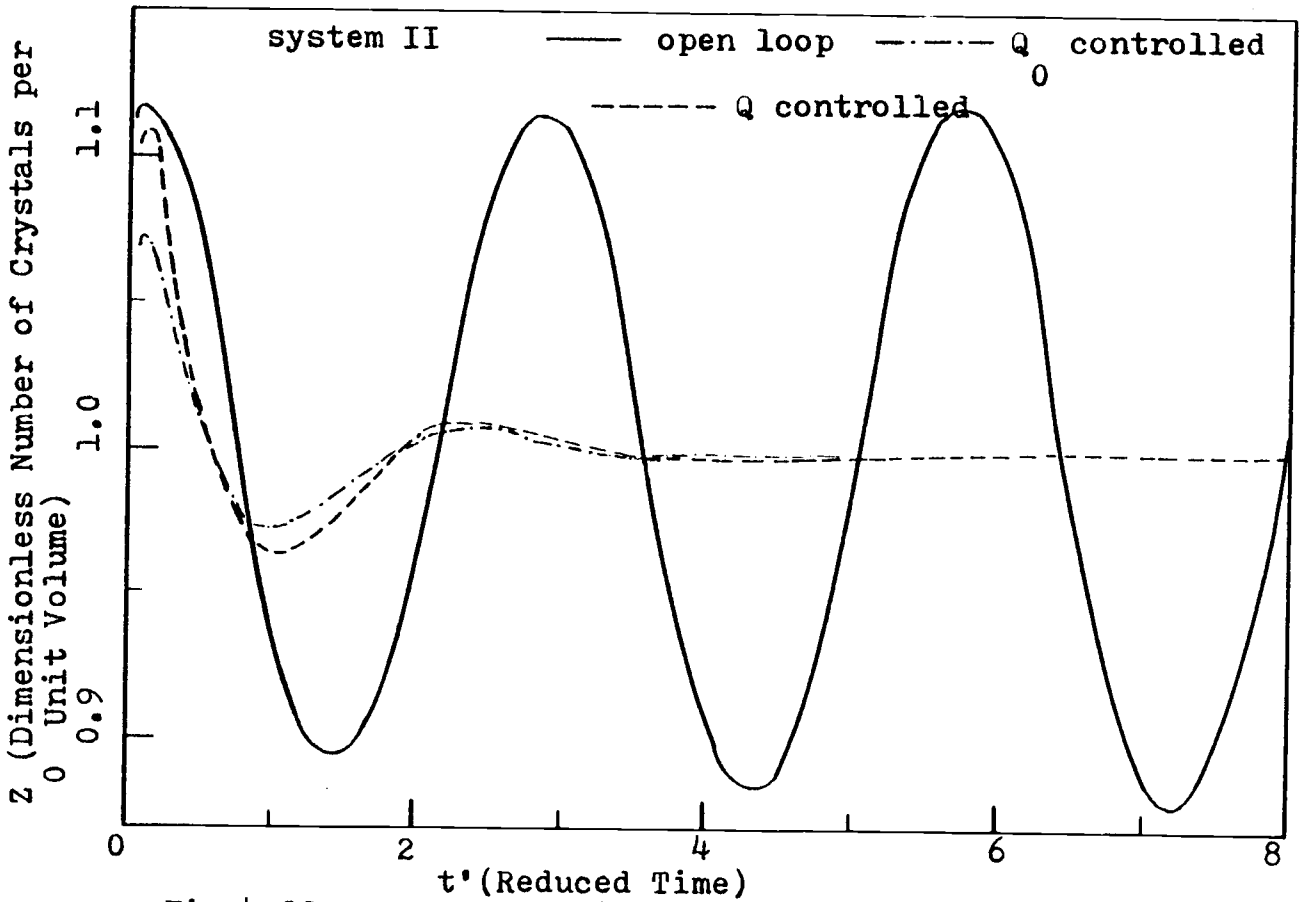

Fig.4-23. Effect of single input modal controller on Z_0 of system II to initial pertubation on F_0.

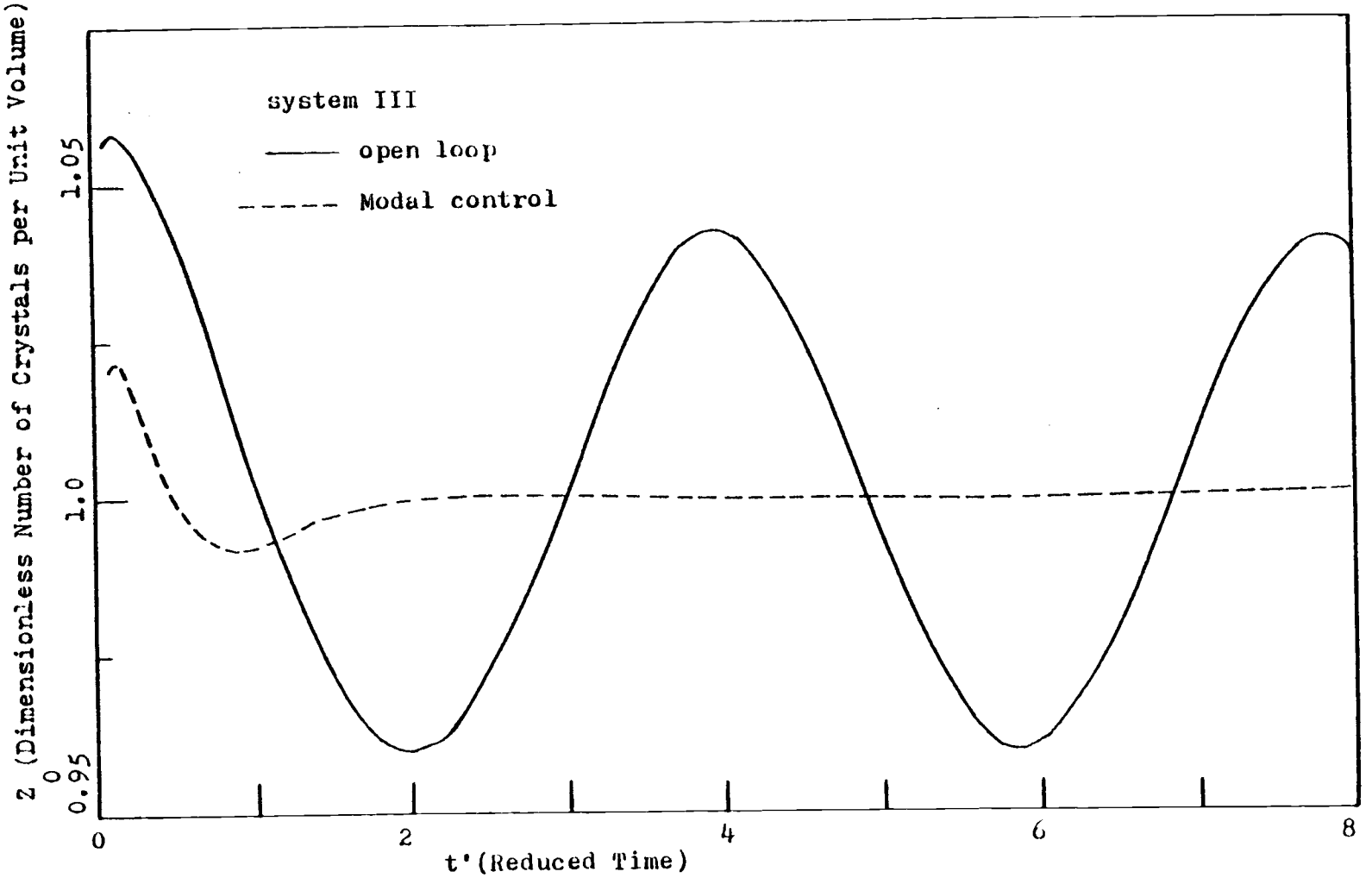

Fig.4-24. Effect of modal controller on Z_0 of system III to initial pertubation on F.

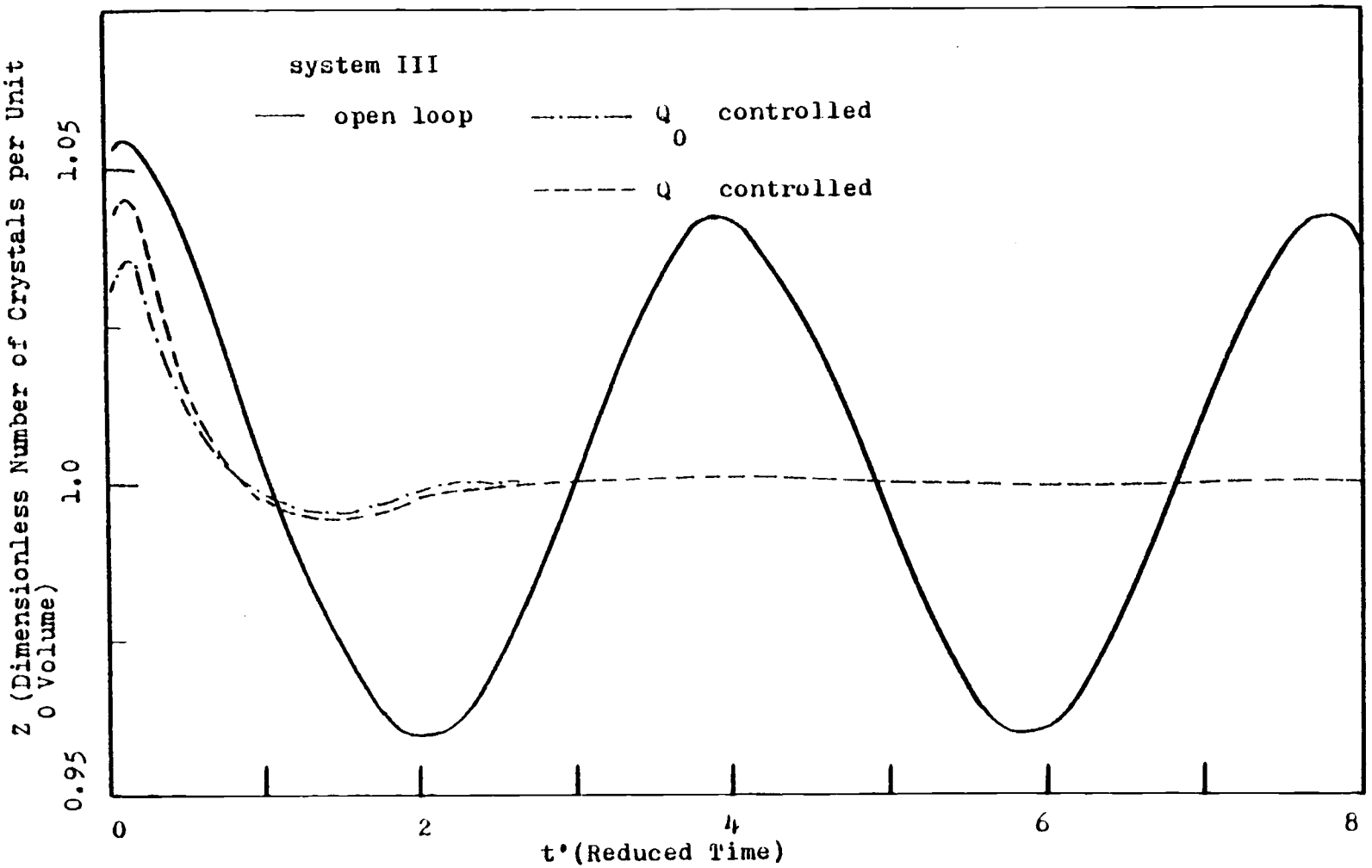

Fig.4-25. Effect of single input modal controller on Z_0 of system III to initial pertubation on F.

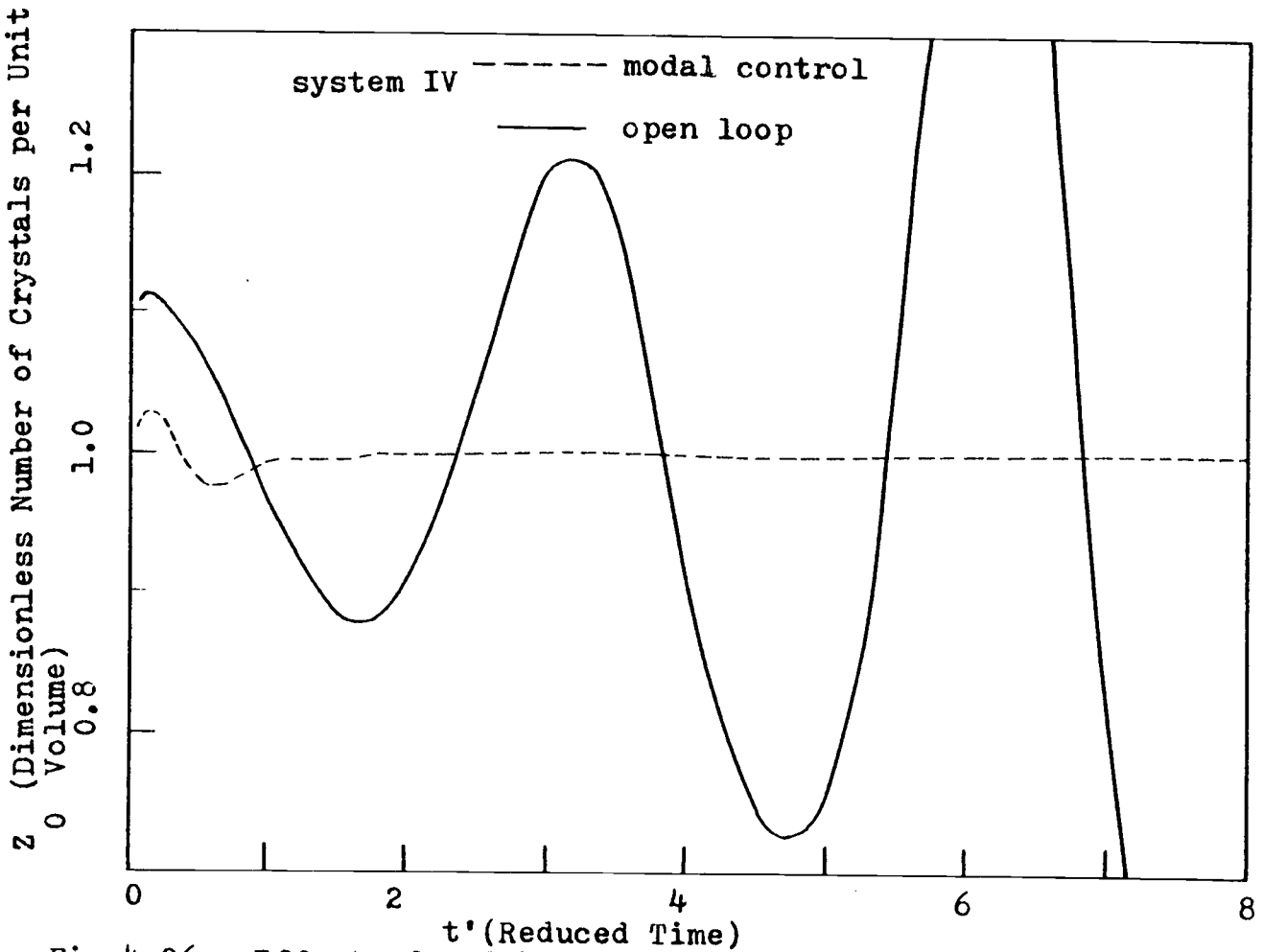

Fig.4-26. Effect of modal controller on Z_0 of system IV to initial pertubation on F.

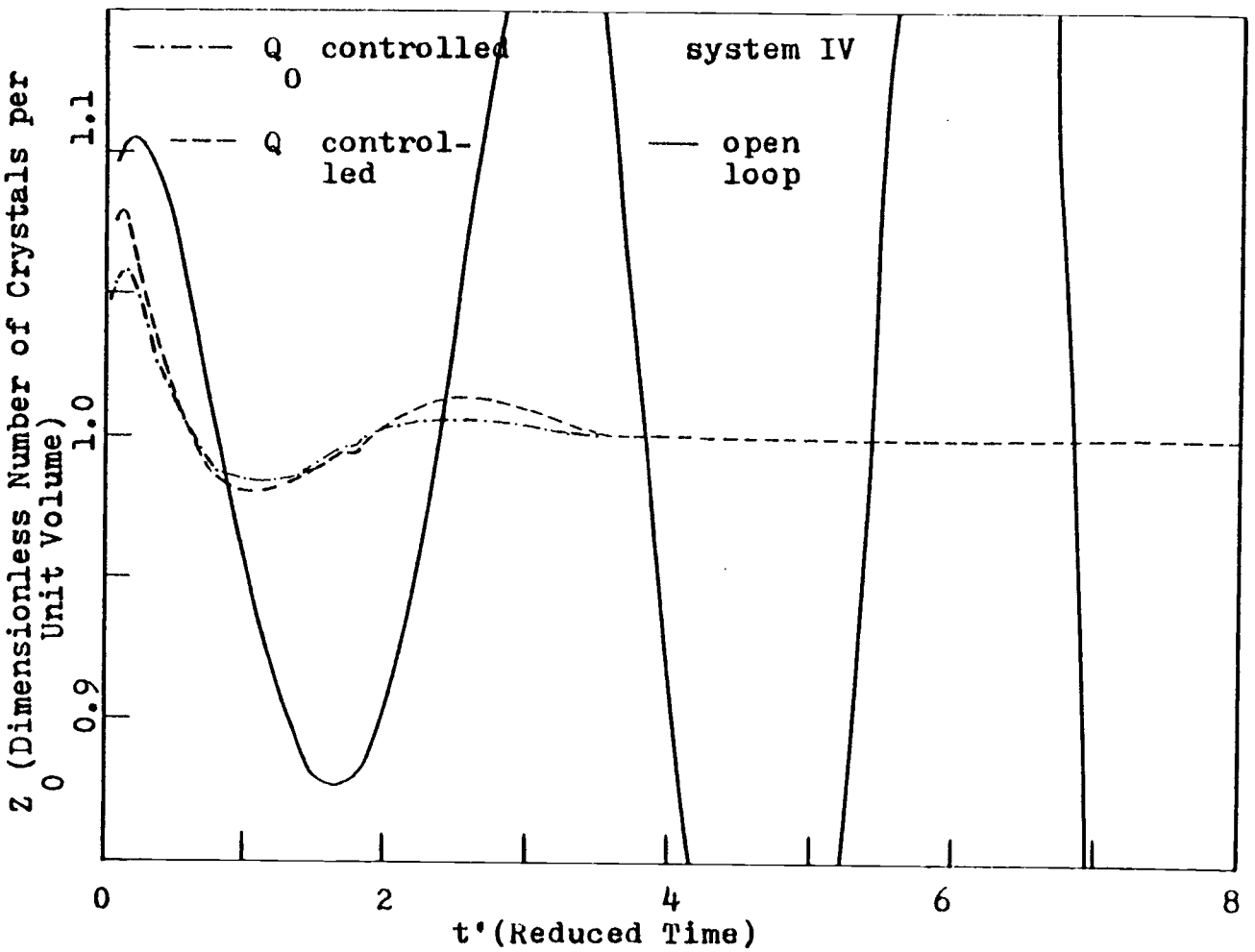

Fig.4-27. Effect of single input modal controller on Z_0 of system IV to initial pertubation on F.

Recently, Chang and Epstein (4) used input concentration, residence time, and seeding/fines dissolving rate as manipulated variables for modal control of an MSMPR crystallizer with linear size dependent growth rate. Although this kind of system is mathematically impossible (1), but their results show the same trend as this work except for the open loop unstable system, where they showed it was not possible to stabilize the unstable system with the same control gain used in a linearized model. A much higher gain was required to force the system back to the steady state. Further, the input concentration could not be used as the controlled variable, it is usually happened as the input noise. Although they shifted the eigenvalues to some arbitary small value, it was not meaningful because in this way the negative one was still the slowest mode and the other eigenvalues were too small to determine system response.

Figures 4-29 to 4-32 show modal controlled behavior of the homogeneous nucleation system for an inlet concentration step change when the system is open-loop stable. Also Figures 4-33 to 4-36 show modal controlled behavior of the secondary nucleation system for an inlet concentration step change when the open loop system is unstable. It can be seen that the modal controller controls the system very successfully. For the stable system, it eliminates the long term oscillatory behavior very effectively, reduces the overshot remarkably, and improves the speed of response; for the unstable system, it transforms the system to a stable one, and eliminates oscillatory behavior.

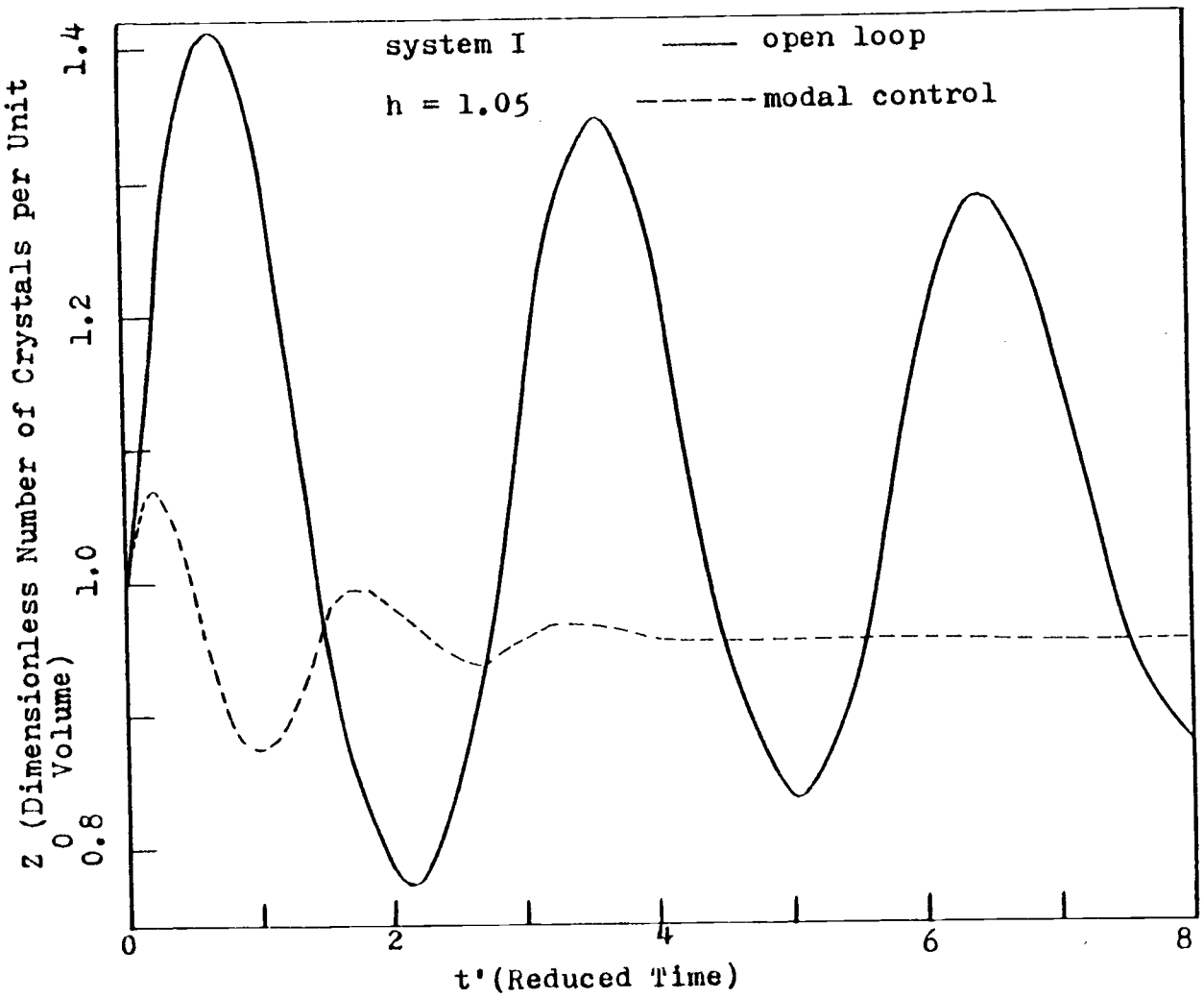

Fig.4-29. Effect of modal controller on Z_0 of system I to input step change.

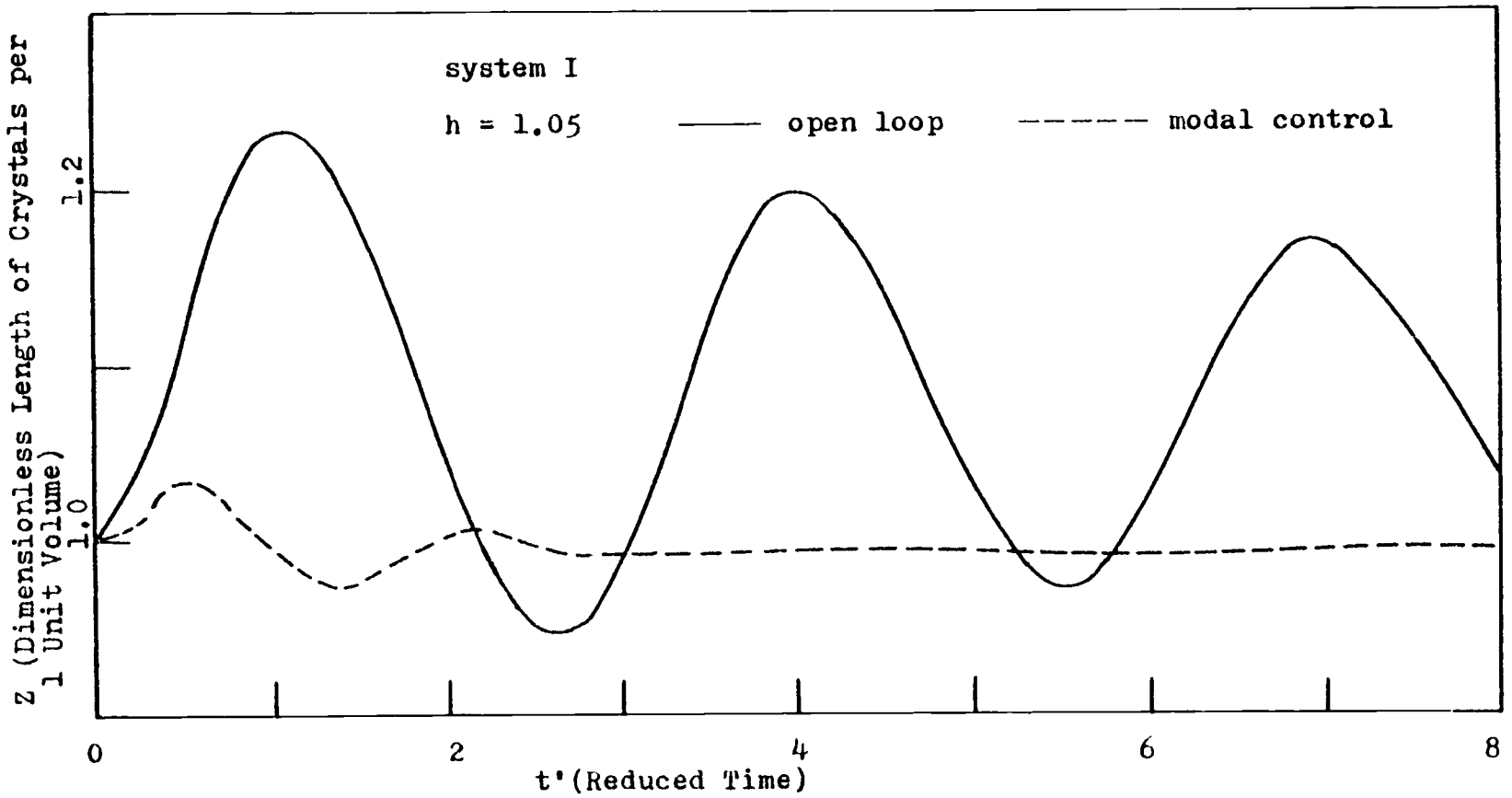

Fig. 4-30. Effect of modal controller on Z_1 of system I to input step change.

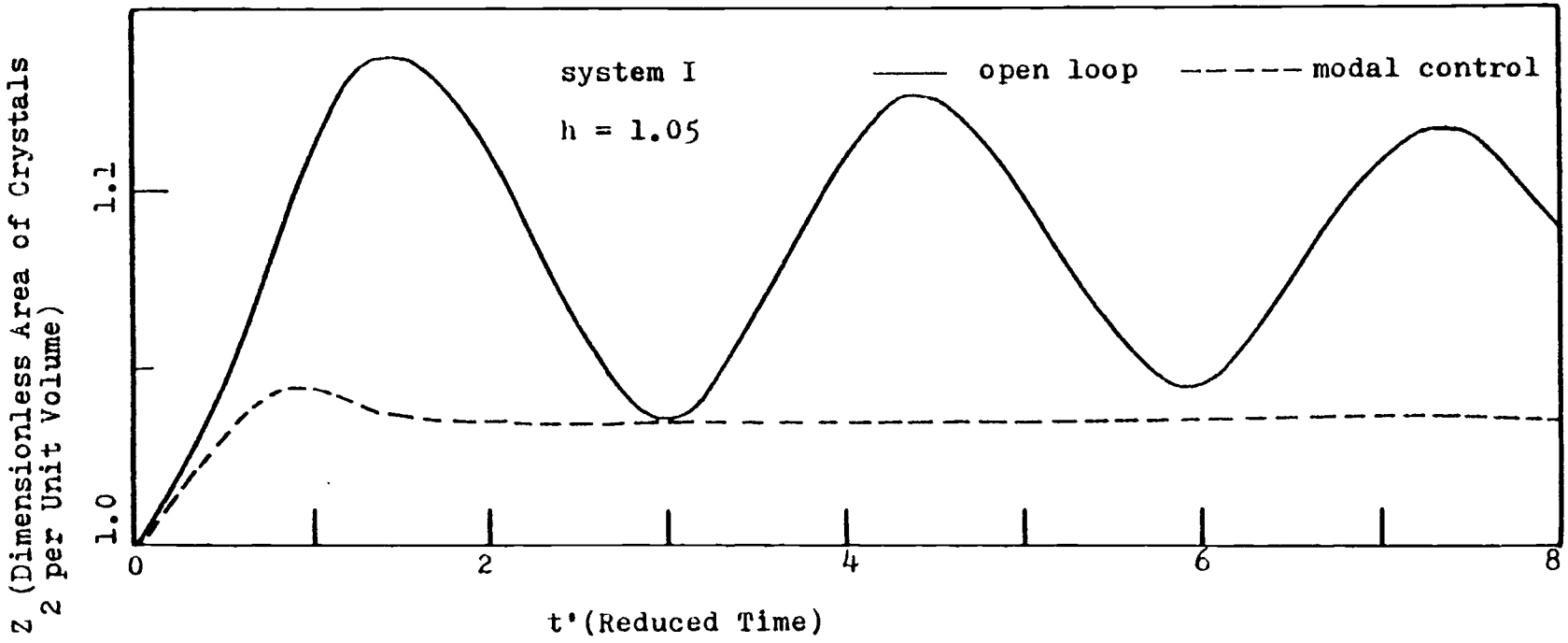

Fig.4-31. Effect of modal controller on Z_2 of system I to input step change.

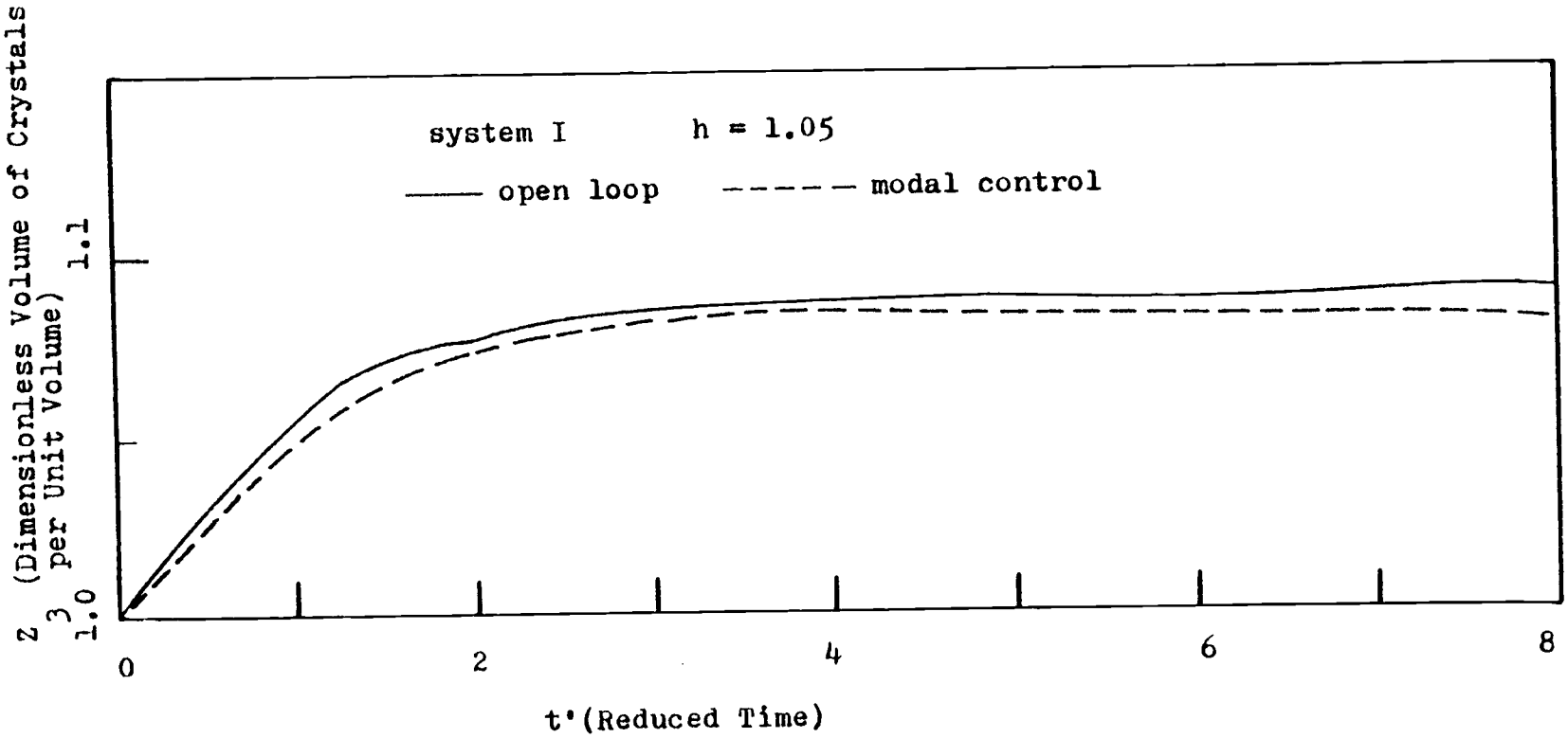

Fig.4-32. Effect of modal controller on Z_3 of system I to input step change.

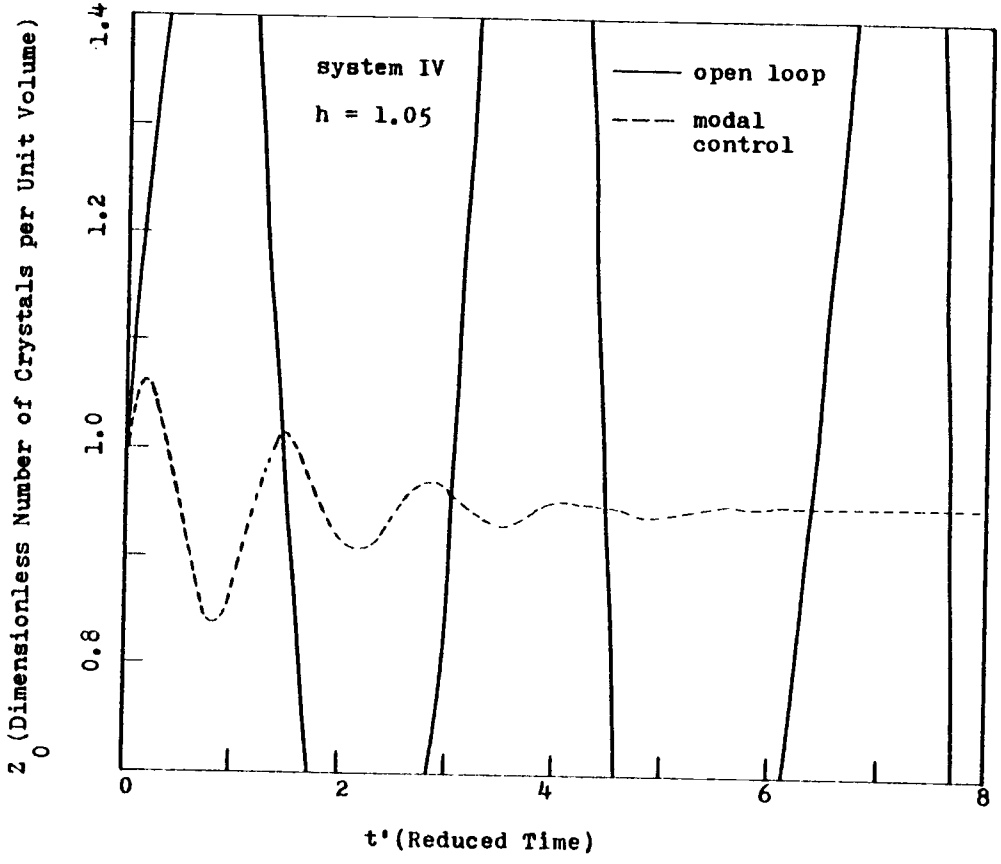

Fig.4-33. Effect of modal controller on Z_0 of system IV to input step change.

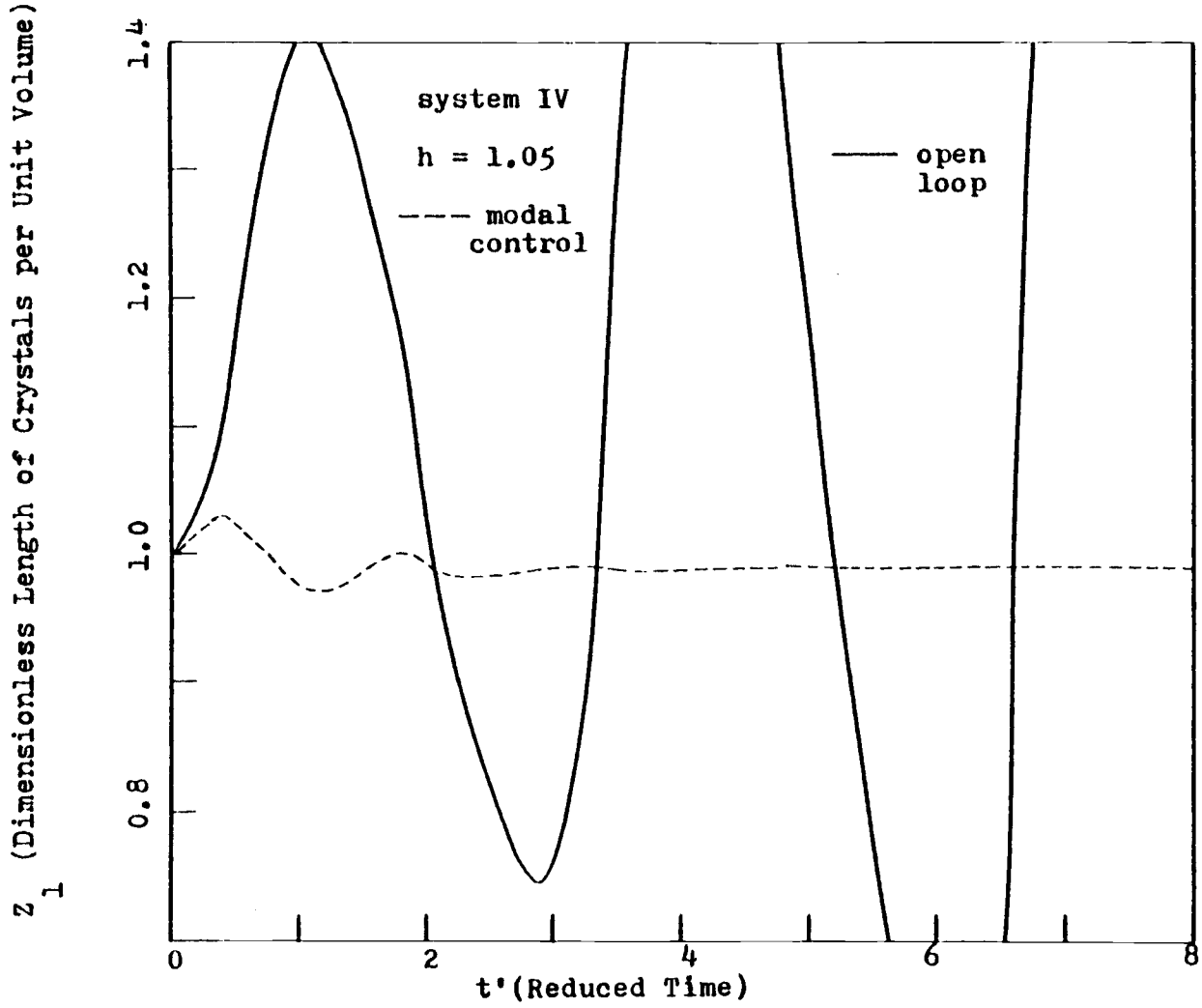

Fig.4-34. Effect of modal controller on Z_1 of system IV to input step change.

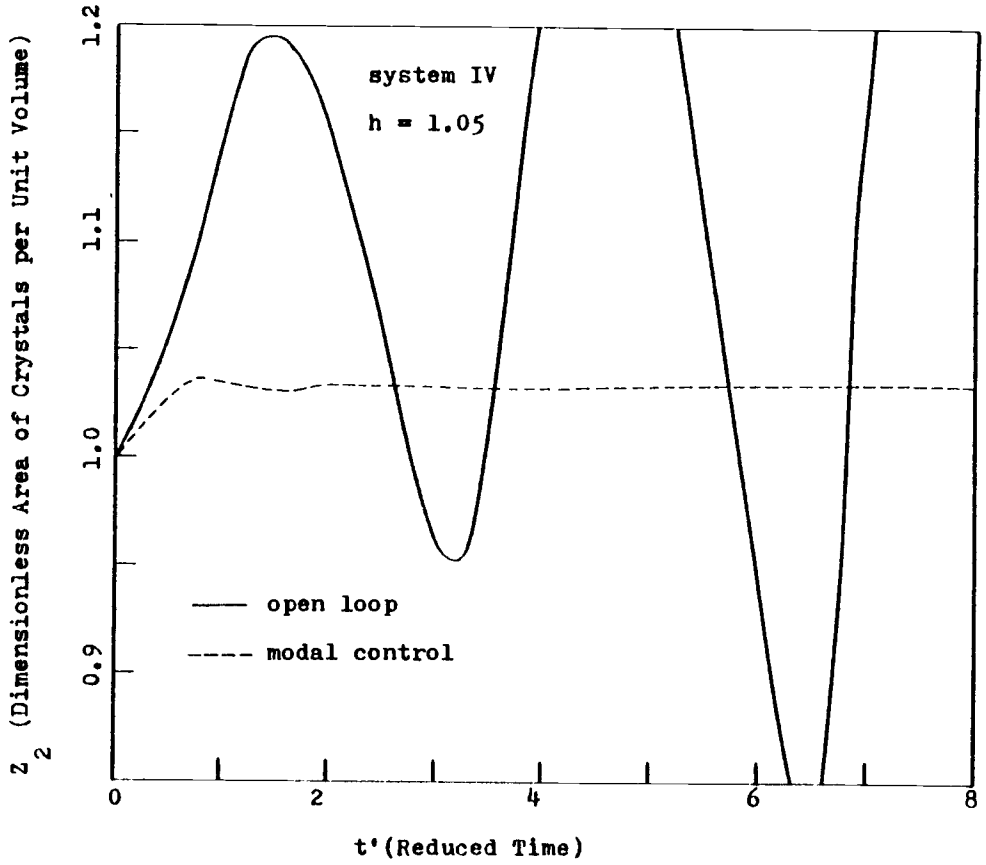

Fig.4-35. Effect of modal controller on Z_2 of system IV to input step change.

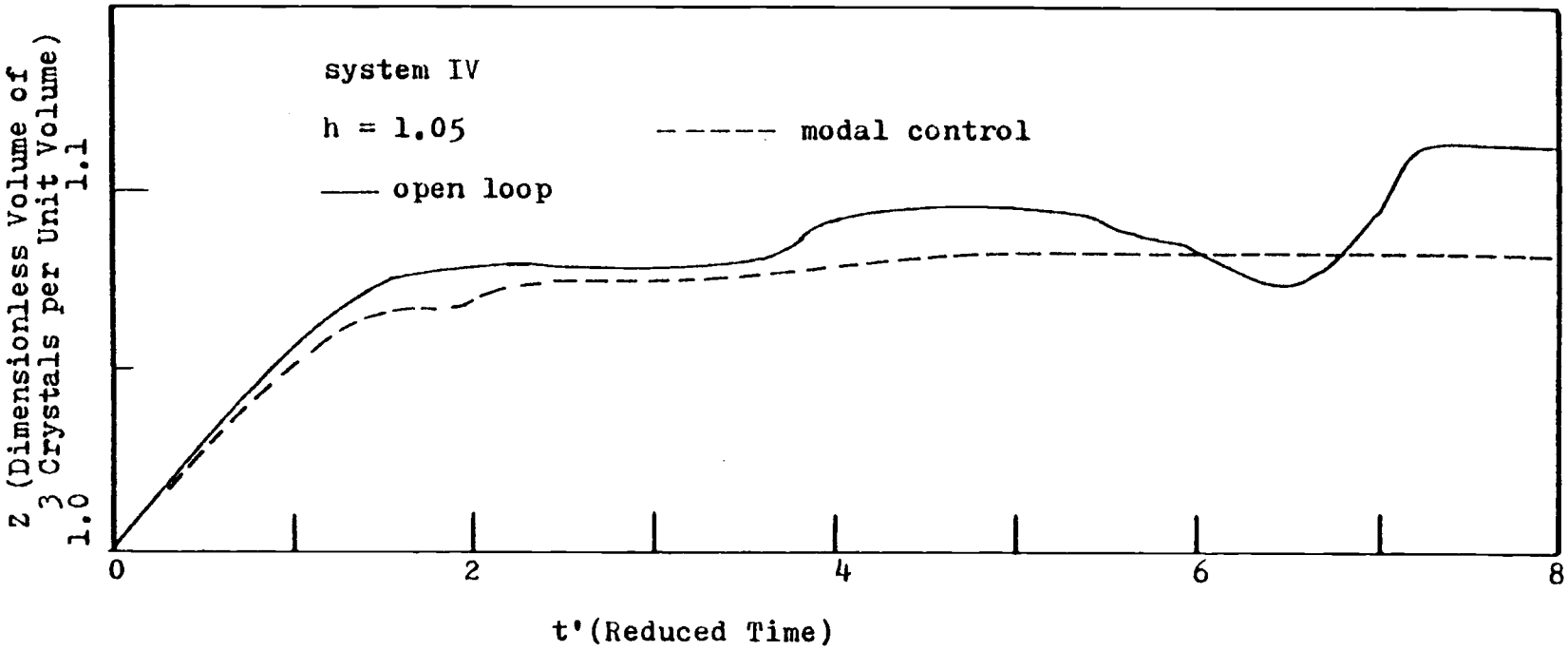

Fig.4-36. Effect of modal controller on Z_3 of system IV to input step change.

Up to now we have not been concerned with how to attain the desired steady state value. This is because the modal control only alters the dynamics of the system. As usual we must use conventional PI (or PID) control to attain the desired steady state operating condition.

Lei et al. (18) studied the control of an MSMPR crystallizer with a point fines trap by conventional proportional feedback control using either bulk throughput rate or fines destruction rate, it was discovered that modes of operation unstable in open loop can be stabilized by measuring the surface area of the fines and manipulating the throughput rate. A corresponding manipulation of the fines recirculation rate rather than of the bulk throughput rate can not readily stabilize an unstable operation. Beckman and Randolph (3) studied the control of a variable yield crystallizer equipped with a fines destruction system and product classifier. Control was simulated by proportional control of nuclei density using fines destruction rate as the manipulated variable. They suggested that nuclei density control scheme is effective both in minimizing the CSD transients and for elimination of instability. But they also showed that when using the slurry density and slurry withdrawal rate as the measured and manipulated variables, the controller can not eliminate the limit cycles. But these studies do not definitely answer whether the control schemes which might stabilize the CSD are effective in reducing the CSD disturbances caused by externally induced upsets. Usually the external upset in a crystallizer would occur in the inlet concentration, and throughput flow rate or fines recirculation rate are usually used to manipulate the system. Again modal control

is effective in such a situation. For this purpose, we use an inner loop modal controller to alter the dynamics (eigenvalues) of the system, while the outer loop controller attains the desired steady state. The error signal is generated by comparing the measured variable with an appropriate set point, taken to be the reference steady state value of the controlled variable. The cascade control scheme is shown schematically in Fig. 4-37 and the block diagram is shown in Fig. 4-38. The Ziegler-Nichols method (based on frequency response) was used to determine optimal settings for a proportional plus integral (PI) controller. There are many possible combinations of observed variables (Z_0, Z_1, Z_2, Z_3) and manipulating variables (Q_0, Q) in addition to choosing multiple-input modal control or single-input modal control. In practice we would also need to take into account the economic factors but that is beyond the scope of this study. Here we choose a few typical cases to show how the controller improves the system output.

Figure 4-39 to 4-42 show the response of the modal controlled system with a PI controller for the step change of inlet concentration where either Z_3 or Z_2 is controlled by manipulating Q. When Z_3 is controlled variable, it returns to steady state very quickly; but for Z_2 as controlled variable, there is still some offset; however improvement of Z_0 (which was not intended) can be considered as an additional benefit which may compensate for the offset remaining in the system.

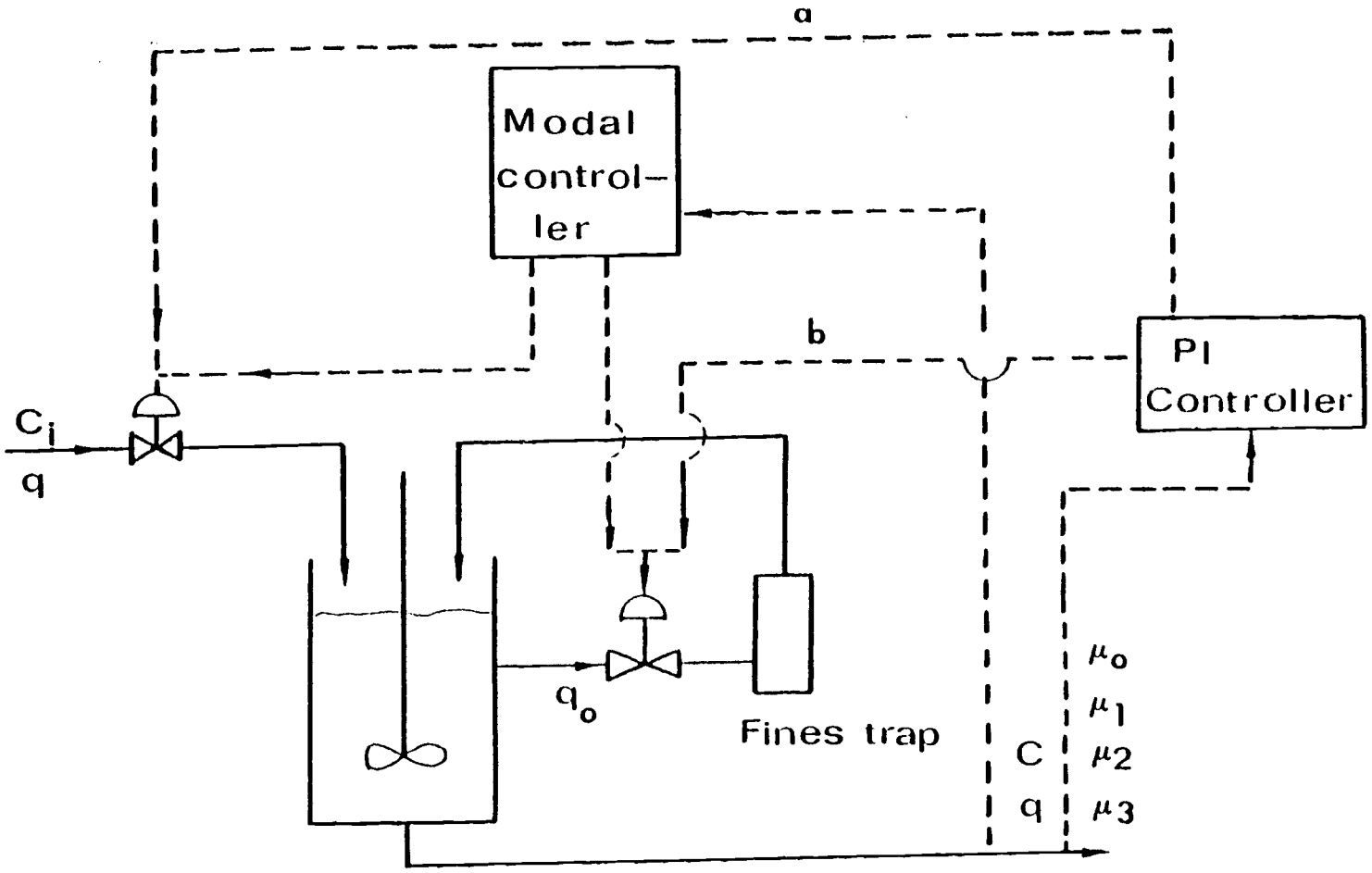

Fig.4-37. Schematic diagram of a modal + PI controlled crystallizer with a point fines trap.

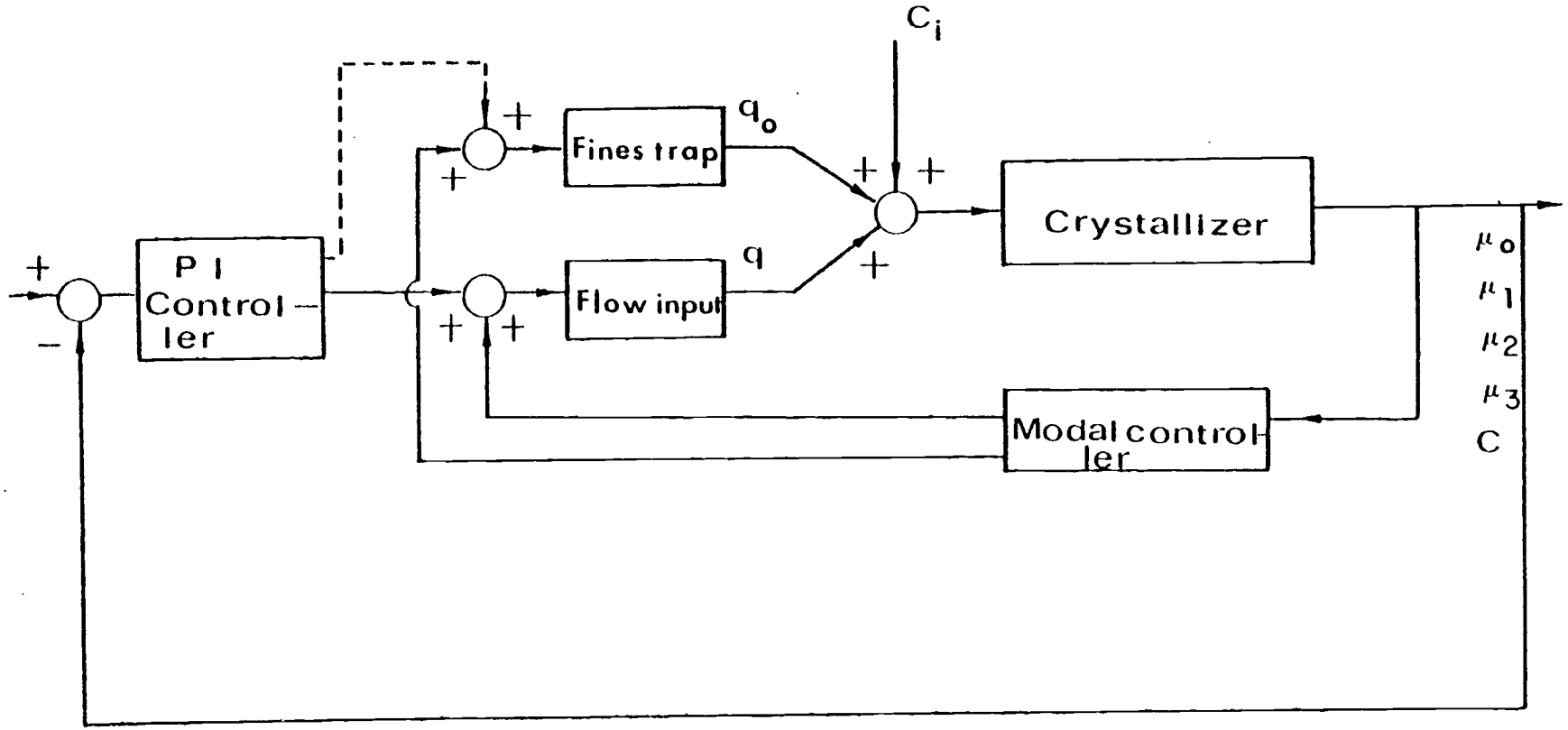

Fig.4-38. Block diagram of a modal + PI controlled crystallizer with a point fines trap.

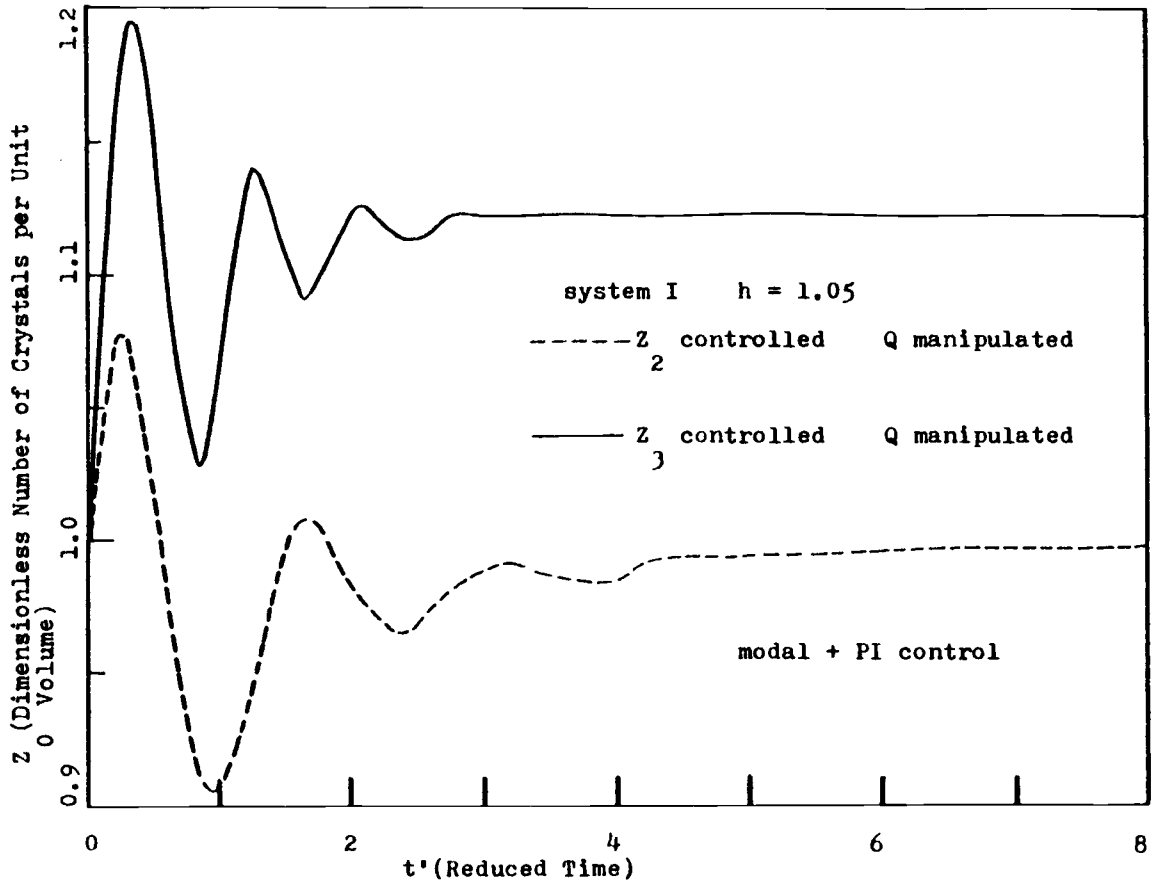

Fig.4-39. Effect of modal + PI controller on Z_0 of system I to input step change.

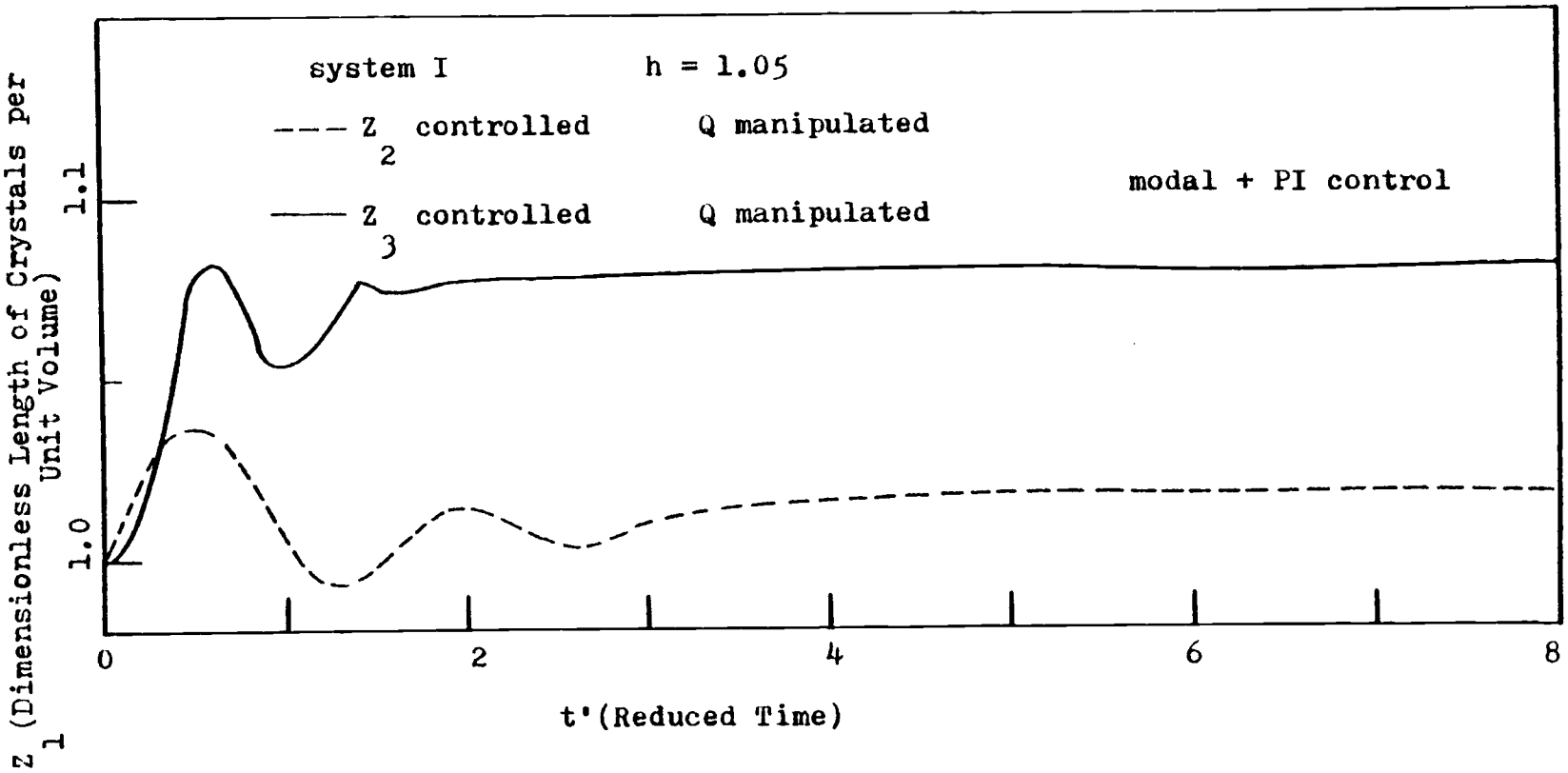

Fig.4-40. Effect of a modal + PI controller on Z_1 of system I to input step change.

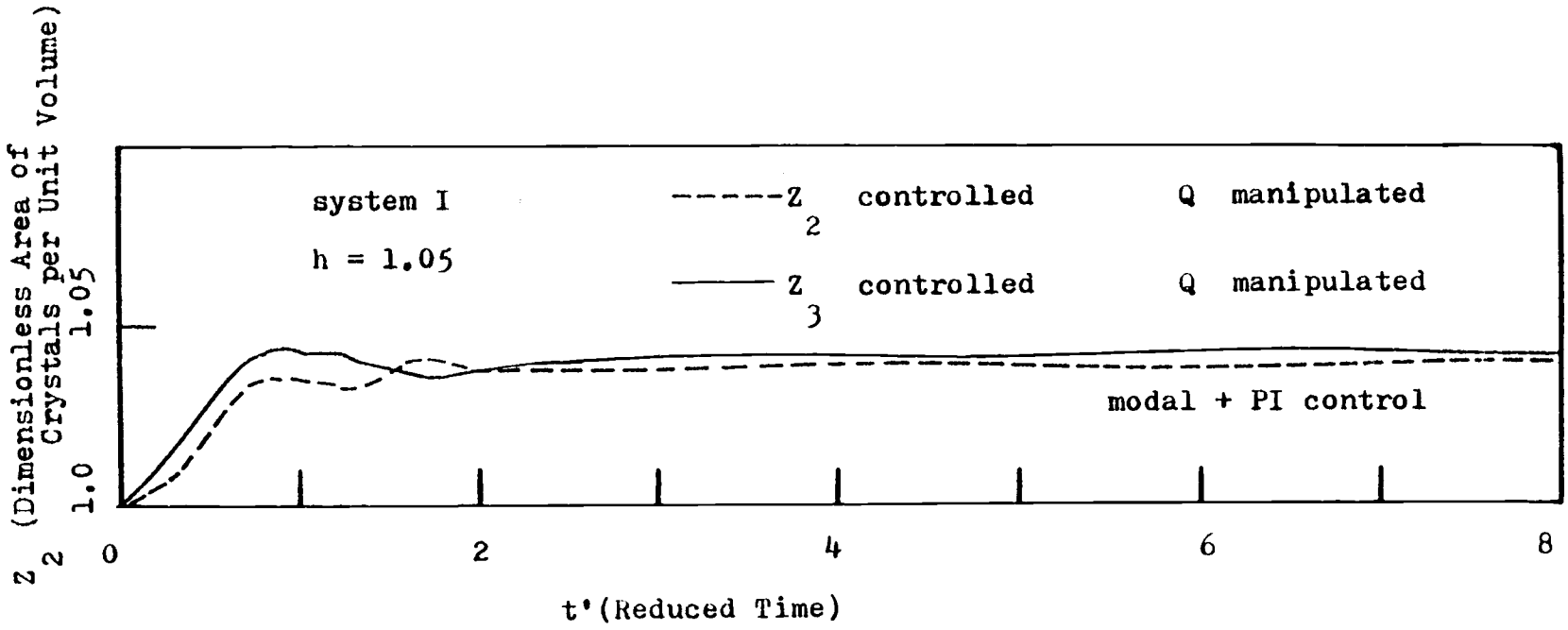

Fig.4-41. Effect of modal + PI controller on Z_2 of system I to input step change.

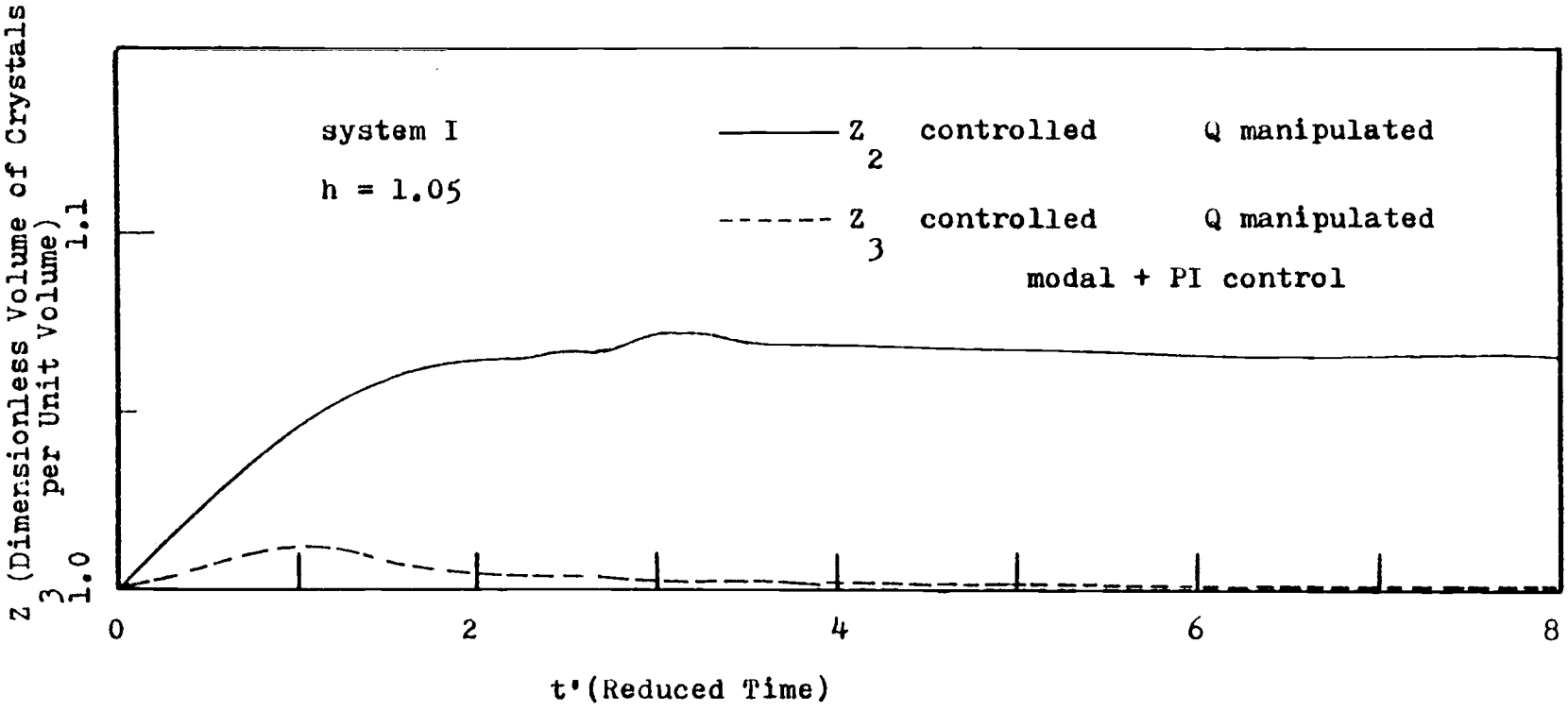

Fig.4-42. Effect of modal + PI controller on Z_3 of system I to input step change.

CHAPTER V. STABILITY ANALYSIS OF AN MSMPR CRYSTALLIZER WITH SIZE DEPENDENT GROWTH RATE

In Chapter III, a stability analysis for MSMPR crystallizer with a fines trap was given for both homogeneous and secondary nucleation. In that calculation it was assumed that the growth rate was independent of the crystal size. This assumption is correct if the rate determining step is the kinetic deposition rate of the surface. It has been shown experimentally (44) that for large crystals (r> >50 micron) the overall mass transfer coefficient at high agitation rates is independent of size. For very small particles this assumption probably does not hold.

In the crystallization process the solute being crystallized must diffuse from the bulk of the solution to the solid-liquid interface of the crystal. At the interface a surface deposition occurs during which the solute becomes a part of the crystal lattice. If the solute diffusion resistance is less than the resistance offered by the surface reaction, the common simplified assumption "McCabe's ΔL law" holds. In a number of systems such as highly hydrated crystal $CuSO_4 \cdot 5H_2O$ (22) and $MgSO_4 \cdot 7H_2O$ (13), it has been observed that growth rate actually increases with increasing crystal size. A diffusion mechanism can be postulated to account for the violation of the McCabe's ΔL law in such a heavily hydrated system when both the water molecules and the solute ions must diffuse to the solid-liquid interface before being integrated in the crystal lattice. For these systems, diffusion resistance plays a large part in the determining the overall reaction rate.

Randolph (24) reported that the size-dependent growth rate affects the CSD in a manner qualitatively the same as size dependent product removal, both result in varying slope on a population density plot, depending on growth and/or removal rate at that size. Thus the question naturally arises, "Does size-dependent growth rate also destabilize CSD?"

Only a few limiting cases of system stability of such size-dependent growth rate have been studied. Sherwin et al. (34) predicted that increasing growth rate with increasing size raises the system stability limits. Their model assumed a growth rate which is linearly proportional to the crystal size. Aushus and Ruckenstein (2) made a first order correction for size-dependent growth and observed that the CSD stability region narrows when the growth rate is mass-transfer controlling, that is size dependent and inversely proportional to a power of the size (below the critical size) and size-independent for large sizes (greater than the critical size). Ishii and Randolph (16) studied the stability of class II MSMPR crystallizers when the growth rate is different below and above a certain critical size. They found a destabilizing effect caused by the size-dependent growth rate.

For an MSMPR crystallizer system with size-dependent growth rate, moment transformation usually cannot form a closed set of equations and the resulting characteristic equation is not a polynomial, thus the Routh test can not be applied. Here the Laplace transformation method will be used to derive the general formula for stability and two useful cases will be discussed. The first case is the system

having different growth rate below and beyond a critical size; the second case is a system which follows the Abegg, Stevens and Larson growth rate equation (1).

(A) Derivation of General Equations

All the assumptions used in Chapter II can still be applied here except the growth rate is not constant, and there is no fines trap.

The growth rate is now expressed as

$$G = G_o(c)\ R(r) \qquad (5\text{-}1)$$

where

$G_o(C) = k_g\ (C-C_s)^{\ell}$ = growth-rate concentration-dependent function

$R\ (r)$ = growth-rate size-dependent function

ℓ = constant

Here we discuss only the homogeneous nucleation model in the class I MSMPR crystallizer without a fines trap. The extension to a secondary nucleation model or an MSMPR crystallizer with a fines trap is straight forward.

(i) The Polulation Balance Equation and Mass Balance Equation

$$V \frac{\partial f}{\partial t} + V \frac{\partial}{\partial r} (Gf) = -qf, \quad r > 0 \tag{5-2a}$$

$$Gf = \varepsilon B, \quad r = 0 \tag{5-2b}$$

$$V \frac{d}{dt} \{(1-\varepsilon)\rho_s + \varepsilon C\} = qC_i - q\{C\varepsilon+(1-\varepsilon)\rho_s\} \tag{5-2c}$$

or $$V \frac{d}{dt} \psi = qC_i - q\psi$$

if $$\psi = (1-\varepsilon)\rho_s + \varepsilon C$$

The physical meanings of these equations and the notations used here are the same as in Chapter II except when specially noted. The boundary condition at size zero equates the generation of particles $\varepsilon B(C)$ to those grown away from the size zero as indicated by the term $Gf\ (0, t)$.

(ii) Steady State Solutions

Since we normalize the linearized equations about their steady state, a diversion to derive the steady state solutions is appropriate now. From Equations (5-2a), (5-2b) and (5-2c) letting $\frac{d}{dt} = 0$, the steady state solution will be

$$f^* = \frac{\varepsilon^* B^*}{G^*} \exp \{- \int_o^r \frac{dr}{\theta^* G^*} \} \tag{5-3a}$$

$$C_i^* = \psi^* \tag{5-3b}$$

(iii) Linearized Equations

It is assumed that a small disturbance is imposed on the crystallizer whose steady state performance is described by Eq. (5-3). The disturbance quantities are all assumed to be so small that the system may be completely linearized about the steady state value. (Steady state values are denoted by the superscript "*").

Thus, we write

$$f(t, r) = f^*(r) + \delta f(t, r) \tag{5-4a}$$

$$\psi(t) = \psi^* + \delta\psi(t) \tag{5-4b}$$

$$q(t) = q^* + \delta q(t) \tag{5-4c}$$

$$C_i(t) = C_i^* + \delta C_i(t) \tag{5-4d}$$

$$G(c, r) = G^* + \frac{\partial G}{\partial C}\,\delta C \tag{5-4e}$$

$$B(C) = B^* + \frac{\partial B}{\partial C}\,\delta C \tag{5-4f}$$

and also

$$\delta C = \frac{\delta\psi - (\rho_s - C^*)k\delta\mu_3}{1 - k\mu_3^*} \tag{5-5}$$

where δC_i, $\delta q(t)$ represents the imposed disturbance.

Substituting Eq. (5-4) into Eq. (5-2) and using steady state solutions, the following linearized equations can be found.

$$\frac{\partial \delta f}{\partial t} + \frac{\partial}{\partial r}(G^* \delta f) + \left[\frac{\partial G}{\partial C} \frac{\partial f^*}{\partial r} + f^* \frac{\partial}{\partial r}\left(\frac{\partial G}{\partial C}\right) \right]$$

$$x \frac{\delta\psi - (\rho_s - C^*) k \delta\mu_3}{1 - k\mu_3^*} = -f^* \frac{\delta q}{V} - \frac{q^*}{V} \delta f$$

$$r > 0 \qquad (5\text{-}6a)$$

$$G^* \delta f + \left(\frac{\partial G}{\partial C} f^* - \frac{\partial B}{\partial C} \varepsilon^*\right) \frac{\delta\psi - (\rho_s - C^*) k \delta\mu_3}{1 - k\mu_3^*} + B^* k \delta\mu_3 = 0$$

$$r = 0 \qquad (5\text{-}6b)$$

$$\frac{d\delta\psi}{dt} = \frac{1}{\theta^*} (\delta C_i - \delta\psi) \qquad (5\text{-}6c)$$

Now define the following dimensionless variables and parameters.

$$\delta f' = \frac{\delta f}{\frac{\varepsilon^* B^*}{G_o^*}}$$

$$\theta^* = \frac{V}{q^*}$$

$$t' = \frac{t}{\theta^*}$$

$$r' = \frac{r}{\theta^* G_o^*}$$

$$H = \frac{f^* G_o^*}{\varepsilon^* B^*}$$

$$\delta\psi' = \frac{\delta\psi}{(\rho_s - C^*)\varepsilon^*}$$

$$\delta C_i' = \frac{\delta C_i}{(\rho_s - C^*)\ \varepsilon^*} \qquad (5\text{-}7)$$

$$g_s = (\rho_s - C^*)\ \frac{1}{G_o^*}\ \frac{\partial G}{\partial C} = R\ (\rho_s - C^*)\ \frac{1}{G_o^*}\ \frac{\partial\ G_o}{\partial\ C} = Rg$$

$$b = \frac{1}{B^*}\ \frac{\partial B}{\partial C}\ (\rho_s - C^*)$$

$$g = (\rho_s - C^*)\ \frac{1}{G_o^*}\ \frac{\partial G_o}{\partial C}$$

Then Eq. (5-6) becomes

$$\frac{\partial \delta f'}{\partial t'} + \frac{\partial}{\partial r'}\ (R\delta f') + \left[g_s \frac{dH}{dr'} + H\ \frac{d}{dr'}(g_s)\ \right]$$

$$(\delta\psi' - \frac{k\mu_3^*}{\varepsilon^*}\ Z_3') = -\ H\delta q' - \delta f'$$

$$r' > 0 \qquad (5\text{-}8a)$$

$$R\delta f' + [g_s H - b]\left[\delta\psi' - \frac{k\mu_3^*}{\varepsilon^*} Z_3'\right]$$

$$+ \frac{k\mu_3^*}{\varepsilon^*} Z_3' = 0$$

$$r' = 0 \qquad (5\text{-}8b)$$

$$\frac{d\delta\psi'}{dt'} = \delta C_i' - \delta\psi' \qquad (5\text{-}8c)$$

Equations (5-8) are the linearized system equations and are independent of the growth rate form.

(iv) Stability Analysis

Now we assume that the only pertubation driving force is the supersaturation. Then we can set $\delta C_i' = 0$ and $\delta q' = 0$ in Eq. (5-8). Now taking the Laplace transform with respect to the reduced time t' reduces the partial differential equation to ordinary differential equations. These Equations (5-8) are transformed applying the initial conditions:

$$\delta f'(0) = 0$$

$$\delta\psi'(0) = 0$$

specifically, let,

$$\tilde{y} = \int_0^\infty y e^{-st'} dt'$$

= Laplace transform of the function y with respect to t'

Then

$$\frac{d}{dr'}\left(R\tilde{\delta f}'\right) + (S+1)\tilde{\delta f}' + \left(g_s\frac{dH}{dr'} + H\frac{dg_s}{dr'}\right)$$

$$\times\left(\tilde{\delta\psi}' - \frac{k\mu_3^*}{\varepsilon^*}\tilde{Z}_3'\right) = 0$$

$$r' > 0 \qquad (5\text{-}9a)$$

$$R\tilde{\delta f}' + (g_s H - b)\tilde{\delta\psi}' = (g_s H - b - 1)$$

$$\times\frac{k\mu_3^*}{\varepsilon^*}\tilde{Z}_3'$$

$$r' = 0 \qquad (5\text{-}9b)$$

$$(S+1)\tilde{\delta\psi}' = 0 \qquad (5\text{-}9c)$$

From Eq. (5-9c), we see that either $\tilde{\delta\psi}' = 0$ or $s = -1$, and since we are only interested in the system's stability we set $\tilde{\delta\psi}' = 0$. This leaves

$$\frac{d}{dr'}\left[R\tilde{\delta f}'\right] + (S+1)\tilde{\delta f}' =$$

$$\left[g_s\frac{dH}{dr'} + H\frac{d}{dr'}g_s\right]\frac{k\mu_3^*}{\varepsilon^*}\tilde{Z}_3'$$

$$r' > 0 \qquad (5\text{-}10a)$$

$$R\tilde{\delta f}' = (g_s H - b - 1) \frac{k\mu_3^*}{\varepsilon^*} \tilde{Z}_3'$$

$$r' = 0 \qquad (5\text{-}10b)$$

Solving Eq. (5-10) as an initial value problem in $\tilde{\delta f}'$ gives

$$\tilde{\delta f}' = \frac{k\mu_3^*}{R\,\varepsilon^*} \exp\left[-\int_0^{r'} \frac{S+1}{R}\, dy\right]$$

$$\times \left\{\int_0^{r'} \left[g_s \frac{dH}{dx} + H \frac{d}{dx} g_s\right] \exp\left[\int_0^{x} \frac{S+1}{R}\, dy\right] dx\right.$$

$$\left. + (g_s H - b - 1)\Big|_{r'=0}\right\} \tilde{Z}_3' = 0 \qquad (5\text{-}11)$$

where x and y are dummy variables, and

$$\tilde{Z}_3' = \frac{\varepsilon^* B^* \theta^{*4} G_o^{*3}}{\mu_3^*} \int_0^{\infty} \tilde{\delta f}' r'^3 dr' \qquad (5\text{-}12)$$

Letting

$$\alpha = 6kB^* \theta^{*4} G_o^{*3}$$

we find

$$\alpha g_s = \alpha \frac{(\rho_s - C^*)}{G_o^*} \frac{\partial G}{\partial C} = R\alpha \frac{(\rho_s - C^*)}{G^*} \frac{\partial G}{\partial C} = R g_c \qquad (5\text{-}13)$$

Substituting Eq. (5-11) into Eq. (5-12) and using Eq. (5-13) gives the characteristic equation of system (5-1).

$$\frac{\alpha}{6} \int_0^\infty \exp\left[-(S+1) \int_0^{r'} \frac{dy}{R(y)}\right] \frac{1}{R(r')}$$

$$\left\{\int_0^{r'} \left[g_s \frac{dH}{dx} + H \frac{d}{dx} g_s\right] \exp\left[(S+1) \int_0^x \frac{dy}{R(y)}\right] dx\right\}$$

$$r'^3 dr' + \frac{1}{6}(g_c RH - b_c)\Big|_{r'=0} \int_0^\infty \frac{1}{R(r')} \exp$$

$$\left[-(S+1) \int_0^{r'} \frac{dy}{R(y)}\right] r'^3 dr' = 1 \qquad (5\text{-}14)$$

Equation (5-14) is the general characteristic equation of the system (5-1). It exists for all size-dependent functions of R. If R = 1, Eq. (5-14) reduces to Eq. (3-16), with $\lambda = 0$; it is the characteristic equation for an MSMPR crystallizer with size-independent growth rate.

The stability of Eq. (5-14) can be studied by examining the pure imaginary roots $s = +i\phi$, and Eq. (5-14) can be rearranged as

$$\frac{1}{6}(g_c RH - b_c)\Big|_{r'=0} = \text{function}(\phi, R, H, g_c) \qquad (5\text{-}15)$$

Since all the kinetic parameters are real numbers, a trial-and-error search on ϕ is made until

$$\text{Im [function } (\phi, R, H, g_c) \text{]} = 0 \tag{5-16a}$$

and then

$$\frac{1}{6}\,(g_c\ RH - b_c)\,\Big|_{r'=0} = \text{Re [function } (\phi, R, H, g_c)] \tag{5-16b}$$

where

$$\text{Im [function } (\phi, R, H, g_c)]$$

$$= \frac{g_c}{(xH)^2+(xI)^2}\,\{(xL)(xH)-(xM)(xH)$$

$$+ \frac{6}{g_c}\,(xI) - (xJ)(xI) - (xK)(xI)\} \tag{5-17a}$$

$$\text{Re [function } (\phi, R, H, g_c)]$$

$$= \frac{g_c}{6}\,\{\frac{6}{g_c}\,(xH) - (xJ)(xH) - (xK)(xH)$$

$$- (xL)(xI) + (xM)(xI)\} \,/\, \{(xH)^2+(xI)^2\} \tag{5-17b}$$

and all the functions are defined as follows

$$(xH) = \int_0^\infty \frac{1}{R(r')}\ \exp\left(-\int_0^{r'} \frac{dy}{R(y)}\right)\ \cos\left(\phi\int_0^{r'} \frac{dy}{R(y)}\right)\ r'^3 dr' \tag{5-18a}$$

$$(xI) = \int_0^{\infty} \frac{1}{R(r')} \exp\left(-\int_0^{r'} \frac{dy}{R(y)}\right) \sin\left(\phi \int_0^{r'} \frac{dy}{R(y)}\right) r'^3 dr' \tag{5-18b}$$

$$(xJ) = \int_0^{\infty} \frac{1}{R(r')} \exp\left(-\int_0^{r'} \frac{dy}{R(y)}\right) \cos\left(\phi \int_0^{r'} \frac{dy}{R(y)}\right)$$

$$\int_0^{r'} \left(R \frac{dH}{dx} + H \frac{dR}{dx}\right) \exp\left(\int_0^{x} \frac{dy}{R(y)}\right) \cos\left(\phi \int_0^{x} \frac{dy}{R(y)}\right)$$

$$dx r'^3 dr' \tag{5-18c}$$

$$(xK) = \int_0^{\infty} \frac{1}{R(r')} \exp\left(-\int_0^{r'} \frac{dy}{R(y)}\right) \sin\left(\phi \int_0^{r'} \frac{dy}{R(y)}\right)$$

$$\int_0^{r'} \left(R \frac{dH}{dx} + H \frac{dR}{dx}\right) \exp\left(\int_0^{x} \frac{dy}{R(y)}\right)$$

$$\sin\left(\phi \int_0^{x} \frac{dy}{R(y)}\right) dx r'^3 dr' \tag{5-18d}$$

$$(xL) = \int_0^{\infty} \frac{1}{R(r')} \exp\left(-\int_0^{r'} \frac{dy}{R(y)}\right) \sin\left(\phi \int_0^{r'} \frac{dy}{R(y)}\right)$$

$$\int_0^{r'} \left(R \frac{dH}{dx} + H \frac{dR}{dx}\right) \exp\left(\int_0^{x} \frac{dy}{R(y)}\right)$$

$$\cos\left(\phi \int_0^{x} \frac{dy}{R(y)}\right) dx r'^3 dr' \tag{5-18e}$$

$$(xM) = \int_0^{\infty} \frac{1}{R(r')} \exp\left(-\int_0^{r'} \frac{dy}{R(y)}\right) \cos\left(\phi \int_0^{r'} \frac{dy}{R(y)}\right)$$

$$\int_0^{r'} \left(R \frac{dH}{dx} + H \frac{dR}{dx}\right) \exp\left(\int_0^{x} \frac{dy}{R(y)}\right)$$

$$\sin\left(\phi \int_0^{x} \frac{dy}{R(y)}\right) dx r'^3 dr' \qquad (5\text{-}18f)$$

If the growth rate model is given, and the values of R and H are known functions of r' only, from Eq. (5-16b), the nucleation sensitivity parameter can be found for a given value of g_c.

All the calculations were made on a digital computer. The computer programs are shown in Appendix C.

(B) Case Study Results and Discussion

(i) The growth rate is defined as

$$G = G_o (C) (1 + a r) \qquad r \leq r_c$$

$$= G_o (C) \qquad r > r_c \qquad (5\text{-}19)$$

If McCabe's ΔL law does not hold, one of the simplest equation to describe the relationship between the growth and the size is the linear equation

$$G = k_g (C - C_s)^{\ell} (1 + a r) \qquad (5\text{-}20)$$

Unfortunately a continuous MSMPR crystallizer with this growth rate is mathematically not possible (1), but due to the simple form and easy mathematical calculation and data fitting, it still appears very often in the literature (such as by Canning and Randolph (43), Sherwin et al. (34), Randolph and Larson (28), Chang and Epstein (4)).

In actuality for small crystals the crystal growth rate is usually size dependent and beyond certain critical size, the growth rate obeys McCabe's ΔL law (44). Garside and Jancic (9) proposed the two region growth rate model in which the population density and the growth rate are not continuous at critical size but the number flux will be continuous at that size. We can find the growth rate equation described by Eq. (5-19) satisfies the requirement that the number flux is continuous at the critical size r_c. Letting $r_c' = r_c/\theta^* G_o^*$, $a' = a\theta^* G_o^*$, the growth rate Eq. (5-19) is shown graphically in Fig. 5-1.

Fig. 5-2 plots the ratio of critical sensitivity nucleation to the sensitivity growth rate parameter b_c/g_c as a function of dimensionless critical size r_c' at which a sudden change in growth rate occurs. The plot is for $g_c = 100$ with a' as the parameter. As r_c' approaches zero the stability limit approaches the MSMPR stability limit at the given g_c value. Note that the CSD is stabilized if the growth rate change occurs at a size less than $\theta^* G_o^*$. Thus the phenomena of slow-growing fines in many systems (44) would be expected to stabilize the system. This result also proves the fact that the fines trap destabilizes the system, because the fines trap withdraws the fines and dissolves them, then recycles the pure solution to the system, so

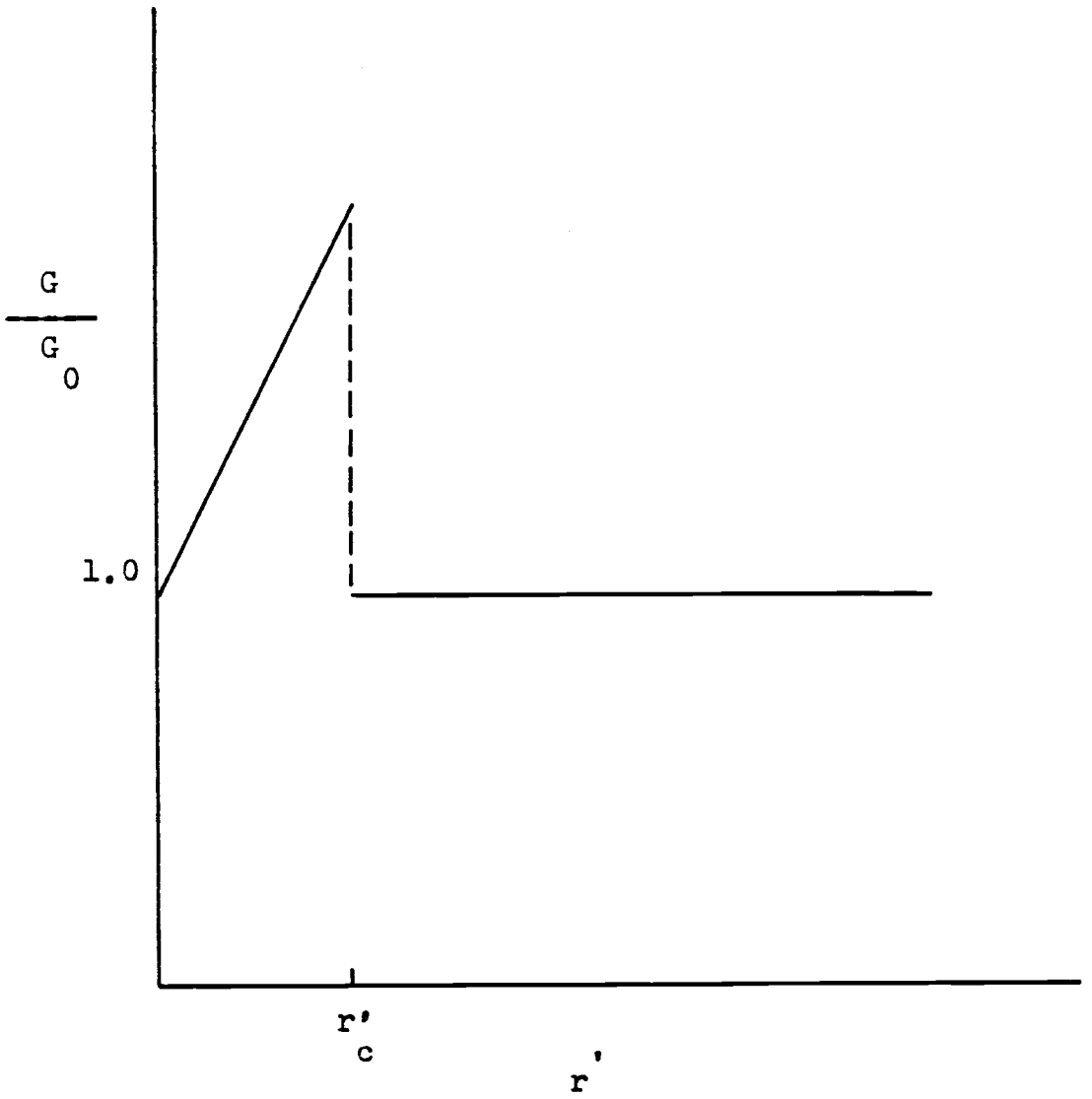

Fig.5-1. Diagram of size-dependent growth rate.

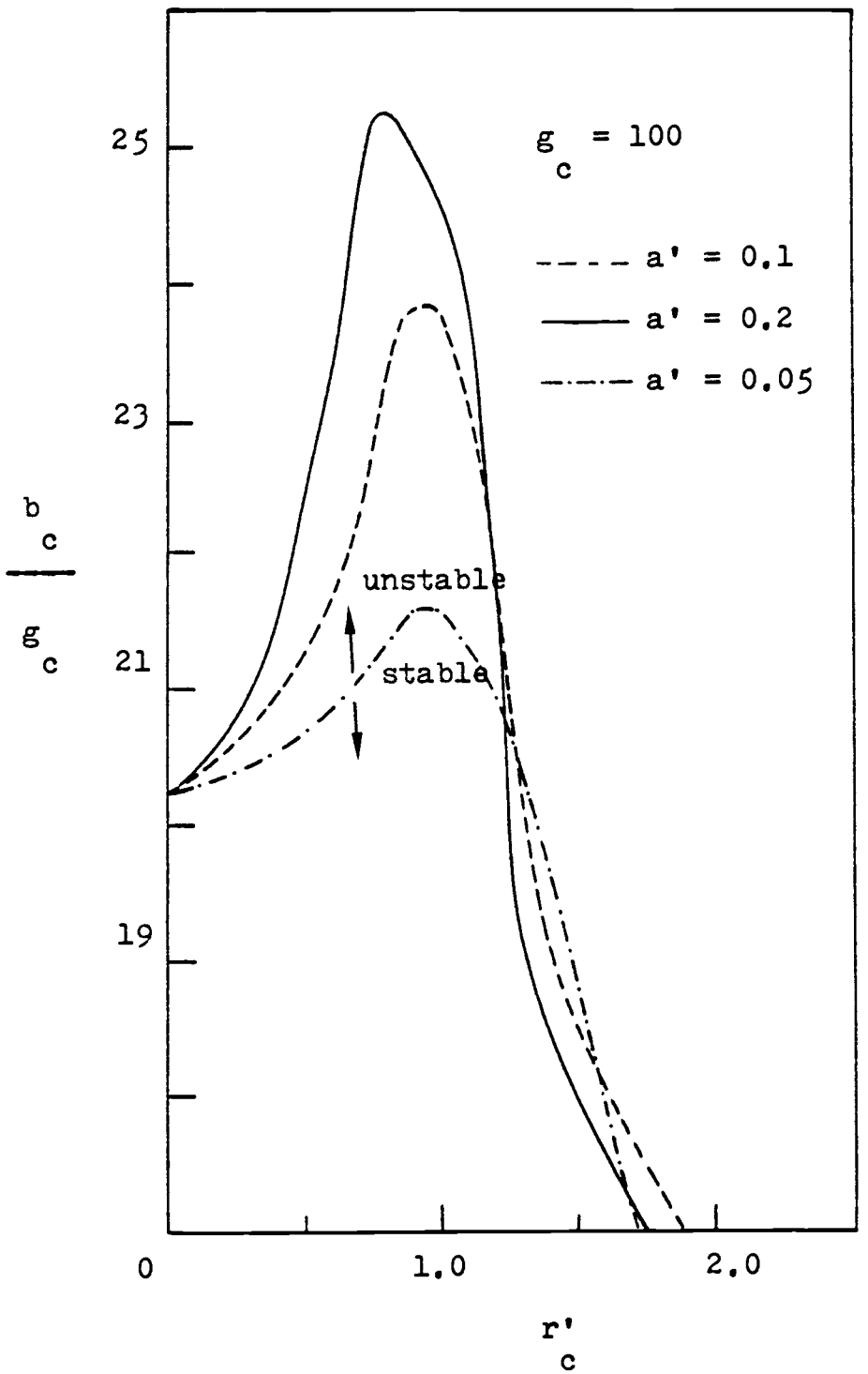

Fig. 5-2. Stability regime for various growth rate parameters.

the net effect is a decrease of fine crystals. In this way the system becomes more unstable as was shown in Chapter III. The greater the value of a $\theta^* G_o^*$, and the smaller the critical size, the more stable the system will be. If, however, the growth rate changes at size greater than about 1.2 $\theta^* G_o^*$, a significant destabilizing effect is predicted.

The latter result is similar to the CSD destabilizing effects of product classification (24). Accelerated product removal and decreasing growth rate gives a similar effect on CSD, but the decreasing growth rate produces more destabilizing than accelerated product removal. As r_c' becomes greater, the b_c/g_c value will become nearly flat (not shown in Fig. 5-2), and the destabilizing effect is very apparent.

Fig. 5-3 shows the effect of g_c on b_c/g_c and $a'=0.1$ for various values of r_c'. It shows that the value b_c/g_c increases as g_c increases and approaches an asymptotic value when g_c becomes very large.

(ii) The growth rate is expressed as

$$G = G_o(C)\ (1 + ar)^m \qquad m < 1 \qquad (5\text{-}21)$$

This is one of the empirical equations describing the effect of crystal size on the growth rate. A good discussion of size-dependent growth rate equations is given by Abegg et al. (1) and White et al. (38). Perhaps the most popular and satisfactory equation among them is the equation proposed by Abegg, Stevens and Larson (1) (the ASL equation). The ASL equation can be written in the form of Eq. (5-21). If the growth rate of nuclei is expressed as $G_o = k_g(C-C_s)^{\ell}$, then

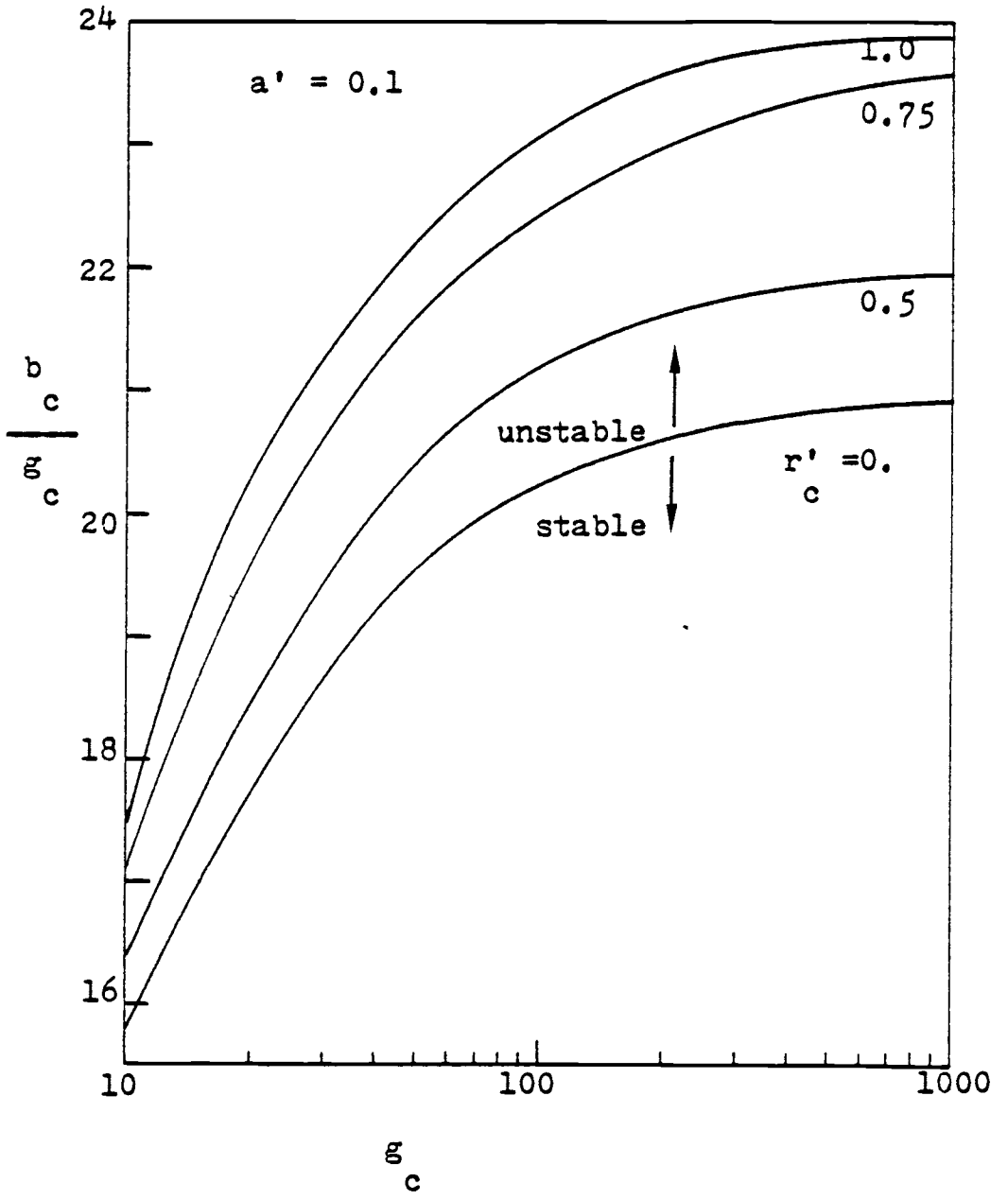

Fig.5-3. Asymtotic stability limit of size-dependent growth rate.

$G = k_g (C-C_s)^{\ell}(1 + a\ r)^m$ is an empirical relationship which may be used to correlate the effects of supersaturation and crystal size on the growth rate by the non-linear least squares fitting.

Fig. 5-4 shows the graphical representation of Eq. (5-21). The growth rate increases as r increases without asymptotic behavior if m is a positive value but the growth rate value is limited by the line $m = 1$; if the value of m is negative, the growth rate decreases as r increases and approaches the asymptotic value of zero.

Garside and Jancic (8) used the ASL equation successfully to fit the experimental data and showed that the kinetic parameter m depends on the crystallizer volume.

Now consider the destabilizing effect due to the size-dependent growth rate.

Fig. 5-5 show the stability limit at $g_c = 100$ as the function of m with parameter a'. If $m = 0$ or $a' = 0$, the critical stability limit approaches the value $b_c/g_c = 20.24$ which is the stability limit for size-independent MSMPR crystallizer. The b_c/g_c value is a monotonic function of m but not a monotonic function of a', if the value of m is fixed. For some values of a', the b_c/g_c value increases with increasing a'; but for other values of a', the b_c/g_c values increase and then decrease with increasing a'. This fact can be seen more clearly as we plot b_c/g_c vs a' using m as the parameter. In Fig. 5-6, as a' approach zero the value of b_c/g_c approach the limiting value at $g_c = 100$; if a' is less than 0.2, with positive value of m, then the bigger the m, the more stabilized the system;

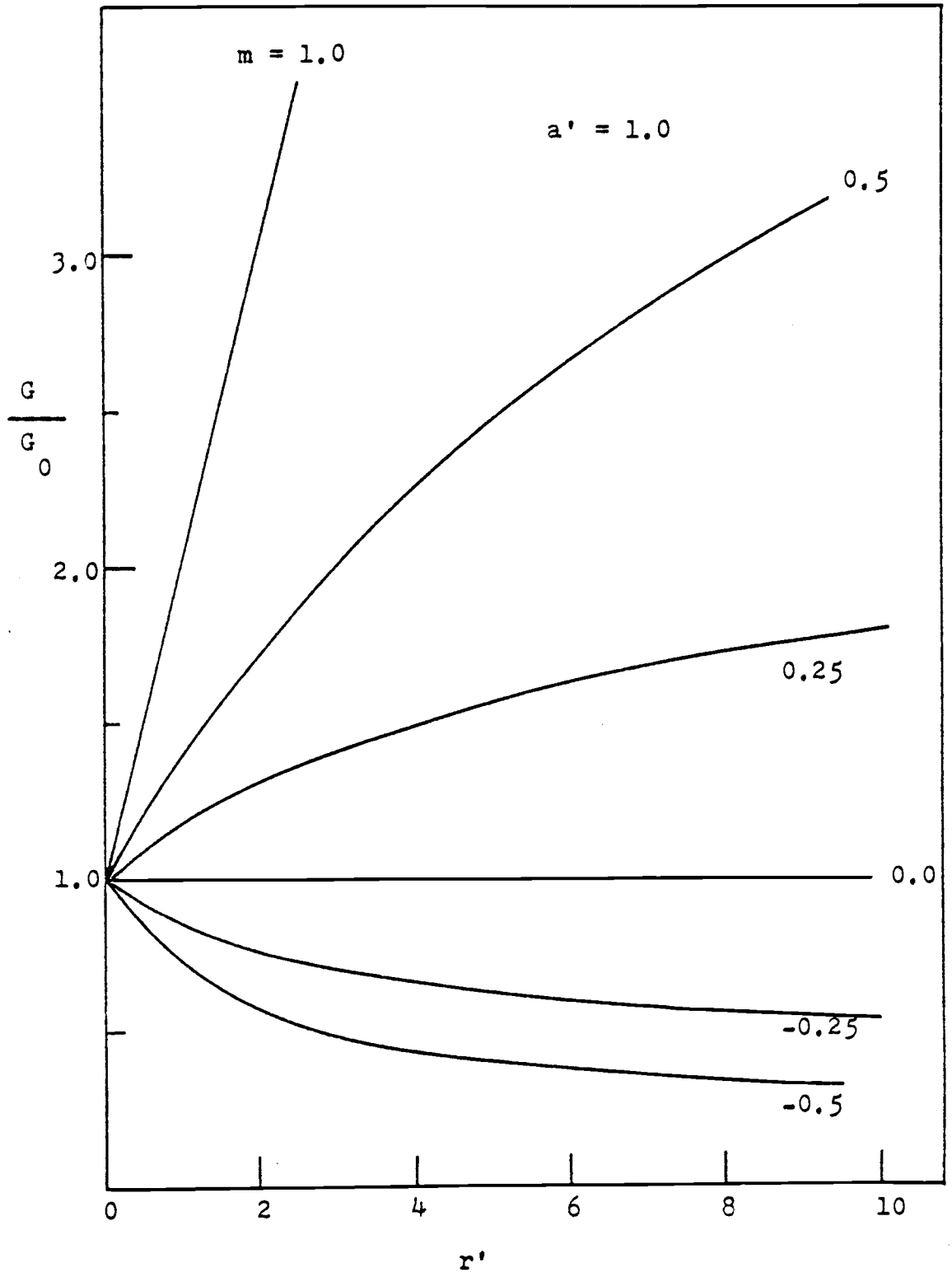

Fig.5-4. Diagram of ASL growth rate equation.

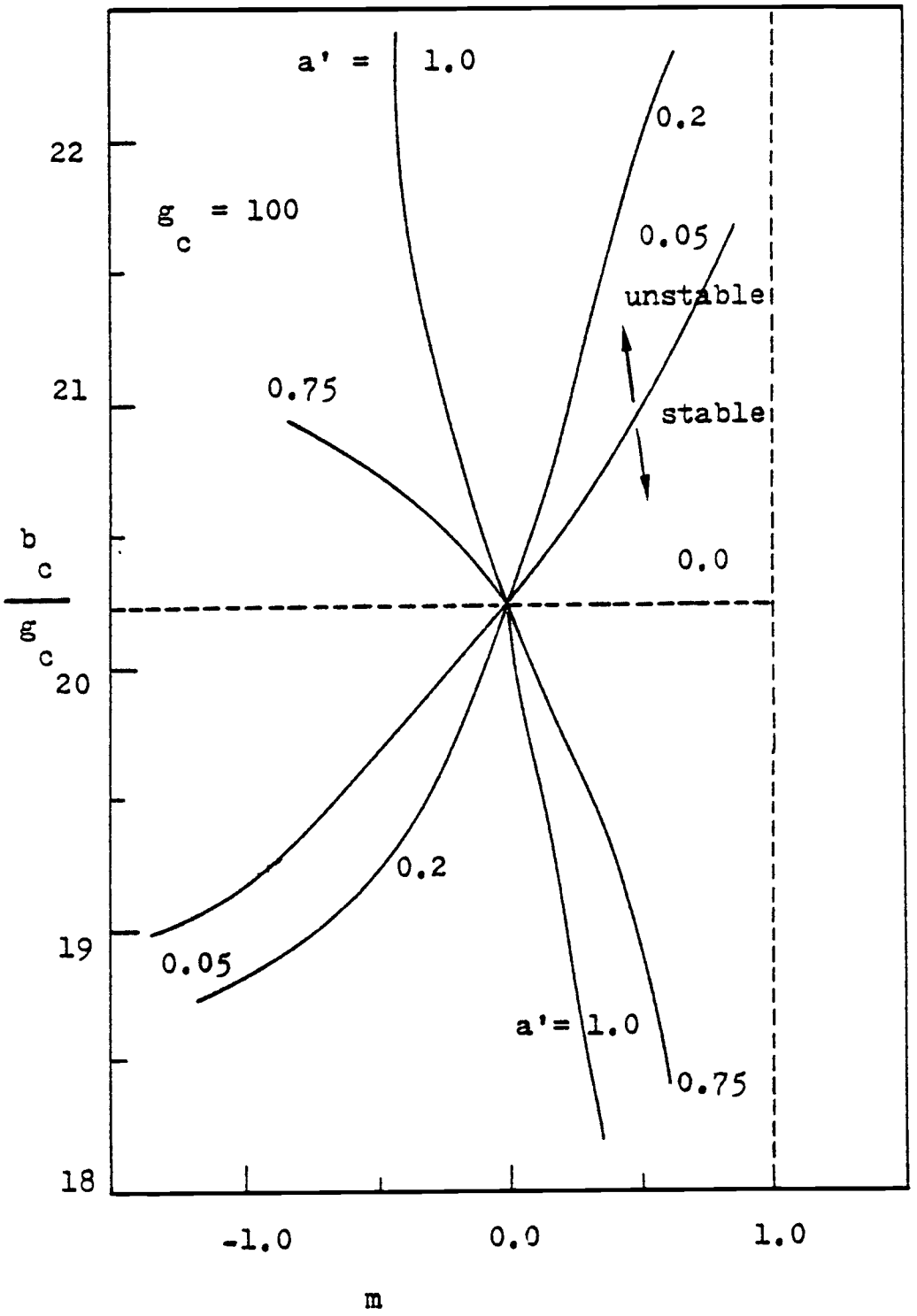

Fig.5-5. Stability regime of ASL growth rate model.

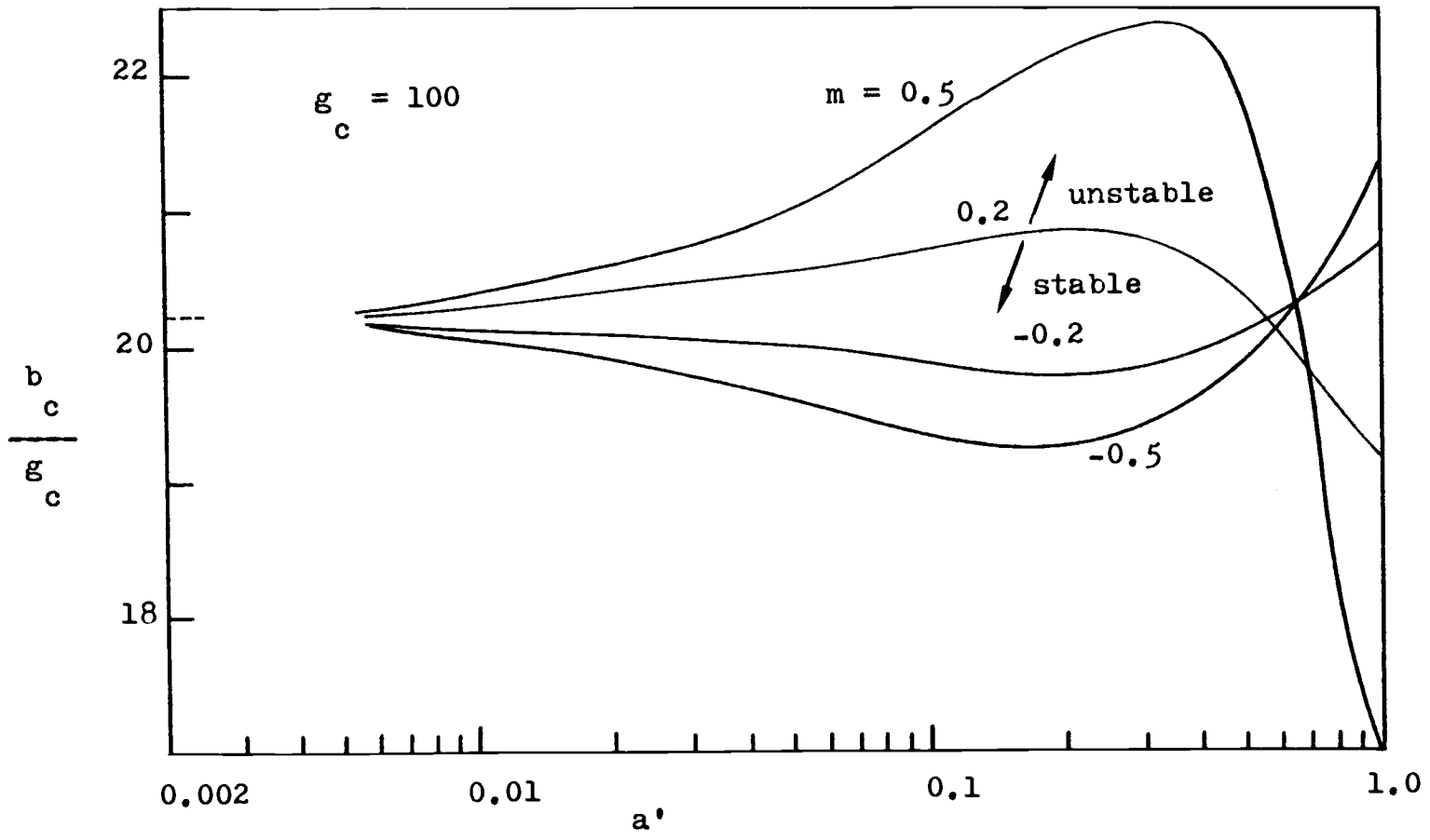

Fig.5-6. Effect of m on stability regime of ASL growth rate model at g_c = 100.

if m is a negative value, the smaller the m, the more destabilized the system. But for a' greater than about 0.4, the stabilizing effect becomes reversed, the greater the m value (positive m value), the more is the destabilizing effect; and also the smaller the m value (negative m value), the more is the stabilizing effect.

Users of the ASL equation often assume a' = 1 (or define $a = 1/\theta^* G_o^*$) in Eq. (5-21) to reduce the two parameters system to one parameter m for simple calculation. When the size-dependent growth rate system is handled in industrial crystallizers, the tendency to produce wider size distribution may well make the operation somewhat more difficult than usual. This is observed by Garside and Jarcic (8) without explanation. The main reason is largely due to destabilized system near a' = 1.

Figure 5-7 shows the stability limit b_c/g_c with various parameters a' = 0.1 and m as the function of g_c. When g_c become very large the value of b_c/g_c approaches asymptotically a certain limiting value.

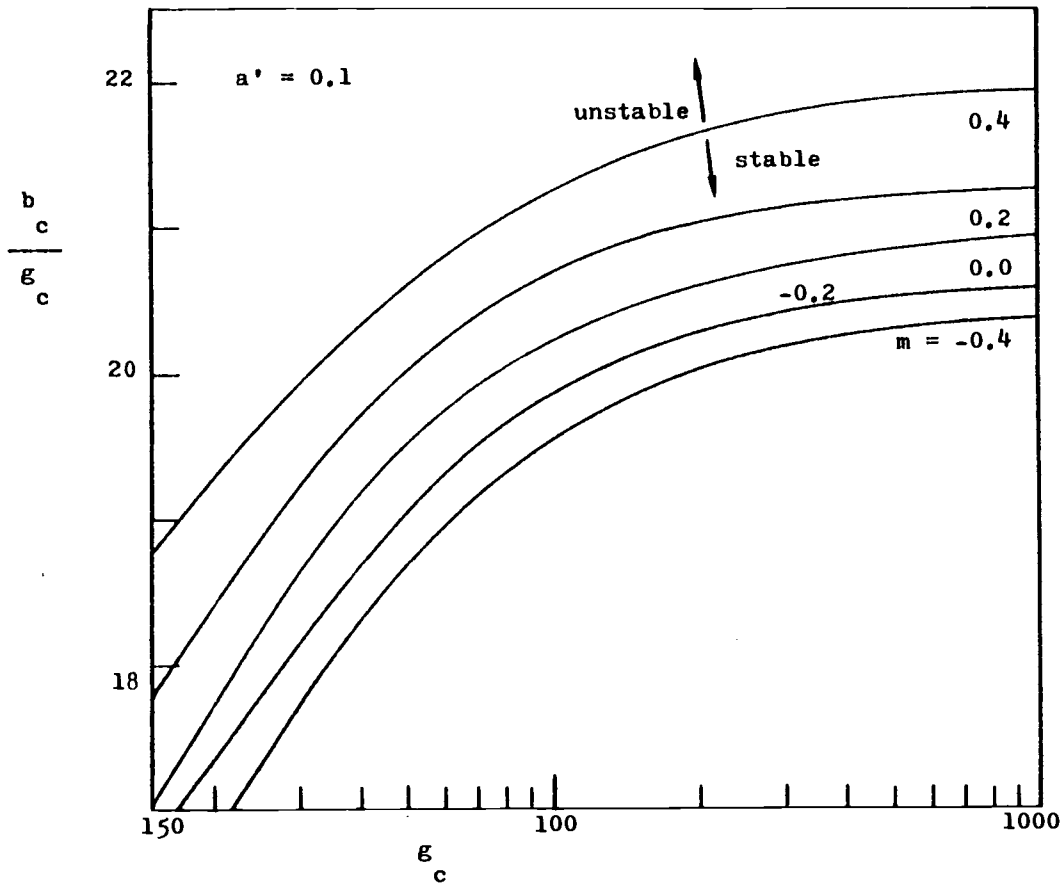

Fig.5-7. Asymtotic stability limit of ASL growth rate model at a' = 0.1.

CHAPTER VI. ON-LINE MEASUREMENT OF PARTICLE SIZE DISTRIBUTION

From Chapter IV we found that modal control is a useful tool to control a continuous MSMPR crystallizer, but whatever control algorithm is employed, a necessary requirement is for an on-line instrument to measure the state of the system. This means measuring the crystal size distribution (CSD).

There are two such devices available in the market, one is a small orifice zone-sensing instrument; the other is a laser light scattering analyzer.

Rovang and Randolph (33) described the zone-sensing device. They made measurement using an on-line Coulter Counter in the fines dissolving loop of a laboratory KCl crystallizer, and they predicted the growth and nucleation data by regression of the CSD data by an on-line real-time mini-computer. But the zone-sensing instrument has some disadvantages: first the small orifice is easily blocked by the particles; and second is the problems due to the electrical noise caused by the flow of conducting fluid.

Randolph et al. (31), using a Leeds and Northrup Microtrac forward low-angle laser light scattering particle analyzer, developed an on-line particle size analysis technique to monitor the laboratory KCl crystallizer. The measured size distribution was analyzed on-line to give running measures of the growth and nucleation rate in the crystallizer. The light scattering instruments have relatively poor precision which requires statistically averaging over thousands of particles. They

concluded that the instrument has considerable potential for monitoring and control of CSD.

Because both the zone-sensing instrument and the laser light scattering analyzer are very expensive, we developed an inexpensive and easy method for on-line measuring of the CSD and monitoring of the crystallizer performance, using an impact type transducer. Up to now due to some mechanical difficulties existing in the transducer we can not measure very fine particles. But the device is inexpensive, only about one-tenth the cost of zone-sensing equipment (the laser analyzer would be more expensive), and still has considerable potential for use in monitoring and control of a crystallizer. A comparison of these three devices is shown in Table 6-1.

(A) Experimental Equipment and Instrumentation

The components used to measure the particle size are shown schematically in Fig. 6-1. They include:

1. Transducer,
2. Test flow tube,
3. Amplifier, and
4. Recording system.

Each of these items will be discussed in detail below.

1. Transducer

A sewing needle shortened to a length of about 25 mm with a diameter of about 300 μ and a phonograph stereo cartridge comprise the

Table 6-1 Comparison of On-line Measurement Equipments

	Cost	Measurable size range	Measuring time	Electrolyte required	Accuracy	Sample required	Size identification method
Coulter Counter	10,000 (a)	20-1600 μ (b)	1-10 min.	yes	(c)	5-15 mg	Statistical method
Laser light scattering analyzer	100,000	0.1-1000 μ (b)	1-2 min	no	(c)	5-50 mg	Statistical method
This work (impact transducer)	1,000 (a)	above 10 μ (b)	depend on particles feeding rate	no	(d)	(e)	Measure the particle size one by one

(a) It does not include recording system or mini-computer.

(b) The equipment should change some parts for whole range measurement.

(c) Not available.

(d) Each particle can be identified accurately, the accuracy of size distribution increase with increasing the number of particles measured.

(e) Need about one thousand particles.

Equipment assembly:

(a) Test flow tube
(b) Trap
(c) Rotameter
(d) Valve
(e) Sewing needle
(f) Amplifier
(g) Oscilloscope
(h) Instrument tape recorder
(i) Oscillographic recorder
(j) Overflow line
(k) Tone arm
(l) Rubber membrane
(m) Particle inlet port

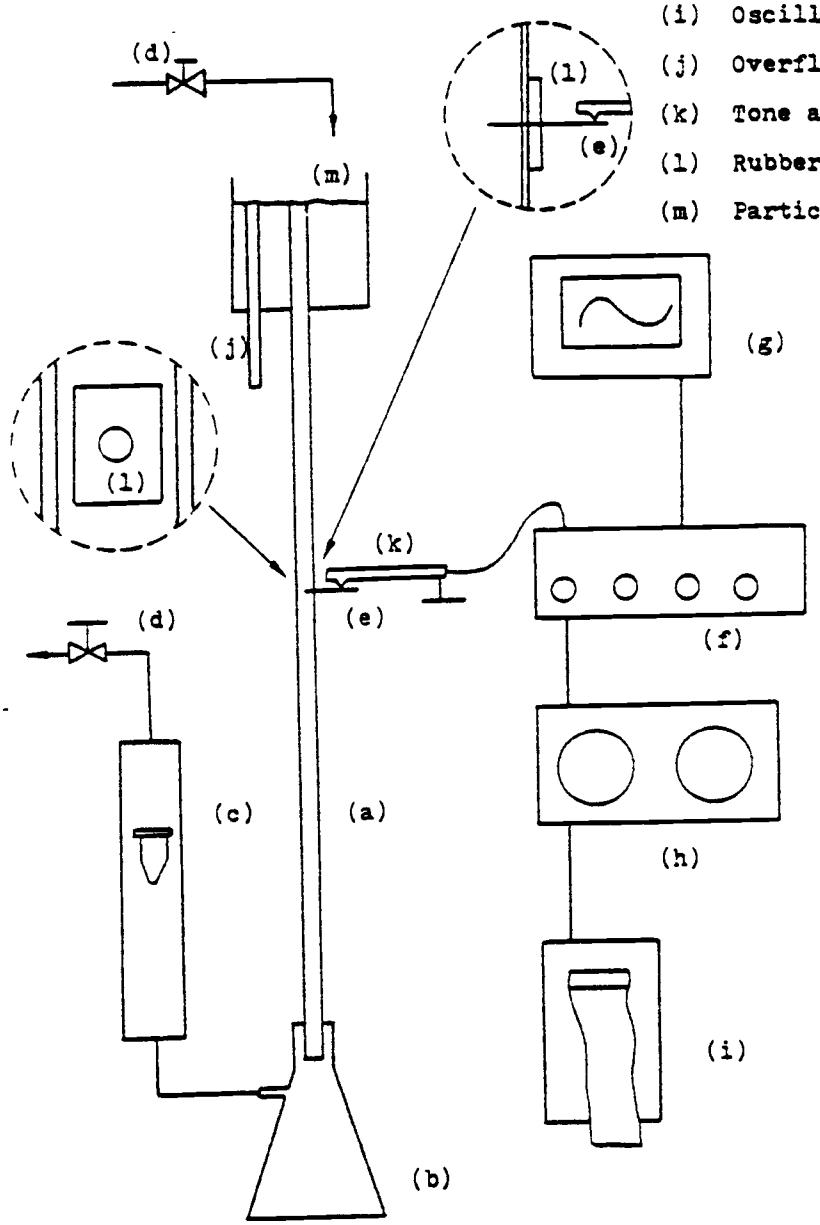

Fig.6-1. Schematic diagram of experimental apparatus.

transducer. The needle is inserted through a rubber membrane with half the needle inside the flow channel, and with the eye outside. The phonograph cartridge rests with its stylus in the needle eye. The needle is chosen so that its eye fits the cartridge stylus. The phonograph stereo cartridge used is a moving coil cartridge (Ortofon MC 10).

The momentum of a particle impacting the needle will give rise to the signal by hitting the needle and this signal is transmitted through the vibration of the cartridge stylus and transformed into an electrical signal.

2. Test Flow Tube

The test flow tube is a 10 mm ID, 1000 mm long glass tube and its structure is shown in Fig. 6-2. There is a 2 mm diameter hole on the middle of the test tube wall. This hole is covered by a thin piece of rubber. The sewing needle protrudes through the rubber into the center of the tube and is supported by the rubber. The rubber thickness is so chosen that where the needle is just supported in the horizontal position. The cartridge was held by a tone arm and positioned with the sewing needle eye and the tone arm in a horizontal position as shown in Fig. 6-1. The upper part of the flow tube is equipped with an overflow pipe so that the water level in test tube is kept constant. The particles are carried downward by water (or by gravity) through the flow tube into the collecting bottle. All particles are collected in this bottle, and the water goes through the rotameter and drains.

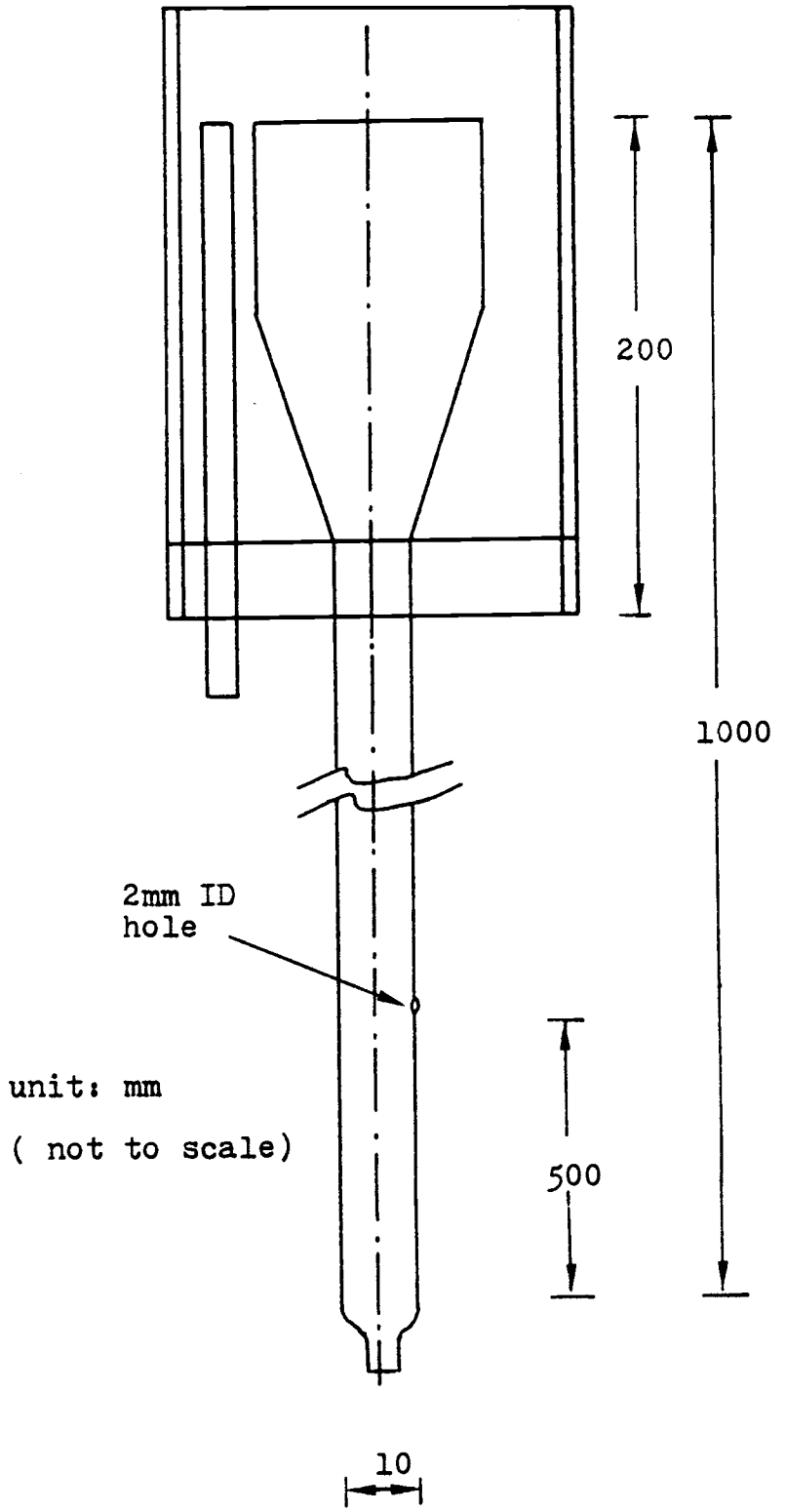

Fig.6-2. Schematic diagram of test flow tube.

3. Amplifier

The amplifier used in the experiment was a Yamaha C-6 natural sound control pre-amplifier.

4. Recording System

The signal output from the preamplifier was monitored by a oscilloscope and recorded by a instrument tape recorder. The instrument recorder used was a Hewlett Packard model 3960A. The signal was recorded at higher speed (15 in/sec) and played back slowly (15/16 in/sec) to an oscillographic recorder (Hewlett Packard model 7402) for recording.

(B) Experimental Procedure

The experimental procedures used to acquire the data is described below.

1. The particles to be measured were mixed with water to make a slurry which was then sucked into a 1 ml syringe.

2. The syringe was put into the test tube inlet port, letting the particles flow out from the syringe and flow down the tube smoothly with the flowing water. Some of the particles hit the needle and give rise to the signal which was then recorded.

(C) Theory

We can consider the probe (or the sewing needle) as an infinitely long cylinder. When the particles carried by the fluid approach the cylinder, due to the effect of inertia, the particles change their loci from the fluid streamline. Some particles will attain the surface of

cylinder and some will miss the cylinder depending on their initial position and their size. When the particles attain the surface of cylinder, the change in momentum of the particles gives rise to the signal. Diffusion affects only very small particles (particle size less than 10 micron), therefore the signal obtained by the probe is caused by the interception and inertia effect. The interception and inertia effects are shown graphically in Fig. 6-3. In Fig. 6-3 (a) the inertia effect is illustrated, far upstream of probe the particle has the same velocity as the fluid. The particle follows the streamline of the fluid, until the particle approaches the cylinder. Then, due to inertia the locus of the particle motion will be different from the fluid streamline and the particle may attain the cylinder. In Fig. 6-3 (b) the interception effect is illustrated. In this the particles follow the fluid streamline even close to the probe (Stokes' number equals zero). In this case, the particle attains the cylinder if its radius is larger than the distance which separates the streamline from the cylinder.

The stereo phonograph cartridge has two perpendicular channels and each channel can be considered as a spring and dashpot assembly. The two spring and dashpot assemblys are used to model the system as shown in Fig. 6-4 (a). The mass of the cylinder is distributed to each assembly as mass M. If the particle hits the position P, due to symmetry the signal in each channel is the same; but if the particle does not hit the position P the signal in each channel will be different and the magnitude depends on the position where the particle hit the cylinder.

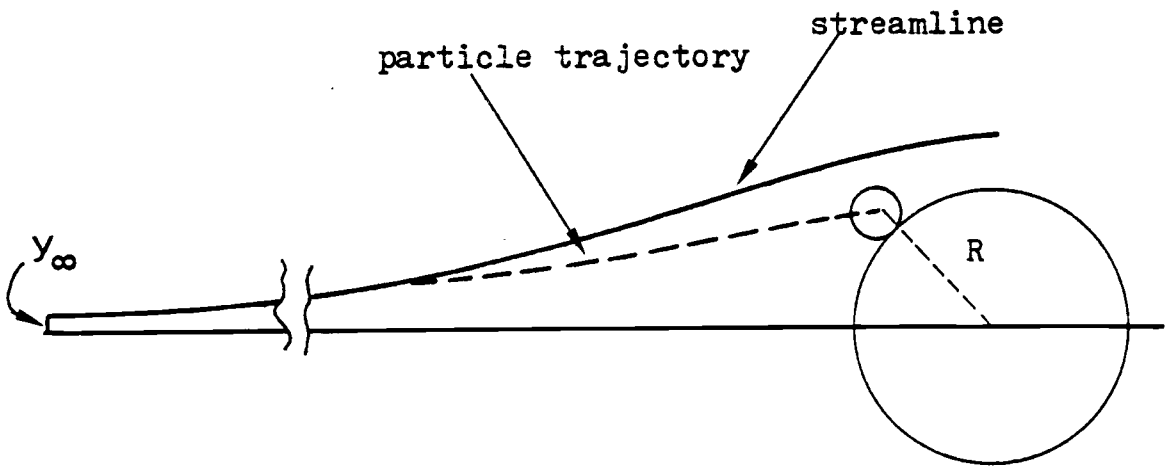

(a) Inertia effect

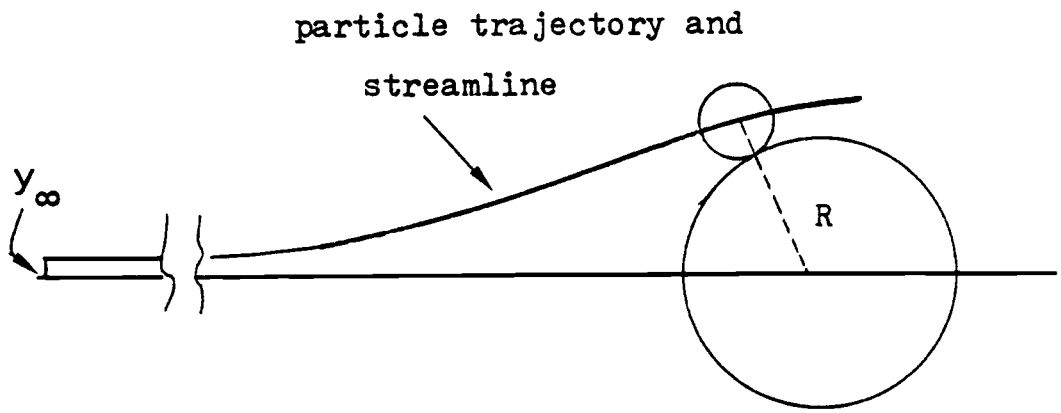

(b) Interception effect

Fig.6-3. Particle trajectory in flow field.

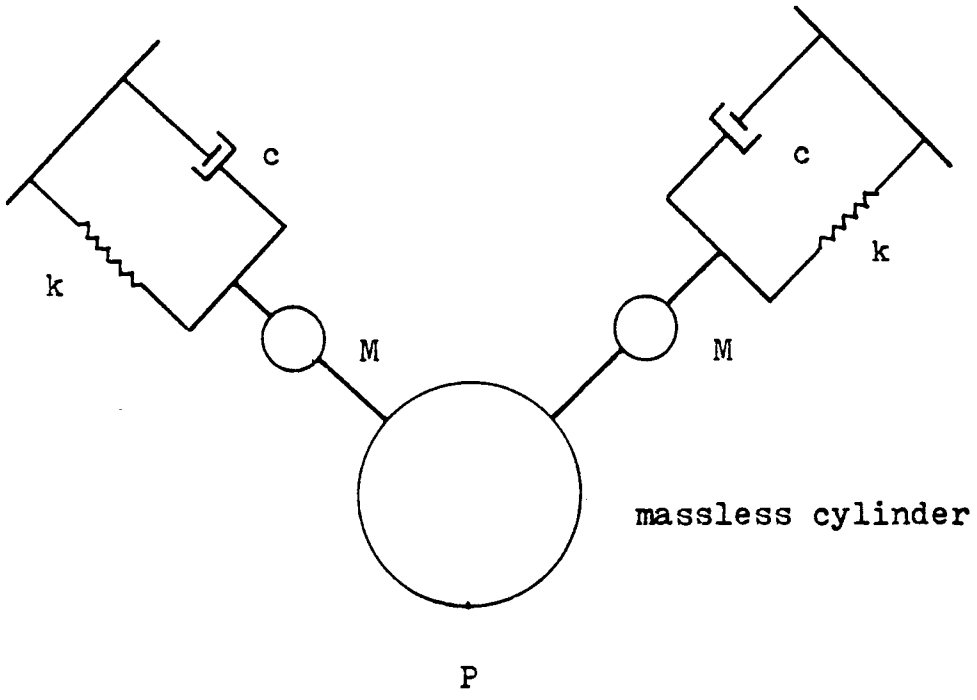

(a)

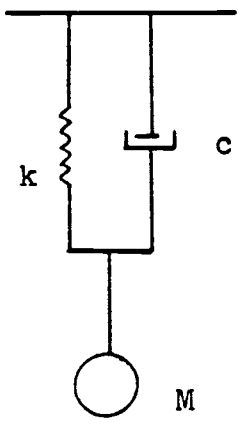

(b)

Fig.6-4. System model.

For each channel, the simple model shown in Fig. 6-4 (b) is equivalent to a second order system and the system equation can be written as (45):

$$M \frac{d^2y}{dt^2} + c \frac{dy}{dt} + ky = F(t) \qquad (6\text{-}1a)$$

$$y(0) = 0 \qquad (6\text{-}1b)$$

$$y'(0) = 0 \qquad (6\text{-}1c)$$

$$F(t) = \frac{mu}{\Delta t} \{U_o(t) - U_o(t-\Delta t)\} \qquad (6\text{-}1d)$$

where

M, c, k = system constants: they represent mass, friction and the spring constant

m = mass of particle (gm)

u = velocity of particle when it hits the cylinder (cm/sec)

y = displacement of system (cm)

t = time (sec)

$U_o(t)$ = unit step function

Δt = contact time between cylinder and particle, that is the time between when the particle hits the stylus and when the particle finally leaves the cylinder. Fig. 6-5 shows this condition: the particle hits the cylinder and travels down the surface of the cylinder until finally it leaves the cylinder.

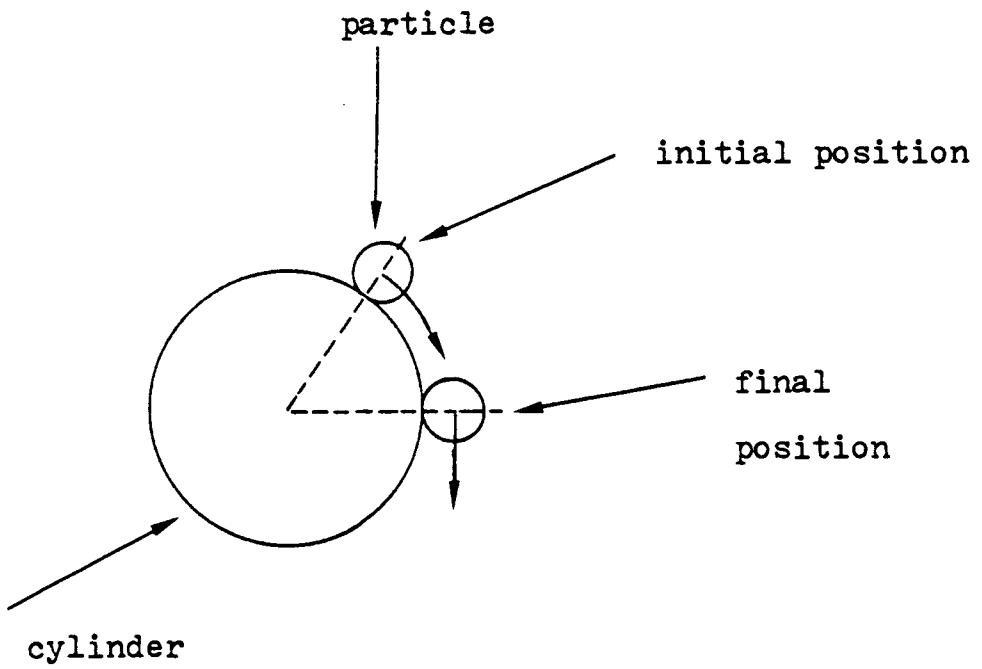

Fig.6-5. Contact pattern between particle and cylinder.

Eq. (6-1d) shows the force acting on the system, if the contact time is small then Eq. (6-1d) can be written as

$$F(t) = mu\ \delta_0(t) \tag{6-1e}$$

where $\delta_0(t)$ represents the unit impulse function.

Usually the cartridge is designed for critical damping and for this condition Eq. (6-1) gives

$$y = \frac{mu}{M} t\ e^{pt} \tag{6-2a}$$

$$p = \frac{c}{-2M} \tag{6-2b}$$

For maximum displacement, we found

$$y_{max} = \frac{2mu}{c} e^{-1} \tag{6-3}$$

Since the recording system records the electrical signal in volts the electrical signal E (volts) will be

$$E = m\ u\ i \tag{6-4}$$

where i is a conversion factor which is determined by calibration with using mono-size particles at a known velocity.

The signal from each channel would be $E_1 = m\, u_1\, i$, or $E_2 = m\, u_2\, i$. By using the geometrical relationship the particle mass m (or particle size) can be determined as described below.

If the particle does not hit at the center position, the two signals E_1 and E_2 will be different. As shown in Fig. 6-6, the velocity vector at the impact point P is u, and this vector u can be resolved into u_T and u_N; the component u_T is in the tangential direction to cylinder and has only a small effect on the motion of the cylinder. For simplicity the frictional force is assumed to be zero and thus, only the vector component in the centripetal direction causes a signal. This component u_N can also be resolved into components in the signal channel direction. (see Fig. 6-6(b)). The angle between channels is 90°; hence

$$u_N = \sqrt{u_1^2 + u_2^2} \qquad \text{and}$$

$$(E_1^2 + E_2^2)^{\frac{1}{2}} = m\, u_N\, i \tag{6-5}$$

The u_N value must be found from the flow condition. The relationship between u_N and the mass of the particle depends on where the particle hits the cylinder. The angular position of impact is given by

$$\theta = 45^{\circ} - \tan^{-1}\left(\frac{u_1}{u_2}\right)$$

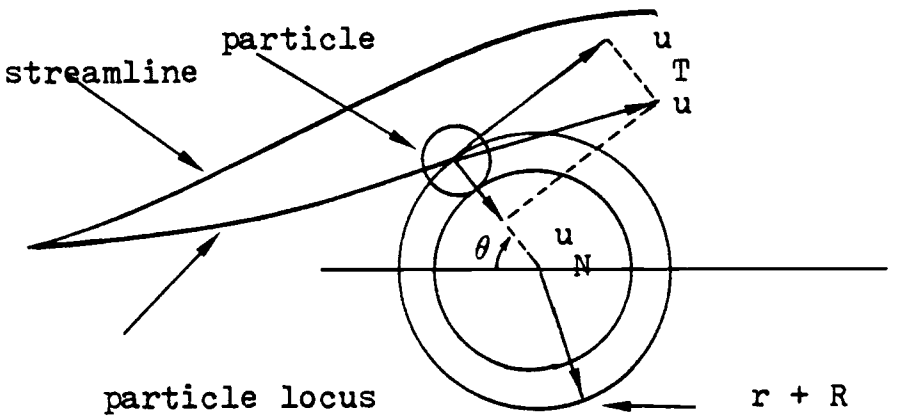

(a)

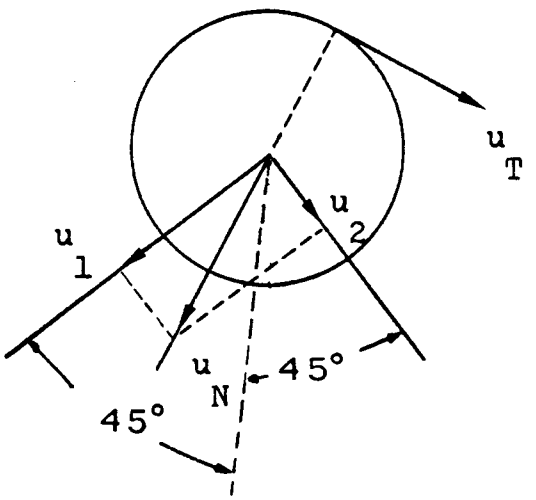

(b)

Fig.6-6. Velocity component at the point of impaction.

(D) Equation of Motion of Particles in the Flow Field

If the fluid is in steady state motion and the particle is sufficiently small to allow the use of the Stokes formula for drag force, then by the Newton's law of motion, the trajectories of particles in the flowing fluid can be written as

$$m \frac{du_x}{dt} = -6 \pi \mu r (u_x - v_x) \qquad (6\text{-}6a)$$

$$m \frac{du_y}{dt} = -6 \pi \mu r (u_y - v_y) \qquad (6\text{-}6b)$$

since

$$u_x = \frac{dx}{dt} . \qquad u_y = \frac{dy}{dt}$$

Let us define the following dimensionless variables

$$x' = \frac{x}{R}$$

$$y' = \frac{y}{R}$$

$$t' = \frac{u_\infty t}{R}$$

$$v_x' = \frac{v_x}{u_\infty}$$

$$v_y' = \frac{v_y}{u_\infty}$$

where:

u_x, u_y = particle velocity in x and y direction respectively

v_x, v_y = fluid velocity in x and y direction respectively

m = mass of particle

r = radius of particle

μ = viscosity of fluid

R = reference length (= radius of cylinder)

u_∞ = upstream fluid velocity

x, y = linear length

then we get the dimensionless equations.

$$St \frac{d^2x'}{dt'^2} + \frac{dx'}{dt'} - v_x' = 0 \qquad (6\text{-}7a)$$

$$St \frac{d^2y'}{dt'^2} + \frac{dy'}{dt'} - v'_y = 0 \qquad (6\text{-}7b)$$

$$St = \frac{2r^2\rho_s u_\infty}{9\mu R} \qquad (6\text{-}7c)$$

= Stokes' number

Stokes' number is the only parameter associated with a non-diffusional field. v_x, and v_y are the fluid velocity and they depend on the type of flow. Here we considered the flow of fluid past an infinitely long cylinder.

With given initial conditions Equations (6-7a) and (6-7b) can be solved to find the velocity at the point of impaction.

Some significant properties of Strokes' number can be found by analyzing special cases. If $St = 0$, then

$$\frac{dx'}{dt'} = v_x'$$

$$\frac{dy'}{dt'} = v_y'$$

This means the particles will follow the streamline of the fluid. In this case only the interception effect is considered. If $St \to \infty$, then

$$\frac{d^2x'}{dt'^2} = 0$$

$$\frac{d^2y'}{dt'^2} = 0$$

This means the particle locus is a straight line.

(E) Probe Limitation

Now let us find what is the lower limit of particle size which can be found by this mehtod.

First, let us assume the flow field is potential flow, then

$$v_x' = 1 - \frac{x'^2 - y'^2}{(x'^2 + y'^2)^2} \tag{6-8a}$$

$$v_y' = \frac{2\,x'y'}{(x'^2 + y'^2)^2} \tag{6-8b}$$

By combining the Equations (6-7) and (6-8), the equation of motion of a particle moving along the stagnation streamline in the direction of stagnation point takes the form

$$St \frac{d\bar{u}}{dt'} + \bar{u} - (1 - \frac{1}{x'^2}) = 0 \tag{6-9}$$

where $\bar{u} = \frac{dx'}{dt'}$

Differentiating the Eq. (6-9) with respect to x' and putting $x' = -1$ and $\bar{u} = 0$, we get

$$St (\frac{d\bar{u}}{dx'})^2 + (\frac{d\bar{u}}{dx'}) + 2 = 0 \tag{6-10}$$

from which $St \leq 1/8$ (6-11)

This value is different from the value obtained by Levich (17) due to different flow model used in the calculation. If $0 < st < St_{cri} = 1/8$, the particles loose all their kinetic energy by the time they collide with the cylinder at the stagnation point, in other words the negligibly small particles can never hit the cylinder. If the particle having $St > St_{cri} = 1/8$, the velocity at the stagnation point is not zero and the particle may or may not hit the cylinder depending on its initial starting point and on its size. For our equipment, $R = 0.015$ cm, $\rho_s = 8.91$ gm/cm^3, $\mu = 0.01$ poise, $u_\infty = 15.1$ cm/sec, the minimum size (radius) that the probe can measure is about eight microns. With other parameter values it may be possible to measure smaller particles, but it must be kept in mind that if the particle size is less than ten microns, diffusional effects become important and our method is not useful.

(F) Accuracy of the Probe

In order to find how accurately we can measure the particle size distribution, let us consider the system as illustrated in Fig. 6-7. And also let us assume:

1) The particles enter the control surface only one particle at a time,

2) No matter what calculation method we use, if the particle hits the probe we can identify its size accurately,

3) Only the particles through the control surface are considered,

4) The particle size distribution is an exponential distribution, that is, the density function of the particle size distribution is

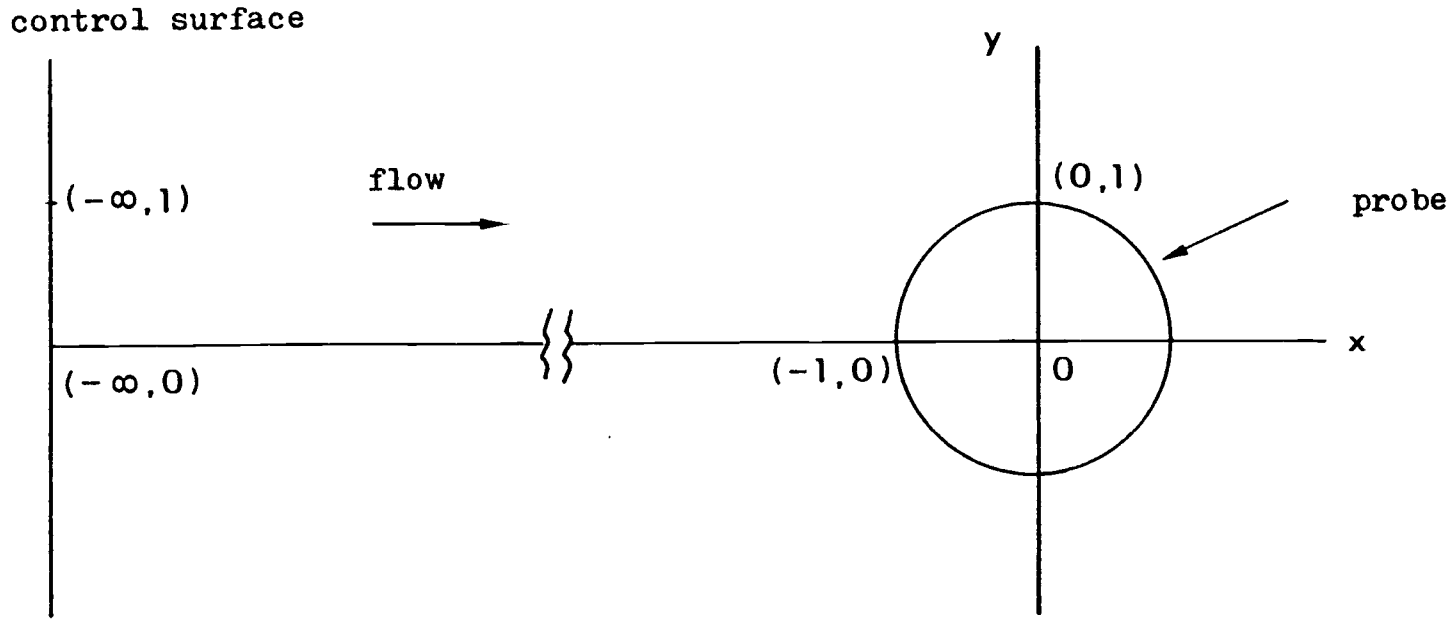

Fig.6-7. System model for simulation.

$f_0 = \exp(-r/R)$ which is the most commonly encountered in the continuous MSMPR crystralizer,

5) The Stokes' number equals zero. The particles will therefore follow streamlines and only the interception effect is considered. This is the most inefficient case,

6) The flow field is the potential flow.

Now consider a randomly selected particle from an exponential size distribution at position $x = -\infty$ with a random position in the cross section of the flow field. The particle will follow the equation of motion of the fluid. Some particles will hit the probe and directly give rise to signals; some particles will miss the probe due to their initial position or their size. Fig. 6-8 shows the simulation results obtained with Monte Carlo simulation. The mean and variance from the Poisson's distribution are both one. The results show that if the total particles taken for consideration are one thousand, then the mean value is about 1.27, about 30% higher than the theoretical value, although the variance approaches the theoretical value. Let us now look at the behavior of these particles in more detail.

If a particle with size r enters the control surface at position y_∞, the particle will be intercepted by the probe only if

$$y_\infty \leq (r+R)^2 - R^2 (r+R)^{-1}$$

if r/R is small, then $y_\infty \leq 2r$. The probability for a particle with size $r/R = 0.1$ to hit the probe is 2% compared to 8% for a size $r/R = 0.5$.

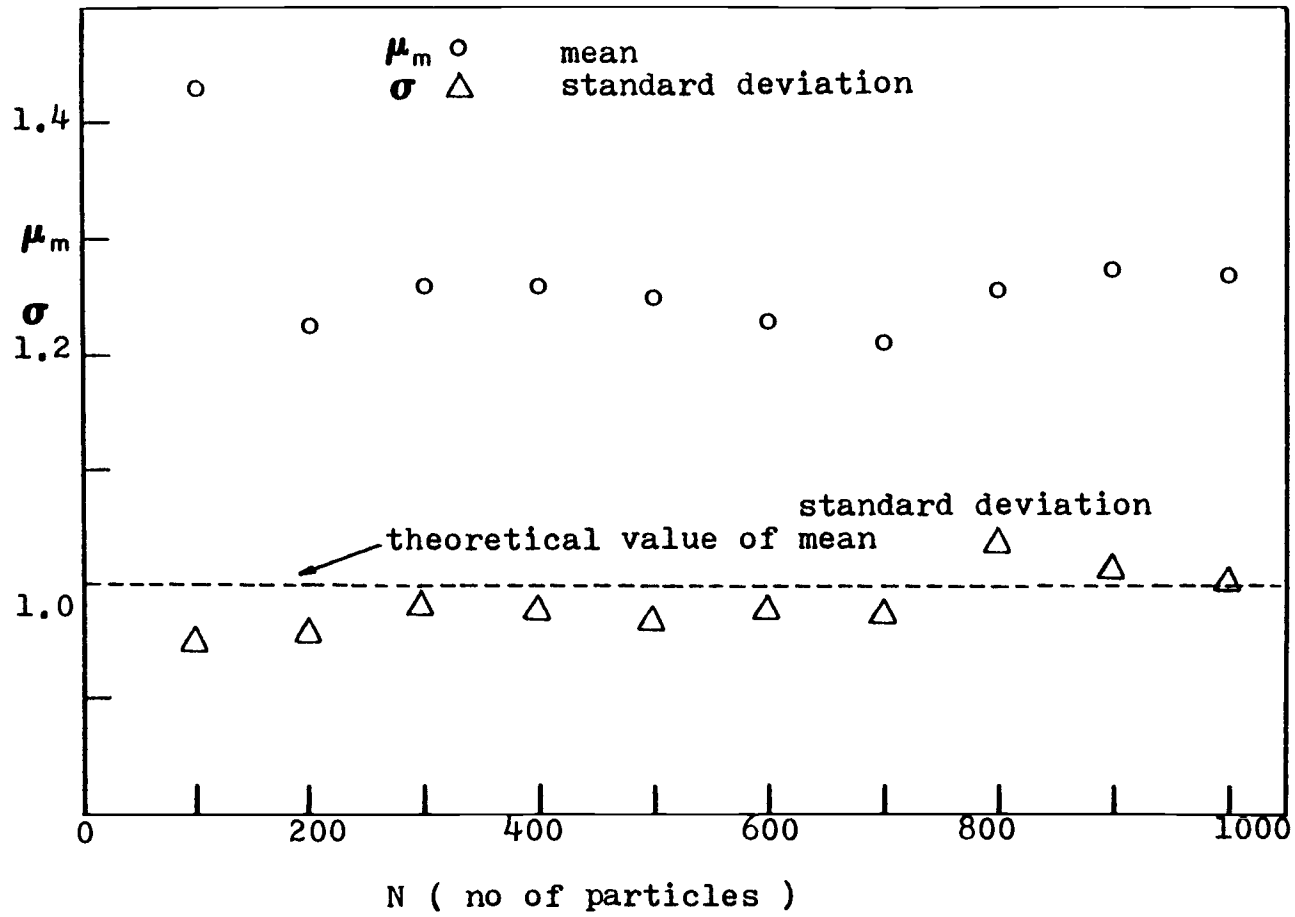

Fig.6-8. Result of simulation.

This means that the probability of hitting the probe increases rapidly as the particle size increases. Therefore, the probe is most efficient for large particles. This result can also found from Fig. 6-9, when the calculated size distribution is plotted against the size and compared with the theoretical values. The result shows when the particle r/R is between o.6 and 1.0 the simulation result is very close to the theoretical one, and the more particles we take the more accurate the result. Since the small particles are easy to miss the probe, this is why the mean value is always greater than the theoretical value.

The distribution of initial positions, y_∞ is given in Table 6-2. The deviation from uniformity is on the average under 7.5%.

The percentage miss of particles from the probe is shown in Fig. 6-10, up to the particles sampling number equal to one thousand, the percentage miss of particles is nearly around twenty six, so about a quarter of the particles can not be taken into account for measurement.

(G) Experimental Results and Discussion

A high quality stereo phonograph cartridge (Ortofon MC 10) was tested and found to be not sensitive enough for our work; it gave useful results only for particle diameters bigger than 300 micron. The particles were small copper spheres. The liquid used as the carrier fluid was water. In our experimental range, the particle size was bigger than the needle size and the terminal velocity of the particle was faster than the fluid velocity. In this situation with the particles settling freely down the flowing fluid, the particles will flow in straight lines

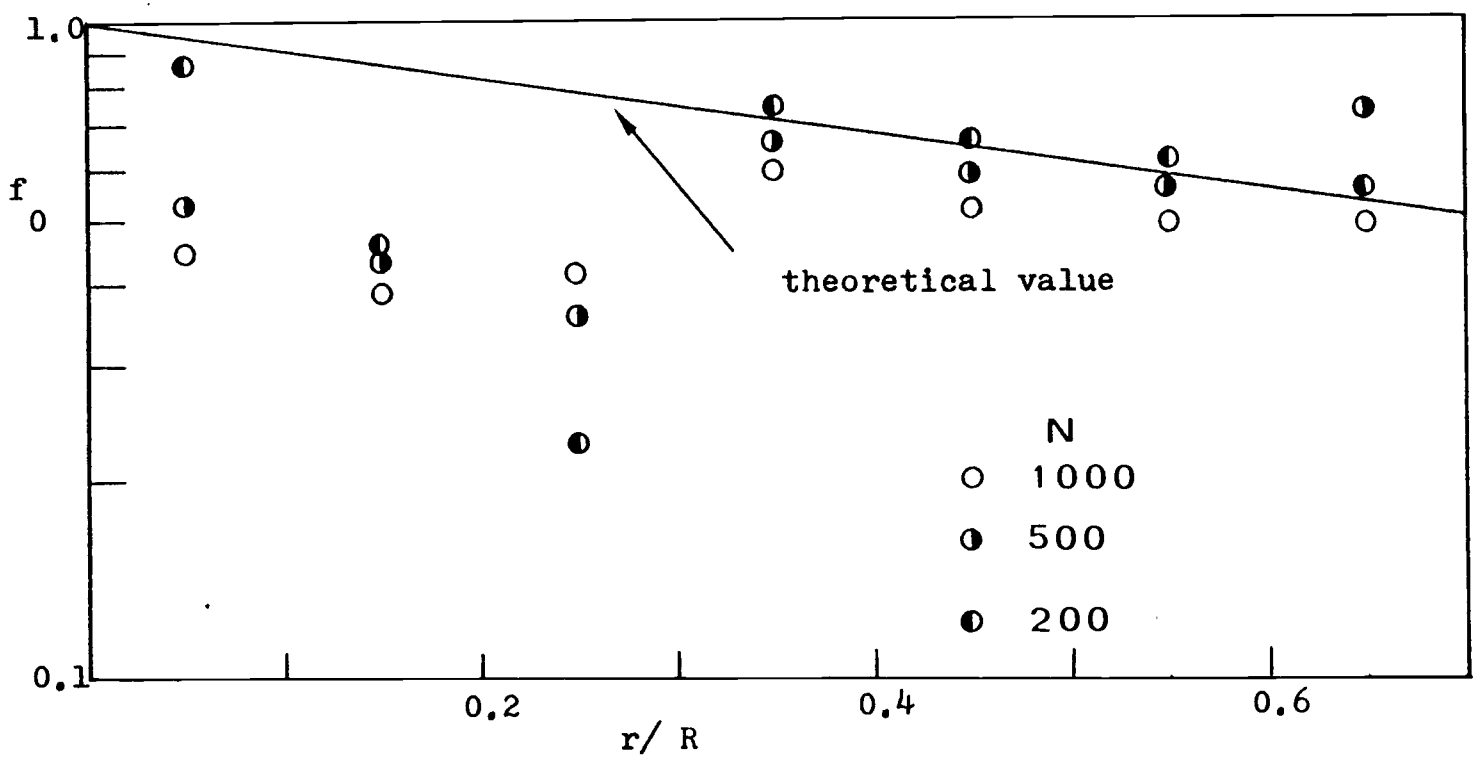

Fig.6-9. Simulation result of particle size distribution.

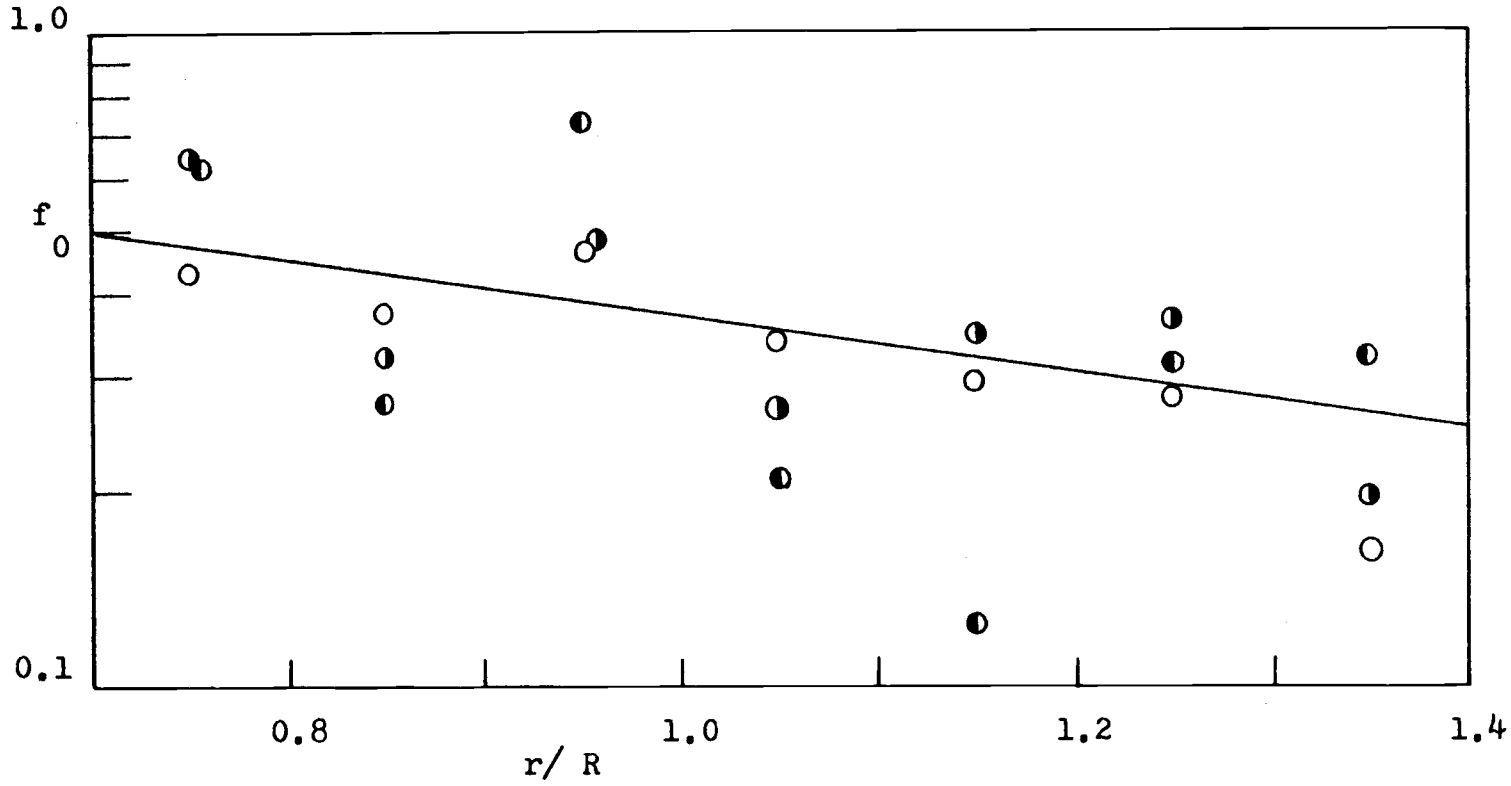

Fig.6-9. (continued)

Table 6-2. Simulation Statistics

Position(y_∞/R)	Number of particles	Expected Value	Deviation
0 ∿ 0.1	109	100	0.09
0.1 ∿ 0.2	96	100	-0.04
0.2 ∿ 0.3	108	100	0.08
0.3 ∿ 0.4	101	100	0.01
0.4 ∿ 0.5	111	100	0.11
0.5 ∿ 0.6	89	100	-0.11
0.6 ∿ 0.7	98	100	-0.02
0.7 ∿ 0.8	108	100	0.08
0.8 ∿ 0.9	95	100	-0.05
0.9 ∿ 1.0	85	100	-0.15
Total:	1000	Total: 1000	

Average absolute deviations = 0.074

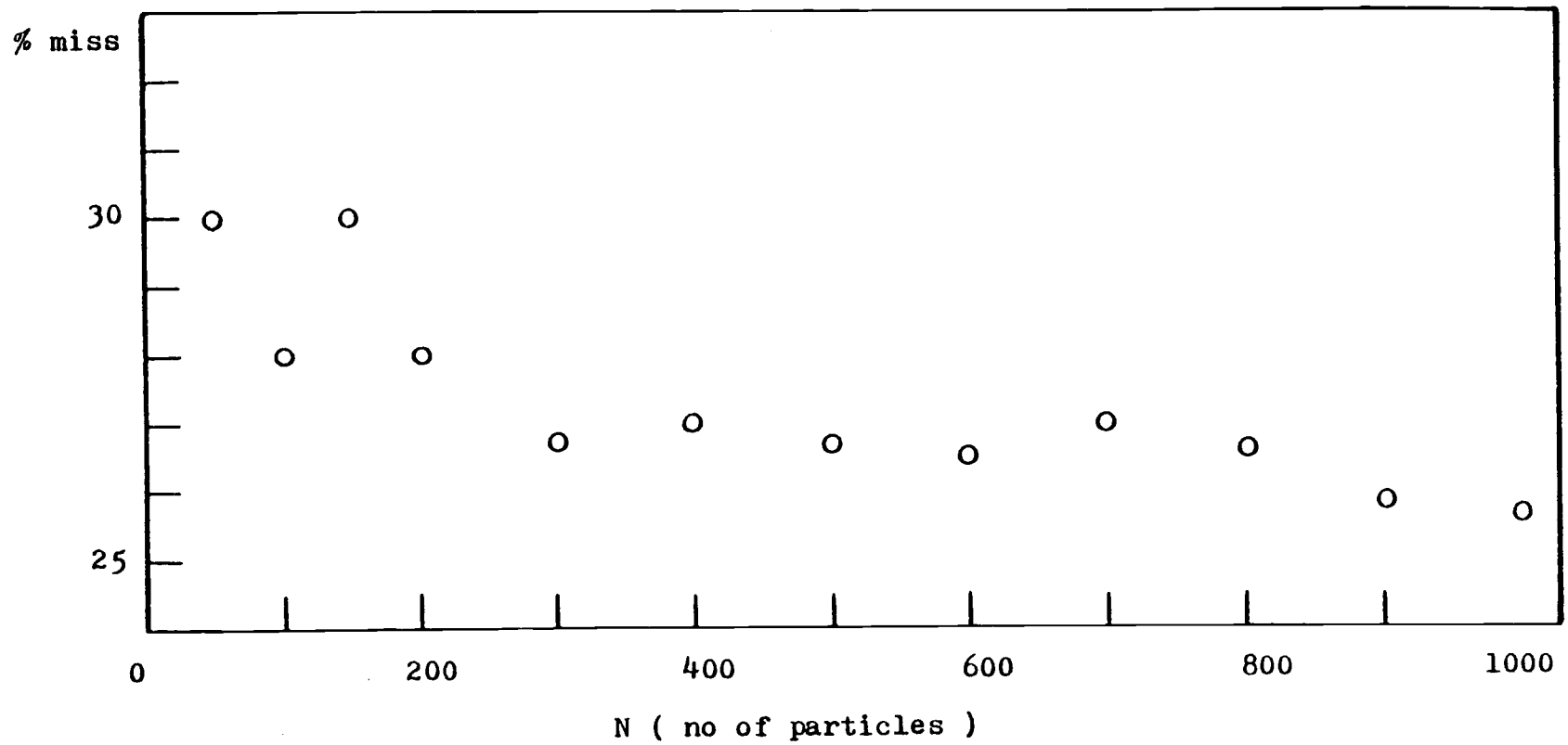

Fig.6-10. Percentage of unuseful particles in size determination simulation.

with their terminal velocity. By using Eq. (6-5) the particle size can be predicted. Fig. 6-11 shows the background noise if the probe is in still air; the noise level is less than the 10 mv. Fig. 6-12 shows the background noise of the probe in still water, and Fig. 6-13 shows the background noise if the water is flowing at the Reynolds number equal to 1510. The noise is about 20 mv; if we increase the fluid velocity the vibration of the system becomes stronger and the base line of the signal shows some cyclic motion.

Various approaches were tried to improve performance but none was very successful. One way to increase the magnitude of the signal is by increasing the fluid velocity, but if the fluid flow pattern in the tube is turbulent the signal and the background noise will both become bigger; therefore, it is not practical to increase the fluid velocity into the turbulent regime.

The friction loss of the needle support is not very important. Direct impulse response tests showed that the needle-cartridge system transmits more than 90% of the energy which would be detected by the cartridge alone.

Fig. 6-14 shows typical signals obtained from the experiments, the signal b and d are suitable for calculating the particle size. Theoretically, the system is critically damped so that the signal curves should show only one peak, but probably due to some change in the properties of the rubber which holds the needle (see Fig. 6-1), the system shows underdamped behavior.

The following results are based on the values for 500 effective particles signal readings.

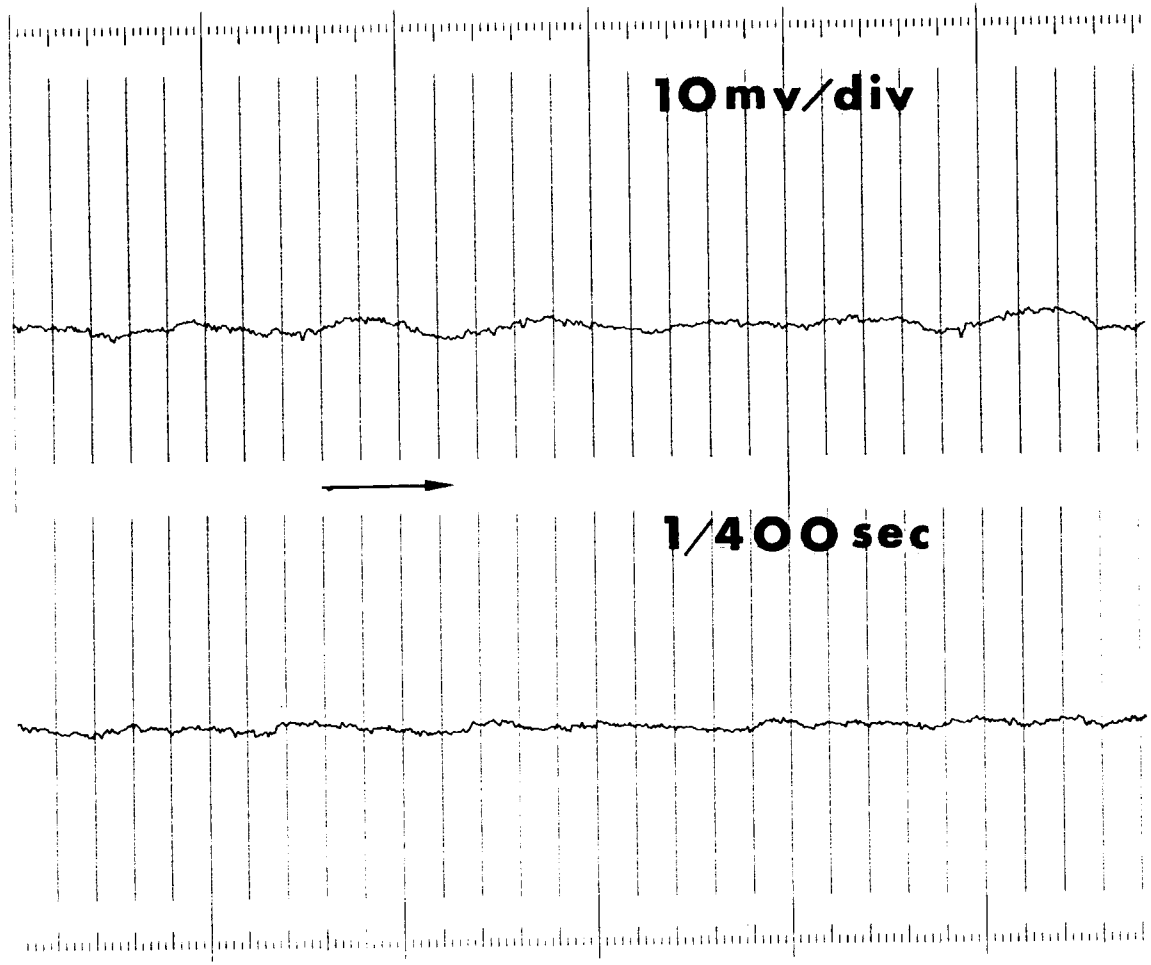

Fig.6-11. Noise level of a probe when in still air

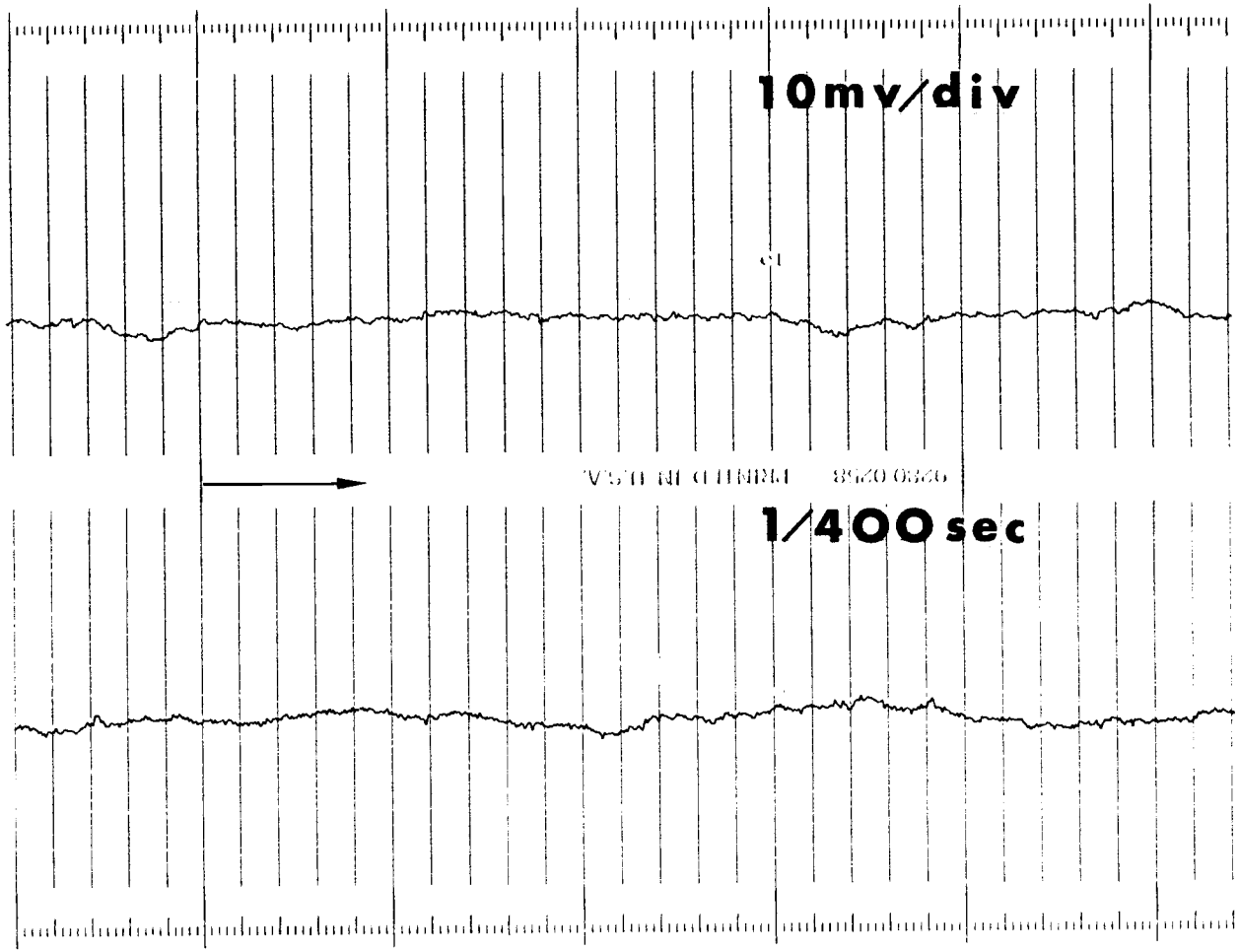

Fig.6-12. Noise level of a probe when in still water.

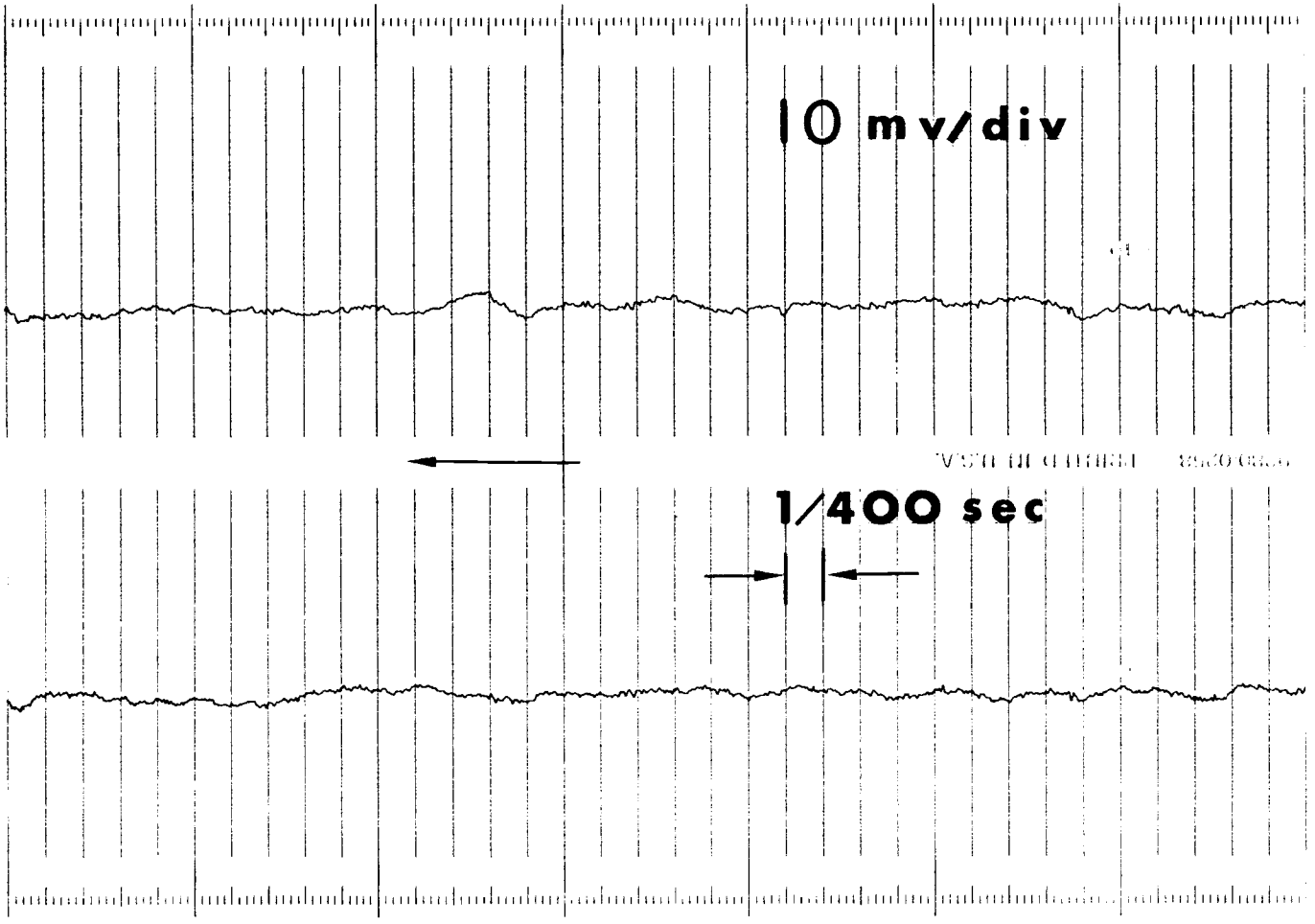

Fig.6-13. Noise level of a probe when in flowing water with Reynolds number equal to 1510.

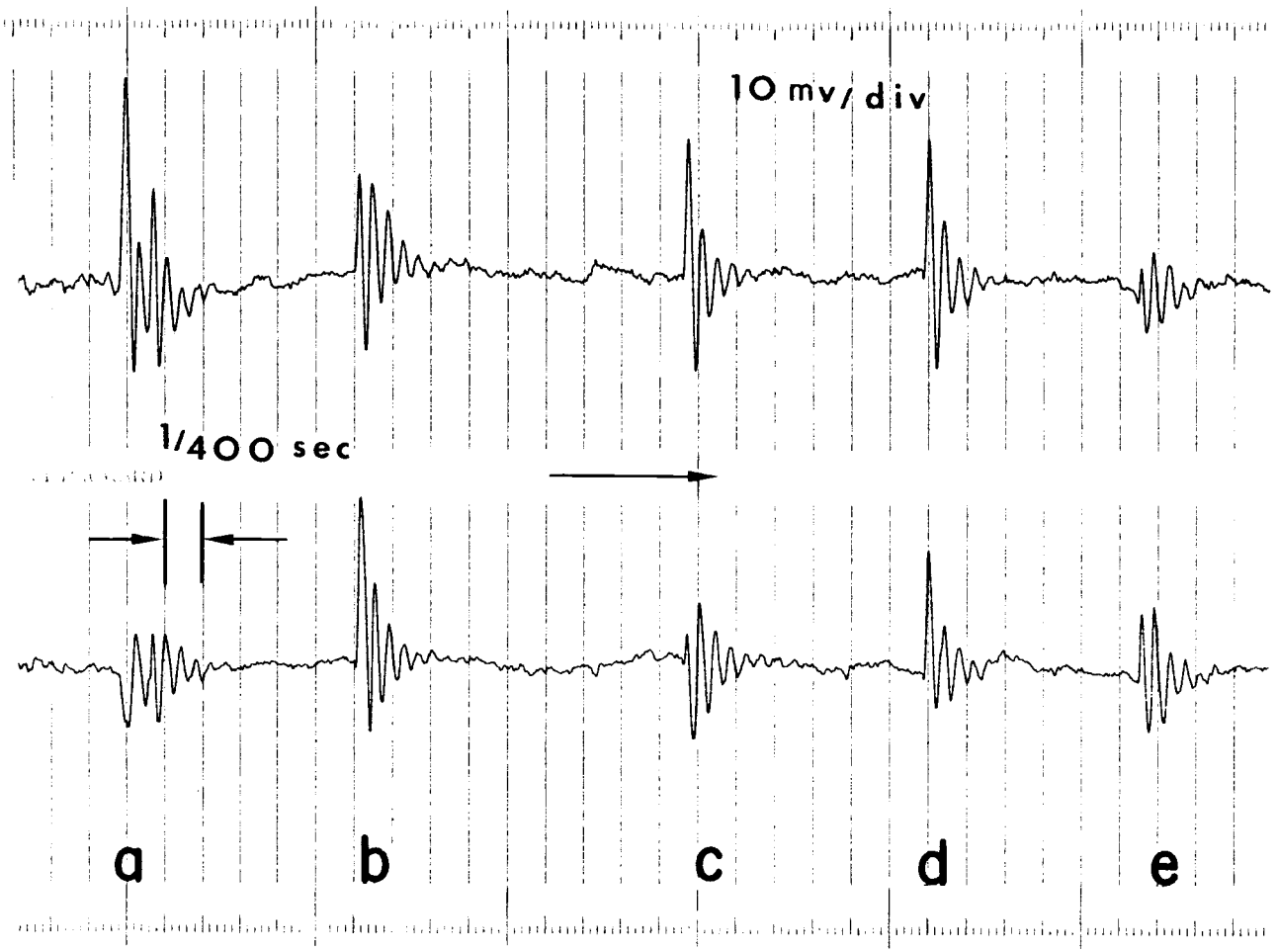

Fig.6-14. Typical signal from the particle size measurement.

Fig. 6-15 and 6-16 show the cumulative undersize fraction curve D (%) vs particle size D_p for particle size from 24 mesh (701 μ) to 28 mesh (589 μ) and 35 mesh (417 μ) to 48 mesh (295 μ) respectively; the experimental values are only slightly different from the theoretical values. When the fluid velocity changes, the results are quite similar, because the particles are flowing down with a terminal velocity, that is larger than the fluid velocity.

Fig. 6-17 shows the cumulative undersize fraction curve D (%) vs particle size D_p when particles between 24 mesh to 28 mesh and 35 mesh to 48 mesh are mixed in equal amounts. From the result we can find that at about 400 μ the under size fraction is less than 50% the theoretical value, more particle samplings will decrease this gap.

This equipment is not perfect and requires further development before practical application is possible. The transducer should be improved to extend the particle measuring range. Signal output should be standarized to eliminate the oscillation behavior. The instrument should also be programmed for operator-free operation.

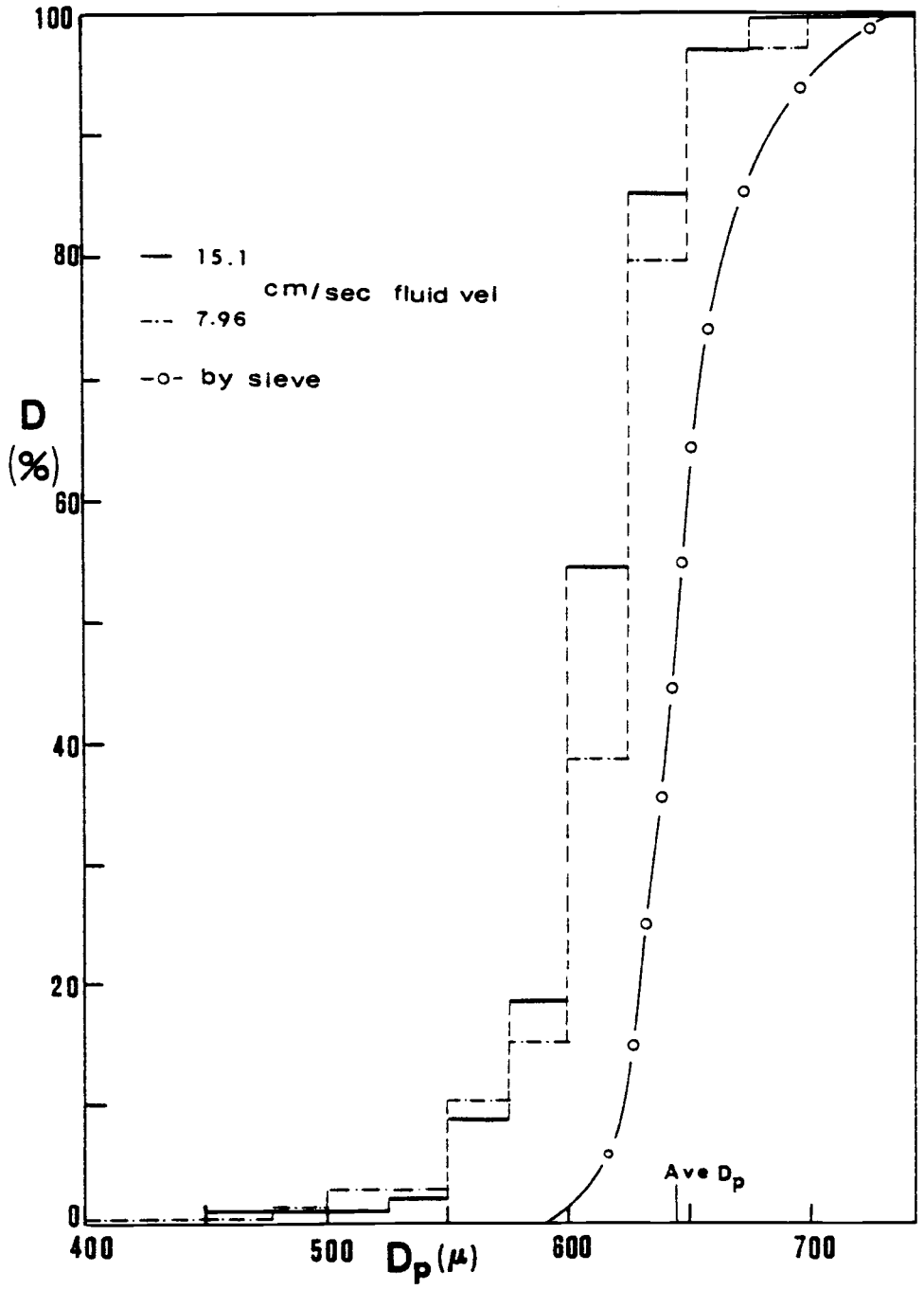

Fig.6-15. Cumulative undersize fraction curve of -24 +28 mesh particles.

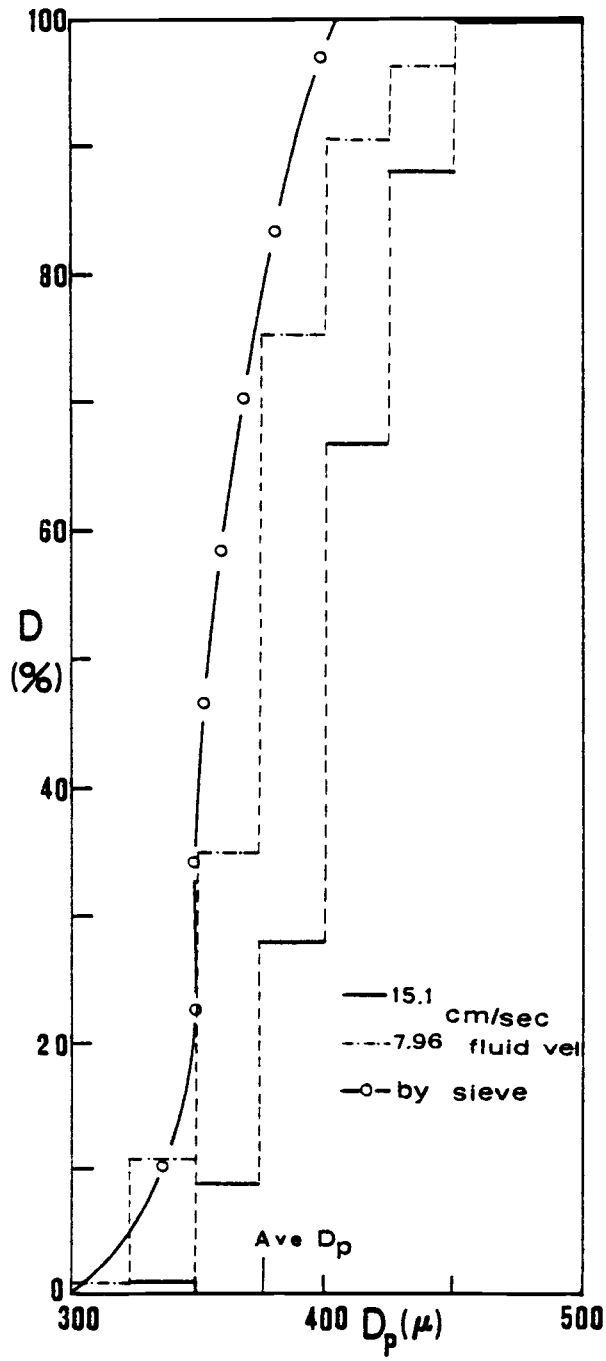

Fig.6-16. Cumulative undersize fraction curve of -35 +48 mesh particles.

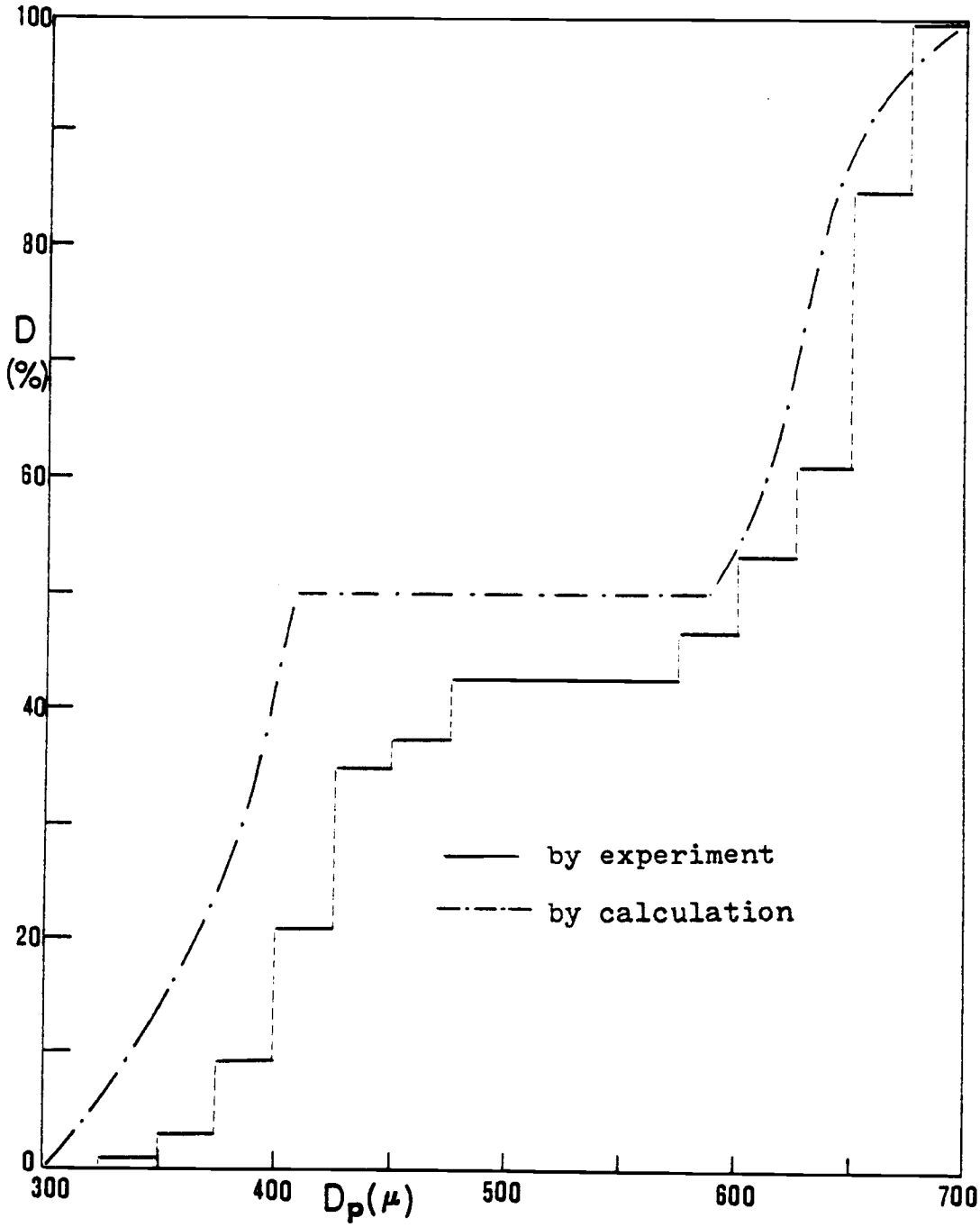

Fig.6-17. Cumulative undersize fraction curve of -24 +48 mesh particles.

CHAPTER VII. CONCLUSIONS

A set of lumped parameter equations were developed in terms of moments of the crystal size distribution for an isothermal continuous mixed suspension mixed product removal class I crystallizer with a fines trap for both the homogeneous and secondary nucleation models. Linear stability analysis was carried out, and linear stability criteria were established for both homogeneous and number dependent secondary nucleation in terms of system kinetic parameters. The results provide insight into the complexity of the interaction between crystal growth and nucleation rate.

Extensive nonlinear and linear simulations of the system equation were performed. The linear stability model predicted the system performance successfully. When the linear stability analysis predicts a stable system, the dynamic response shows long-term self-sustained oscillation; when the stability analysis predicts the unstable system, the dynamic response shows the amplitude of the system variables will become bigger and bigger as the time elapses.

The capability of modal control for elimination of the limit cycles in the above cases was investigated. The results of simulations indicated that modal control was a useful tool for control the continuous MSMPR crystallizer with a fines trap, and showed remarkable improvement in the performance of both the stable and unstable system. The output of the systems was measured using the throughput or fines recirculation rate or both as the manipulated variables. From the simulation results, it was

found that when using both the throughput rate and fines recirculation rate as the manipulated variable the system is better controlled; and using the fines recirculation rate is better than using the throughput rate. Although using the throughput rate is not so effective as the previous two methods, it is still useful for control of a continuous MSMPR crystallizer.

The stability of MSMPR crystallizer where McCabe's ΔL law was violated (i.e. the growth rate is size-dependent) was investigated. The general characteristic equation was formulated. In this situation the characteristic equation is not a simple polynomial form, and the Routh test for stability is no longer applicable. Two cases of size-dependent growth rate were solved to illustrate how size-dependent growth destabilized the system.

Finally, a new and simple method for on-line measurement of particle size distribution was investigated. This method measures the momentum of a particle when it hits a very small cylindrical probe to determine the particle size. The instrument tested was not adequate but the technique has considerable potential for monitoring and control of CSD, and deserves further investigation.

REFERENCES

1. Abegg, C. F., J. D. Stevens and M. A. Larson, "Crystal Size Distributions in Continuous Crystallizer when Growth Rate is Size Dependent", AIChEJ., 14, 1, 118 (1968).

2. Anshus, B. E. and E. Ruckenstein, "On Stability of a Well Stirred Isothermal Crystallizer", Chem Eng. Sci. 28, 501 (1973).

3. Beckman, J R. and A. D. Randolph, "CSD Dynamics in a Classified Crystallizer, Part II", AIChEJ., 23, 4, 510 (1977).

4. Chang, C. T. and M. A. F. Epstein, "Modal Control Strategies for Continous Crystallizers", Paper presented for AIChE Philadelphia National Meeting, June (1980).

5. Crossley, T. R., "Generalized Single-Input Modal Control Theory", Int. J. Control, 24, 1, 1 (1976).

6. Desai, R. M., J. W. Rachow and D. C. Timm, "Collision Breeding: A Function of Crystal Moments and Degree of Mixing", AIChEJ., 20, 1, 43 (1974).

7. Epstein, M. A. F. and L. Sowul, "Phase space analysis of Limit-Cycle Development in CMSMPR Crystallizers using 3-dimensional Computer Graphics", AIChE Symp. Ser., No. 193, vol. 76, 6 (1980).

8. Garside, J. and S. J. Jancic, "Prediction and Measurement of Crystal Size Distributions for Size-Dependent Growth", Chem. Eng. Sci. 33, 1623 (1978).

9. Garside, J. and S. J. Jancic, "Measurement and Scale-Up of Secondary Nucleation Kinetics for the Potash Alum-Water System", AIChEJ., 25, 6, 948 (1979).

10. Gould L. A. and M. A. Murray-Lasso, "On the Modal Control of Distributed Systems with Distributed Feedback", IEEE Trans. On Automatic Control, AC-11, No. 4, 729 (1966).

11. Gupta, G. and D. C. Timm, "Predictive/Corrective Control for Continuous Crystallizers", CEP Symp. Ser., No. 110, Vol. 67, 121 (1971)

12. Han, C. D., "A Control Study on Isothermal Mixed Crystallizers", Ind. Eng. Chem. Process Des. Dev., 8, 2, 150 (1969).

13. Hixson, A. W. and K. L. Knox, "Effect of Agitation on Rate of Growth of Single Crystal", Ind. Eng. Chem. 43, 2144 (1951).

14. Hulburt, H.M. and S. Katz, "Some Problems in Particle Technology", Chem. Eng. Sci. 19, 555 (1964).

15. Hulburt, H M. and D. G. Stefango, "Design Models for Continuous Crystallizers with Double Drawoff", CEP Symp. Ser., No. 95, Vol. 65, 50 (1969).

16. Ishii, T. and A. D. Randolph, "Stability of the High Yield MSMPR Crystallizer with Size-Dependent Growth Rate", AIChEJ., 26, 3, 507 (1980).

17. Levich, V.G., "Physicochemical Hydrodynamics", Prentice-Hall Inc. (1962).

18. Lei, S., R. Shinnar and S. Katz, "The Regulation of a Continuous Crystallizer with Fines Trap", CEP Symp. Ser., No. 110, Vol. 67, 129 (1971).

19. Lei, W., R. Shinnar and S. Katz, "The Stability and Dynamic Behavior of a Continuous Crystallizer with a Fines Trap", AIChEJ., 17, 6, 1459 (1971).

20. Liss, B. and R. Shinnar, "The Dynamic Behavior of Continuous Crystallizers in which Nucleation and Growth depend on Properties of the Crystal Magma", AIChE Symp. Ser., No. 153, Vol 72, 28 (1976).

21. Mayne, D. Q. and P. Murdoch, "Modal Control fo Linear Time Invariant Systems", Int. J. Control, 11, 2, 223 (1970).

22. McCabe, W. L. and R. P. Stevens, "Rate of Growth of Crystals in Aqueous Solutions", Chem. Eng. Prog. 47, 168 (1951).

23. Nyvlt, J. and J. W. Mullin, "The Perioic Behavior of Continuous Crystallizers", Chem. Eng. Sci. 25, 131 (1970).

24. Randolph, A. D., "CSD Dynamics, Stability, and Control", AIChE Symp. Ser., No. 193, Vol 76, 1 (1980).

25. Randolph, A. D., "A Population Balance for Countable Entities", Can. J. Chem. Eng. 42, 280 (1964).

26. Randolph, A. D., G. L. Beer and J. P. Keener, "Stability of Class II Classified Product Crystallizer with Fines Removal", AIChEJ., 19, 6, 1140 (1973).

27. Randolph, A. D., J. R. Beckman and Z. I. Kraljevich, "CSD Dynamics in a Classified Crystallizer, Part I", AIChEJ., 23, 4, 500 (1977).

28. Randolph, A. D. and M. A. Larson, "Theory of Particulate Processes", Academic Press, New York (1971).

29. Randolph, A. D. and M. A. Larson, "Analog Simulation of Dynamic Behavior in a Mixed Crystal Suspension", CEP Symp. Ser., No. 55 Vol. 61, 147 (1965).

30. Randolph, A. D. and M. A. Larson, "Transient and Steady state Size Distributions in Continuous Mixed Suspension Crystallizers", AIChEJ., 8, 5, 639 (1962).

31. Randolph, A. D., E. T. White and C. D. Low, "On-Line Measurement of Fine-Crystal Response to Crystallizer Disturbances", Paper presented for AIChE Philadelphia National Meeting, June (1980).

32. Rosenbrock, H. H., "Distinctive Problems of Process Control", Chem. Eng. Prog. 58, 9, 43 (1962).

33. Rovang, R. D. and A. D. Randolph, "On-Line Particle Size Analysis in the Fines Loop of a KCL Crystallizer", AIChE Symp. Ser., No. 193, Vol. 76, 18 (1980).

34. Sherwin, M.B., R. Shinnar and S. Katz, "Dynamic Behavior of the Well-Mixed Isothermal Crystallizer", AIChEJ., 13, 6, 1141 (1967)

35. Sherwin, M.B., R. Shinnar and S. Katz, "Dynamic Behavior of the Isothermal Well-Stirred Crystallizer with Classified Outlet", CEP Symp. Ser., No. 95, Vol. 65, 75 (1969).

36. Sowul, L. and M. A. F. Epstein, "Crystallization Kinetics of Sucrose in a CMSMPR Evaporative Crystallizer", Ind. Eng. Chem. Process Des. Dev., 20, 2, 197 (1981).

37. Takahashi, Y., H. Thal-Larson, E. Goldenberg, W. V. Loscutoff and P. R. Ragetly, "Mode Oriented Design Viewpoint for Linear, Lumped-Parameter Multivariable Control Systems", J. Basic Eng. Trans. ASME., 90, 222 (1968).

38. White, E. T., L. L. Bendig and M. A. Larson, "The Effect of Size on the Growth Rate of Potassium Sulfate Crystals", AIChE Symp. Ser., No. 153, Vol. 72, 41 (1976).

39. Finn, R. K. and R. E. Wilson, "Population Dynamics of a Continuous Propagator for Microorganisms", Ag. Food Chem. Vol. 2, No. 2, 66 (1954).

40. Omi, S., T. Ueda and H. Kubota, "Continuous Operation of Emulsion Polymerization of Styrene", J. of Chem. Eng. (Japan), 22, 193 (1969).

41. Omi, S., T. Ueda and H. Kubota, "Experimental Study of Continuous Emulsion Polymerization of Styrene", J. of Chem. Eng. (Japan), 41, 50 (1971).

42. Ellis, J. K. and G. W. T. White, "An Introduction to Modal Analysis and Control", Part 1 & 2, Control, April, May (1965).

43. Canning, T. F. and A. D. Randolph, "Some Aspects of Crystallization Theory: System that Violate McCabe's Delta L Law", AIChEJ., 13, 1, 5 (1967).

44. Garside, J. and S. J. Jancic, "Growth and Dissolution of Potash Alum Crystals in the Subsive Size Range", AIChEJ., 22, 5, 887 (1976).

45. Coughanowr, D. R. and L. B. Koppel, "Process Systems Analysis and Control", McGraw-Hill Book Company, New York (1965)

APPENDICES

Appendix A. Stability Limit of Number Dependent Secondary Nucleation

From Eq. (3-5), the characteristic equation represent the system will be:

$$S^4 + (4 + g_1 e^{-\lambda} - b_n)\, S^3$$

$$+ (6 + 4g_1 e^{-\lambda} - 3\, b_n - \lambda g_1 b_n e^{-\lambda})\, S^2$$

$$+ (4 + 6g_1 e^{-\lambda} - 3b_n - 3g_1 b_n e^{-\lambda})\, S$$

$$+ (3g_1 e^{-\lambda} + 1 + \lambda g_1 e^{-\lambda} - b_n - 3g_1 b_n e^{-\lambda} + b_1 e^{-\lambda}) = 0$$

Application of the Routh test to the above equation results in the conditions for the system. These conditions are from Eq. (3-6)

$$4 + g_1 e^{-\lambda} - b_n > 0 \qquad \text{(A-1a)}$$

$$b_1 e^{-\lambda} > 3g_1 e^{-\lambda} - 1 - \lambda g_1 e^{-\lambda} + b_n + 3\, b_n g_1 e^{-\lambda} \qquad \text{(A-1b)}$$

$$(4-b_n)(g_1 e^{-\lambda})^2 + (16-8b_n+b_n^2)(g_1 e^{-\lambda})$$

$$+ (20-15b_n+3b_n^2) > 0 \qquad \text{(A-1c)}$$

$$b_1 e^{-\lambda} < \{(21-15b_n + 3\,b_n^{\,2} - \lambda\,)(g_1 e^{-\lambda})^3$$

$$+(87-81b_n-8\lambda+2\lambda b_n+27b_n^{\,2}-3b_n^{\,3})(g_1 e^{-\lambda})^2$$

$$+(128-148b_n+8\lambda b_n-16\lambda+62b_n^{\,2}-\lambda b_n^{\,2}-9b_n^{\,3})(g_1 e^{-\lambda})$$

$$+(64-96b_n+48b_n^{\,2}-8b_n^{\,3})\} \,/(4+g_1 e^{-\lambda} - b_n)^2 \qquad \text{(A-1d)}$$

In order to represent the stability region more clearly, one must rearrange the Eq. (A-1). From Eq. (A-1b) and Eq. (A-1d), one get

$$(b_n+3b_n g_1 e^{-\lambda}-\lambda g_1 e^{-\lambda}- 1 - 3g_1 e^{-\lambda}) < b_1 e^{-\lambda} <$$

$$\{(21-15b_n+3b_n^{\,2} - \lambda)(g_1 e^{-\lambda})^3 + (87-81b_n-8\lambda+2\lambda b_n+27b_n^{\,2}-3b_n^{\,3})$$

$$(g_1 e^{-\lambda})^2 + (128-148b_n+8\lambda b_n-16\lambda+62b_n^{\,2}-\lambda b_n^{\,2}-9b_n^{\,3})(g_1 e^{-\lambda})$$

$$+ (64-96b_n+48b_n^{\,2}-8b_n^{\,3})\} \,/\, (4+g_1 e^{-\lambda}-b_n)^2$$

Multiplying both sides of above equation by $(4+g_1 e^{-\lambda}-b_n)^2$ and after simplification, one can get

$$(24-18b_n+3b_n^{\,2})(g_1 e^{-\lambda})^3 + (112-112b_n+33b_n^{\,2}-3b_n^{\,3})(g_1 e^{-\lambda})^2$$

$$+ (184-23b_n+91b_n^{\,2}-12b_n^{\,3})(g_1 e^{-\lambda}) + (80-120b_n+57b_n^{\,2}- 9b_n^{\,3})$$

$$> (b_1 e^{-\lambda}+\lambda g_1 e^{-\lambda}+1+3g_1 e^{-\lambda}-b_n-3b_n g_1 e^{-\lambda})(4+g_1 e^{-\lambda}-b_n)^2 > 0 \qquad \text{(A-2)}$$

Let

$$f(g_1e^{-\lambda}) = (24-18b_n+3b_n^2)(g_1e^{-\lambda})^3 + (112-112b_n+33b_n^2-3b_n^3)$$
$$(g_1e^{-\lambda})^2 + (184-230b_n+91b_n^2-12b_n^3)(g_1e^{-\lambda})$$
$$+ (80-120b_n+57b_n^2-9b_n^3)$$

$$h(b_1, g_1, \lambda, b_n) = (b_1e^{-\lambda}+\lambda g_1e^{-\lambda}+ 1 +3g_1e^{-\lambda}-b_n-3b_ng_1e^{-\lambda})$$
$$(4+g_1e^{-\lambda}-b_n)^2$$

Then the stability limit $h(b_1, g_1, \lambda, b_n)$ lies between $f(g_1e^{-\lambda})$ and zero. If let $f(g_1e^{-\lambda}) = 0$, one gets three roots as

$$(g_1e^{-\lambda})_1 = \frac{-(4-b_n) + \sqrt{(4-b_n)^2-4\,\frac{(20-15b_n+3b_n^2)}{4-b_n}}}{2}$$

$$(g_1e^{-\lambda})_2 = \frac{-(4-b_n) - \sqrt{(4-b_n)^2-4\,\frac{(20-15b_n+3b_n^2)}{4-b_n}}}{2}$$

$$(g_1e^{-\lambda})_3 = \frac{-3b_n + 4}{3b_n - 6}$$

$(g_1e^{-\lambda})_1$ and $(g_1e^{-\lambda})_2$ are real or complex value depend on $b_n \gtrless 4$.

(i) If $b_n > 4$, then $(g_1e^{-\lambda})_1$, $(g_1e^{-\lambda})_2$, and $(g_1e^{-\lambda})_3$ are three real roots. The relationship of Eq. (A-2) is shown in Fig. A-1(a), so the stable region must be $g_1e^{-\lambda} > (g_1e^{-\lambda})_1$ or $g_1e^{-\lambda}$ between $((g_1e^{-\lambda})_2, (g_1e^{-\lambda})_3)$ and from Eq. (A-1a)

$$(g_1e^{-\lambda}) > b_n - 4$$

so
$$g_1e^{-\lambda} > \frac{-(4-b_n) + \sqrt{(4-b_n)^2 - \frac{4(20-15b_n+3b_n^2)}{4-b_n}}}{2}$$

but this relation violate the requirement of Eq. (A-1b). Thus no stability limit can be found in region $b_n > 4$.

(ii) If $b_n < 4$, then $f(g_1e^{-\lambda}) = 0$ has only one real roots $(g_1e^{-\lambda})_3$, and the relationship of Eq. (A-2) is shown in Fig. A-1(b). From requirement of Eq. (A-1a), $(g_1e^{-\lambda})_3 > b_n - 4$, then $b_n < 2$.

Finally one can conclude that if $b_n < 2$, the stable region will be $g_1e^{-\lambda} > -\frac{3b_n-4}{3b_n-6}$, and there is no stable region for $b_n > 2$.

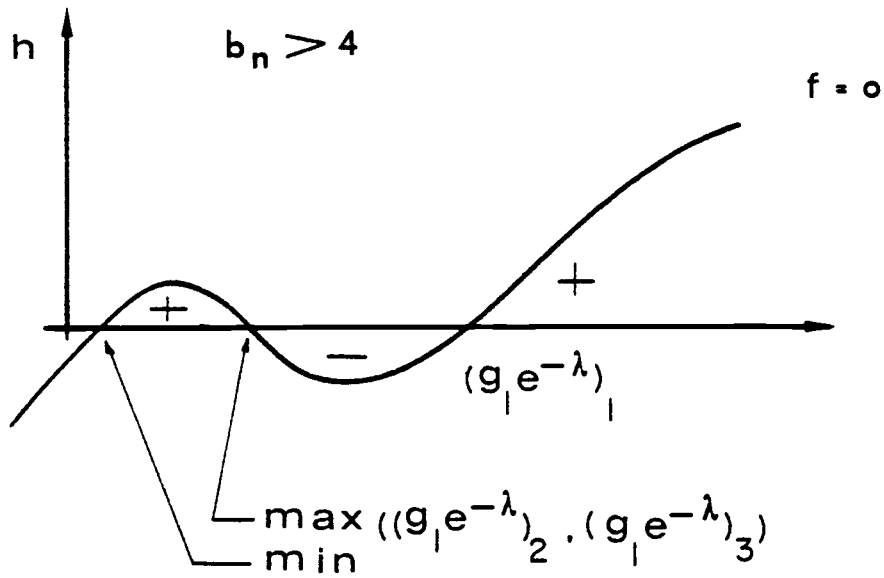

(a)

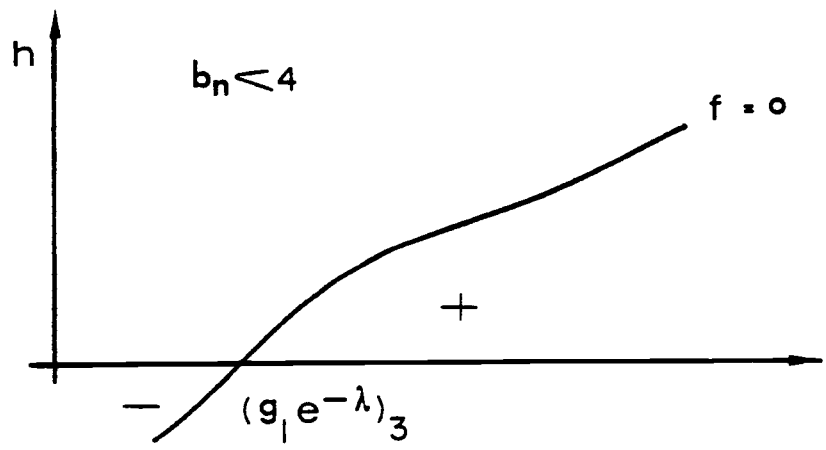

(b)

Fig.A-1. Locus of stable region for number dependent nucleation model.

Appendix B. The Non-linear Dimensionless Equations.

(a) Homogeneous Nucleation Model

From Eq. (2-8) defining $Z_n = \frac{\mu_n}{\mu_n^*}$ $Q = \frac{q}{q^*}$ $Q_0 = \frac{q_0}{q_0^*}$, one can get the following non-linear dimensionless equations.

$$\frac{dZ_0}{dt'} = \frac{B}{B^*}\frac{e^{\lambda}}{\varepsilon^*} \exp\left[\frac{-\lambda}{\frac{G}{G^*}} Q_0\right] [1 - (1-\varepsilon^*)Z_3] - QZ_0 \tag{B-1a}$$

$$\frac{dZ_1}{dt'} = - QZ_1 + \frac{G}{G^*} Z_0 \tag{B-1b}$$

$$\frac{dZ_2}{dt'} = -QZ_2 + \frac{G}{G^*} Z_1 \tag{B-1c}$$

$$\frac{dZ_3}{dt'} = - QZ_3 + \frac{G}{G^*}Z_2 \tag{B-1d}$$

$$\frac{dF}{dt'} = Qh - QF \tag{B-1e}$$

$$\frac{G}{G^*} = f_1(F, Z_3) \tag{B-1f}$$

$$\frac{B}{B^*} = f_2(F, Z_3) \tag{B-1g}$$

(b) Secondary Nucleation Model

From Eq. (2-12), taking moment transformation one can get the following dimensionless equations.

$$\frac{dZ_0}{dt'} = - QZ_0 + \frac{B}{B^*} e^{-\lambda} \exp \left[\frac{-\lambda}{\frac{G}{G^*}} Q_0 \right] \qquad \text{(B-2a)}$$

$$\frac{dZ_1}{dt'} = - QZ_1 + \frac{G}{G^*} Z_0 \qquad \text{(B-2b)}$$

$$\frac{dZ_2}{dt'} = - QZ_2 + \frac{G}{G^*} Z_1 \qquad \text{(B-2c)}$$

$$\frac{dZ_3}{dt'} = - QZ_3 + \frac{G}{G^*} Z_2 \qquad \text{(B-2d)}$$

$$\frac{dF}{dt'} = Qh - QF \qquad \text{(B-2e)}$$

$$\frac{G}{G^*} = f_3 (F, Z_3) \qquad \text{(B-2f)}$$

$$\frac{B}{B^*} = f_4 (F, Z_0, Z_3) \qquad \text{(B-2g)}$$

APPENDIX C

Computer Programs for Computation

```
      XPHI=XHALF
      CALL GENEFUN(GA,YH)
      FHALF=YH
      IF(ABS(FHALF).LE.EPS) GO TO 10
      IF(FHALF*FL.GT.0.0) GO TO 80
      XR=XHALF
      FR=FHALF
      GO TO 90
   80 XL=XHALF
      FL=FHALF
   90 CONTINUE
      WRITE(6,170)ITER
      STOP
   50 XHALF=XPHI
      FHALF=FL
      GO TO 10
   20 XHALF=XPHI
      FHALF=FR
   10 WRITE(6,180)XHALF,FHALF
      Y=GA/6.0*(XH*6.0/GA-XJ*XH-XK*XH-XLL*XI
     1     +XM*XI)/(XH**2+XI**2)
      WRITE(6,190)Y
      STOP
CC
  120 FORMAT(// *  GIVEN DATA*///*  GA = *,F10.2,
     1         * RC = *,F10.4,*  A = *,F10.4
     2  //* CALCULATED  RESULT*//)
  150 FORMAT(//* NO INTERVAL CAN BE FOUND UP TO NEAR XL =*,
     1        F10.6)
  160 FORMAT(//*  THE INTERVAL FOR XPHI IS BETWEEN XL =*,
     1        F10.6,5X,*TO XR =*,F10.6,5X//* FL = *,E14.4
     2    ,5X,*FR = *,E14.4)
  170 FORMAT(//* NO VALUE OF XPHI CAN BE FOUND FOR GIVEN*,
     1           *ITERATION ITER =*,I6)
  180 FORMAT(//* THE XPHI VALUE=*,F10.4,5X,* THE IMAGINARY*,
     1    * VALUE = *,E14.4)
  190 FORMAT(//* THE ACTUAL VALUE=*,F12.4)
      END
CC
CC
      FUNCTION FINF(F,RC)
CC    SUBPROGRAM FOR NUMERICAL INTEGRATION OF F FROM LOWER
CC    BOUND RC TO INFINITE
CC    DCADRE: IMSL SUBROUTINE
      EXTERNAL F
      AINF=RC
CC    THIS VALUE IS SET ARBITARY AND SHOULD
CC    ADJUST IF NECESSARY
      BINF=10.
CC
      RERR=1.0E-4
      AERR=0.
      C=DCADRE(F,AINF,BINF,AERR,RERR,ERROR,IER)
      IF(IER.NE.0.AND.IER.NE.65.AND.IER.NE.66) GO TO 30
```

```
      PROGRAM CHARAC(INPUT,OUTPUT,TAPE6=OUTPUT)
      COMMON A,XPHI,RC,A1,CE,CA
      COMMON/C1/XH,XI,XJ,XK,XLL,XM
CC
CC    STABILITY ANALYSIS OF MSMPR WITH
CC    GROWTH RATE G = GC*F(R)
CC    F(R) = 1.0 + A*R, IF R LESS THAN OR EQUAL RC
CC    F(R) = 1.0 , IF R GREATER THAN RC
CC
CC
CC    GIVEN DATA
CC
CC    GA=GC*ALPH
CC    RC=CRITICAL PARTICLE SIZE
CC    A =PARAMETER IN  (1.0+ A*R )
CC
      GA=100.
      RC=1.75
      A=0.05
      A1=-1.0/A-1.0
      WRITE(6,120) GA,RC,A
CC
      CE=(1.0+A*RC)**(-1.0/A)
      CA=(ALOG(1.0+A*RC))/A
CC
      EPS=1.0E-3
      EPSI=1.0E-8
      N=20
      ITER=50
CC    TRIAL VALUE OF XPHI
      XL=1.0
CC
CC    FIND INTERVAL WITHIN WHICH ROOT LIES
      XPHI=XL
      CALL GENEFUN(GA,YA)
      FL=YA
      IF(ABS(FL).LE.EPSI) GO TO 50
      DO 60 I=1,N
      XR=XL+5.0
      XPHI=XR
      CALL GENEFUN(GA,YB)
      FR=YB
      IF(ABS(FR).LE.EPSI) GO TO 20
      IF(FL*FR.LT.0.0) GO TO 30
      XL=XR
      FL=FR
   60 CONTINUE
      WRITE(6,150)XL
      STOP
   30 WRITE(6,160)XL,XR,FL,FR
CC
CC    INTERVAL HALVING SEARCH METHOD
      DO 90 J=1,ITER
      XHALF=(XL+XR)/2.0
```

```
      DO 20 I=1,50
      AINF=BINF
      BINF=AINF+2.0
      D=DCADRE(F,AINF,BINF,AERR,RERR,ERROR,IER)
      IF(IER.NE.0.AND.IER.NE.65.AND.IER.NE.66) GO TO 30
      ER=ABS(D/C)
      IF(ER.LT.0.0005) GO TO 60
      C=C+D
   20 CONTINUE
      WRITE(6,180)BINF
      STOP
   60 FINF=C
      RETURN
   30 WRITE(6,150)IER
      STOP
CC
  150 FORMAT(//* IER =*,I5,* THE INTEGRATION FAILS*)
  180 FORMAT(//* UPPER LIMIT =*,F10.6,* IS STILL NOT BIG *
     1         ,*ENOUGH*)
      END
CC
CC
      FUNCTION FFIX(F,XA,XB)
CC    SUBPROGRAM FOR NUMERICAL INTEGRATION OF F FROM
CC    XA TO XB
CC    DCADRE: IMSL SUBROUTINE
      EXTERNAL F
      RERR=1.0E-4
      AERR=0.0
      C=DCADRE(F,XA,XB,AERR,RERR,ERROR,IER)
      IF(IER.NE.0.AND.IER.NE.65.AND.IER.NE.66) GO TO 30
      FFIX=C
      RETURN
   30 WRITE(6,150)IER
      STOP
CC
  150 FORMAT(//* IER =*,I5,* THE INTEGRATION FAILS*)
      END
CC
CC
      SUBROUTINE GENEFUN(GA,Y)
      EXTERNAL F1,F2,F3,F4,F5,F6,F7,F8,F9,F10
      COMMON A,XPHI,RC,A1,CE,CA,CT
      COMMON/C1/XH,XI,XJ,XK,XLL,XM
CC
      CT=XPHI*CA
CC
      XH=FFIX(F1,0.,RC)+FINF(F2,RC)*CE
      XI=FFIX(F3,0.,RC)+FINF(F4,RC)*CE
      XJP=FFIX(F5,0.,RC)+FINF(F6,RC)*CE
      XJ=XJP*(-1.0)/XPHI
      XKP=FFIX(F5,0.,RC)-FFIX(F3,0.,RC)-FINF(F4,RC)*CE
     1      +FINF(F6,RC)*CE
      XK=XKP/XPHI
```

```
      XLP=FFIX(F7,0.,RC)+FINF(F8,RC)*CE
      XLL=-XLP/XPHI
      XMP=FFIX(F9,0.,RC)-FFIX(F1,0.,RC)-FINF(F2,RC)*CE
     1       +FINF(F10,RC)*CE
      XM=XMP/XPHI
      Y= XLL*XH-XM*XH+6.0*XI/GA-XJ*XI-XK*XI
      RETURN
      END
CC
CC
      FUNCTION F1(X)
      COMMON A,XPHI,RC,A1
      P=1.0+A*X
      F1=(P)**(A1)*COS(XPHI/A*ALOG(P))*X**3
      RETURN
      END
CC
CC
      FUNCTION F2(X)
      COMMON A,XPHI,RC,A1,CE,CA,CT
      F2= EXP(-(X-RC))*COS(CT
     1           +XPHI*(X-RC))*X**3
      RETURN
      END
CC
CC
      FUNCTION F3(X)
      COMMON A, XPHI,RC,A1
      P=1.0+A*X
      F3=(P)**(A1)*SIN(XPHI/A*ALOG(P))
     1       *X**3
      RETURN
      END
CC
CC
      FUNCTION F4(X)
      COMMON A,XPHI,RC,A1,CE,CA,CT
      F4= EXP(-(X-RC))*SIN(CT
     1         +XPHI*(X-RC))*X**3
      RETURN
      END
CC
CC
      FUNCTION F5(X)
      COMMON A, XPHI,RC,A1
      P=1.0+A*X
      F5=(P)**(A1)*(SIN(2.0*XPHI/A*ALOG(P)))
     1         /2.0*X**3
      RETURN
      END
CC
CC
      FUNCTION F6(X)
      COMMON A,XPHI,RC,A1,CE,CA,CT
```

```
      F6=EXP(-(X-RC))*(SIN(2.0*(CT+XPHI*(X-RC))))
     1     /2.0*X**3
      RETURN
      END
CC
CC
      FUNCTION F7(X)
      COMMON A,XPHI,RC,A1
      P=1.0+A*X
      F7=(P)**(A1)*(SIN(XPHI/A*ALOG(P
     1        )))**2*X**3
      RETURN
      END
CC
CC
      FUNCTION F8(X)
      COMMON A, XPHI,RC,A1,CE,CA,CT
      F8= EXP(-(X-RC))*(SIN(CT
     1      +XPHI*(X-RC)))**2*X**3
      RETURN
      END
CC
CC
      FUNCTION F9(X)
      COMMON A, XPHI,RC,A1
      P=1.0+A*X
      F9=(P)**(A1)*(COS(XPHI/A*ALOG(P
     1       )))**2*X**3
      RETURN
      END
CC
CC
      FUNCTION F10(X)
      COMMON A,XPHI,RC,A1,CE,CA,CT
      F10= EXP(-(X-RC))*(COS(CT
     1          +XPHI*(X-RC)))**2*X**3
      RETURN
      END
 -END OF FILE-
```

```
      PROGRAM CHARAC(INPUT,OUTPUT,TAPE6=OUTPUT)
      COMMON A,XPHI,B,CE,CA
      COMMON/C1/XH,XI,XJ,XK,XLL,XM
CC
CC    STABILITY ANALYSIS OF MSMPR WITH
CC    GROWTH RATE G = GC * F(R)
CC    F(R)= (1.0 + A*R )**B, B LESS THAN ONE
CC
CC
CC    GIVEN DATA
CC
CC    GA=GC*ALPH
CC    A,B =PARAMETER IN  (1.0+ A*R )**B
CC
      GA=20.
      B=+0.2
      A=0.05
      WRITE(6,120) GA,B,A
CC
      CA=1.0/(A*(1.0-B))
      CE=EXP(CA)
CC
      EPS=1.0E-3
      EPSI=1.0E-8
      N=20
      ITER=50
CC    TRIAL VALUE OF XPHI
      XL=1.0
CC
CC    FIND INTERVAL WITHIN WHICH ROOT LIES
      XPHI=XL
      CALL GENEFUN(GA,YA)
      FL=YA
      IF(ABS(FL).LE.EPSI) GO TO 50
      DO 60 I=1,N
      XR=XL+5.0
      XPHI=XR
      CALL GENEFUN(GA,YB)
      FR=YB
      IF(ABS(FR).LE.EPSI) GO TO 20
      IF(FL*FR.LT.0.0) GO TO 30
      XL=XR
      FL=FR
   60 CONTINUE
      WRITE(6,150)XL
      STOP
   30 WRITE(6,160)XL,XR,FL,FR
CC
CC    INTERVAL HALVING SEARCH METHOD
      DO 90 J=1,ITER
      XHALF=(XL+XR)/2.0
      XPHI=XHALF
      CALL GENEFUN(GA,YH)
      FHALF=YH
```

```
      IF(ABS(FHALF).LE.EPS) GO TO 10
      IF(FHALF*FL.GT.0.0) GO TO 80
      XR=XHALF
      FR=FHALF
      GO TO 90
   80 XL=XHALF
      FL=FHALF
   90 CONTINUE
      WRITE(6,170)ITER
      STOP
   50 XHALF=XPHI
      FHALF=FL
      GO TO 10
   20 XHALF=XPHI
      FHALF=FR
   10 WRITE(6,180)XHALF,FHALF
      Y=GA/6.0*(XH*6.0/GA-XJ*XH-XK*XH-XLL*XI
     1     +XM*XI)/(XH**2+XI**2)
      WRITE(6,190)Y
      STOP
CC
  120 FORMAT(// *  GIVEN DATA*///*  GA = *,F10.2,
     1         *  B = *,F10.4,*  A = *,F10.4
     2  //* CALCULATED  RESULT*//)
  150 FORMAT(//* NO INTERVAL CAN BE FOUND UP TO NEAR XL =*,
     1        F10.6)
  160 FORMAT(//*  THE INTERVAL FOR XPHI IS BETWEEN XL =*,
     1        F10.6,5X,*TO XR =*,F10.6,5X//* FL = *,E14.4
     2    ,5X,*FR = *,E14.4)
  170 FORMAT(//* NO VALUE OF XPHI CAN BE FOUND FOR GIVEN*,
     1           *ITERATION ITER =*,I6)
  180 FORMAT(//* THE XPHI VALUE=*,F10.4,5X,* THE IMAGINARY*,
     1    * VALUE = *,E14.4)
  190 FORMAT(//* THE ACTUAL VALUE=*,F12.4)
      END
CC
CC
      FUNCTION FINF(F,RC)
CC    SUBPROGRAM FOR NUMERICAL INTEGRATION OF F FROM LOWER
CC    BOUND RC TO INFINITE
CC    DCADRE: IMSL SUBROUTINE
      EXTERNAL F
      AINF=RC
CC    THIS VALUE IS SET ARBITARY AND SHOULD
CC    ADJUST IF NECESSARY
      BINF=10.
CC
      RERR=1.0E-4
      AERR=0.
      C=DCADRE(F,AINF,BINF,AERR,RERR,ERROR,IER)
      IF(IER.NE.0.AND.IER.NE.65.AND.IER.NE.66) GO TO 30
      DO 20 I=1,90
      AINF=BINF
      BINF=AINF+2.0
```

```
      D=DCADRE(F,AINF,BINF,AERR,RERR,ERROR,IER)
      IF(IER.NE.0.AND.IER.NE.65.AND.IER.NE.66) GO TO 30
      ER=ABS(D/C)
      IF(ER.LT.0.0005) GO TO 60
      C=C+D
   20 CONTINUE
      WRITE(6,180)BINF
      STOP
   60 FINF=C
      RETURN
   30 WRITE(6,150)IER
      STOP
CC
  150 FORMAT(//* IER =*,I5,* THE INTEGRATION FAILS*)
  180 FORMAT(//* UPPER LIMIT =*,F10.6,* IS STILL NOT BIG *
     1          ,*ENOUGH*)
      END
CC
CC
      SUBROUTINE GENEFUN(GA,YI)
      EXTERNAL F1,F2,F3,F4,F5
      COMMON A,XPHI,B,CE,CA
      COMMON/C1/XH,XI,XJ,XK,XLL,XM
CC
      XH=FINF(F1,0.0)*CE
      XI=FINF(F2,0.0)*CE
      XJ=-FINF(F3,0.0)*CE/2.0/XPHI
      XK=-XJ-XI/XPHI
      XLL=-FINF(F4,0.0)*CE/XPHI
      XMP=FINF(F5,0.0)*CE
      XM=(XMP-XH)/XPHI
      YI= XLL*XH-XM*XH+6.0*XI/GA-XJ*XI-XK*XI
      RETURN
      END
CC
CC
      FUNCTION F1(X)
      COMMON A,XPHI,B,CE,CA
      P=1.0+A*X
      RY=P**(-B)*CA
      RYY=RY*P
      F1=RY/CA*EXP(-RYY)*COS(XPHI*(RYY-CA))
     1       *X**3
      RETURN
      END
CC
CC
      FUNCTION F2(X)
      COMMON A,XPHI,B,CE,CA
      P=1.0+A*X
      RY=P**(-B)*CA
      RYY=RY*P
      F2=RY/CA*EXP(-RYY)*SIN(XPHI*(RYY-CA))
     1       *X**3
```

```
      RETURN
      END
CC
CC
      FUNCTION F3(X)
      COMMON A,XPHI,B,CE,CA
      P=1.0+A*X
      RY=P**(-B)*CA
      RYY=RY*P
      F3=RY/CA*EXP(-RYY)*SIN(2.0*XPHI*
     1    (RYY-CA))*X**3
      RETURN
      END
CC
CC
      FUNCTION F4(X)
      COMMON A,XPHI,B,CE,CA
      P=1.0+A*X
      RY=P**(-B)*CA
      RYY=RY*P
      F4=RY/CA*EXP(-RYY)*(SIN(XPHI*(RYY-CA)))
     1     **2*X**3
      RETURN
      END
CC
CC
      FUNCTION F5(X)
      COMMON A,XPHI,B,CE,CA
      P=1.0+A*X
      RY=P**(-B)*CA
      RYY=RY*P
      F5=RY/CA*EXP(-RYY)*(COS(XPHI*(RYY-CA)))
     1     **2*X**3
      RETURN
      END
 -END OF FILE-
```

LIST OF SYMBOLS

$\underline{A}$ - State space matrix

a - Constant in growth rate

a' - $a\, G_o^* \theta^*$

B - Nucleation rate (no/cm^3 sec)

$\underline{B}$ - Matrix defined by Eq. (2-11b) or Eq. (2-14b)

b_c - Nucleation Sensitivity rate (-)

b_1 - $(b_c - \alpha)/\varepsilon^*$ (-)

b_n - $\mu_0^*/B^* \frac{\partial B}{\partial \mu_0}$ (-)

b - $\frac{(\rho s - c^*)}{B^*} \frac{\partial B}{\partial c}$

C - Concentration (gm/cm^3)

C_i - Inlet concentration (gm/cm^3)

C_m - Critical concentration in Mier nucleation model (gm/cm^3)

C_s - Saturation concentration (gm/cm^3)

c - Friction constant (Chapter 6 only)

$\underline{D}$ - Matrix defined by Eq. (2-11c) or Eq. (2-14c)

D_p - Particle diameter (Chapter 6 only)

E, E_1, E_2 - Electrical voltage (volt)

$F(t)$ - Forcing function (Chapter 6 only)

F - Ψ/Ψ^* (-)

F' - $-\delta\Psi/\Psi^*$ (-)

f - Population density (no/cm^3cm)

G - Growth rate (cm/sec)

G_o - Growth rate concentration dependent function (cm/sec)

g - $(C_s - C^*)/G_o^* \frac{\partial G_o}{\partial C}$

g_c - Growth Sensitivity rate (-)

g_1 - g_c/ε^* (-)

g_c' - αg

g_s - Defined by Eq. (5-7)

H - Defined by Eq. (5-7)

h - C_i/C_i^* (-)

h' - $\delta C_i/C_i^*$ (-)

i,i' - Conversion factor

k - Spring constant (Chapter 6 only)

k - Geometric shape factor (1/no)

k_g - Growth rate constant

k_b - Nucleation rate constant

L - $(\rho_s - C_s)/(C_i^* - C_s)$ (-)

l - constant

M - Mass of cylinder (Chapter 6 only)

M - $(C^* - C_s)/(C_i^* - C_s)$ (-)

m - constant

m - mass of particle (Chapter 6 only)

N - Number of particles

n - Interger number (-)

n' - Constant in Mier nucleation model (-)

P - $1/\alpha\ (L-M)(1-k\mu_3^*)(1-C_s/C_i^*)$ (-)

P - Defined by Eq. (6-2b)

Q - q/q^* (-)

Q_0 - q_0/q_0^* (-)

q - Throughput volumetric flow rate (cm^3/sec)

q' - $\delta q/q^*$ (-)

q_0 - Fines recirculation rate (cm^3/sec)

q_0' - $\delta q_0/q_0^*$ (-)

$R(r)$ - Growth rate size dependent function (-)

R - Reference radius (Chapter 6 only)

r - Characteristic size of crystal (cm)

r' - $r/G_o^*\theta^*$ (-)

r_c - Critical size (cm)

r_c' - Dimensionless critical size (-)

r_o - A critical size for fines destruction (cm)

St - Stokes' number (-)

s - Laplace transformation variable

t - Time (sec)

t' - Reduced time = t/θ^* (-)

t' - $t\ u_\infty/R$ (Chapter 6 only)

U - Velocity of particle (cm/sec) (Chapter 6 only)

$\underline{U}$ - Control variable vector

u_x, u_y, u_1, u_2 - Velocity component of particle in x, y, 1, 2 direction (cm/sec)

u_N - Velocity component of particles in normal direction (cm/sec)

u_T - Velocity component of particles in tangential direction (cm/sec)

u_∞ - Reference velocity (cm/sec)

V - Volume of crystallizer (cm^3)

$\underline{V}$ - Input vector

v_x, v_y - Velocity component of the fluid in x, y direction (cm/sec)

v_x', v_y' - Dimensionless velocity component of fluid in x, y direction (cm/sec)

$\underline{X}$ - State space matrix

x - Dummy variable

x - Displacement (Chapter 6 only)

x' - x/R (Chapter 6 only)

y - Dummy variable

y - Displacement (Chapter 6 only)

y_∞ - y coordinate of particle at upstream

y' - y/R (Chapter 6 only)

Z_n - μ_n/μ_n^* (-)

Z_n' $-\delta\mu_n/\mu_n^*$ (-)

GREEK LETTERS

α - $6kB^* G^{*3} \theta^{*4}$ (-)

δ - Refers to the pertubation variables of the system

$\delta C_i'$ - Defined by Eq. (5-7)

$\delta f'$ - Defined by Eq. (5-7)

$\delta\psi'$ - Defined by Eq. (5-7)

ε - Liquid volumetric fraction in the crystallizer (-)

θ - The overall holdup time of the crystallizer (sec)

θ_0 - Retention time of small particles (sec)

λ - $r_o q_0^*/V G^*$, parameter of the fines trap (-)

μ - Viscosity (gm/cm sec)

μ_m - Mean

μ_n - n-th moment of population density f (no cm^{n-3})

ρ_s - Density of crystals (gm/cm^3)

σ^2 - Variance

ϕ - Parameter

ψ - Crystal-solute resource function (gm/cm^3)

SUPERSCRIPT

$*$ - Refer to the steady state value

$\sim$ - Refer to Laplace transformation

AFFIX

δ - Denote pertubation from the steady state value